



DEGREE PROJECT IN INDUSTRIAL ENGINEERING AND
MANAGEMENT,
SECOND CYCLE, 30 CREDITS
STOCKHOLM, SWEDEN 2018

Local positioning system for mobile robots using ultra wideband technology

FILIP LENSUND

MIKAEL SJÖSTEDT



Master Thesis ITM-EX 2018:163
Local positioning system for mobile robots using ultra wide-band technology

Mikael Sjöstedt
Filip Lensund

Approved: 15/6 - 2018	Examiner: Lei Feng	Supervisor: Martin Edin Grimheden
	Commissioner: Cybercom Group AB	Contact Person: Filip Stenbeck

Abstract

This thesis explores the possibility of using ultra wideband technology to localize an outdoor mobile robot. More explicitly, this project focuses on the multilateration problem where the topology of the static reference anchors are changed. Instead of having stationary anchors they are placed on a mobile robot and by pinpointing one single static tag node the position of the robot is established. The research uses a robotic lawn mover from Husqvarna, the Automover 430X. The robot is used as a base platform for this thesis to evaluate if this approach is applicable for other generic robots in the same size. The feasibility of this solution is demonstrated through simulation using Matlab and the robot simulation environment Gazebo. Results show that this specific topology is feasible for tracking a specific point but is also suitable for positioning a mobile robot if coupled with an accurate heading sensor. The system was evaluated for several scenarios of which all indicated an adequate accuracy, provided that data from an encoder was used. The upper limit for the position error in a one sided 95% confidence interval was 0.469 m at a range of 40 m.

Keywords: ultra wide-band, UWB, localization, positioning, outdoor positioning, multilateration, reversed multilateration



Examensarbete ITM-EX 2018:163

Lokalt positioneringssystem för mobila robotar med ultra wideband teknik

Mikael Sjöstedt
Filip Lensund

Godkänt: 15/6 - 2018	Examinator: Lei Feng	Handledare: Martin Edin Grimheden
	Uppdragsgivare: Cybercom Group AB	Kontaktperson: Filip Stenbeck

Sammanfattning

Detta examensarbete tar sig an problemet att lokalisera en långsamtgående mobil robot i en utomhusmiljö genom att använda sig av ultra wideband radioteknik. Vanligtvis placeras stationära noder i miljön som används för att positionera en ensam nod i dess närhet. Detta projekt tar sig an frågeställningen om det är möjligt att vända på problemet och placera dessa *stationära* noder på den mobila roboten för att sedan fixera robotens position genom att bestämma var den ensamma noden är placerad. Husqvarnas robotgräsklippare Automover 430X har använts som plattform för att evaluera och testa om denna tes är applicerbar för andra generiska robotar i samma storlek. Positionsuppskattningen utförs genom simulationer i Matlab samt simulationsmiljön Gazebo som tar hänsyn till diverse fysiska fenomen. Resultaten pekar på att denna topologi är möjlig för att lösa multilatereringsproblem om en riktningssensor med hög precision används. För alla scenarion som simulerades indikerades att en någorlunda god precision kan uppnås och det krävdes att systemet kombinerades med annan indata, som en enkoder i detta fall för att förbättra estimeringen. Den övre gränsen för felet i ett 95% konfidensintervall var 0.469 m på ett avstånd upp till 40 m.

Acknowledgements

We would like to thank our company supervisors Filip Stenbeck and Oden Lobell for their continuous feedback along the whole project. Our supervisor at KTH, Associate Professor and Division Manager Martin Edin Grimheden for his scientific guidance. The Cybercom group for housing us for these six months and the thesis group at Cybercom for many elaborate discussions.

Mikael Sjöstedt, Filip Lensund Stockholm, May 2018

Contents

List of Figures	xi
List of Abbreviations	xii
1 Introduction	1
2 Background	3
2.1 Problem formulation	3
2.2 The positioning problem	3
2.3 Previous work	7
2.4 Research question	12
2.5 Scope	12
2.6 Requirements	12
2.7 Method	13
2.8 Ethics	13
3 Theory	15
3.1 Rover model	15
3.2 Radio	17
3.3 Ranging methods	19
3.3.1 Two-Way Ranging	20
3.4 Positioning techniques	22
3.4.1 Linear Least squares and Non-linear least square	23
3.5 Filtering	25
3.5.1 Discrete Kalman filter	25
3.6 Performance evaluation	29
3.7 Reference frame	29
3.8 Orientation angle	31
4 Unit tests & Simulation	35
4.1 Micro controllers	35
4.2 DWM1000	36
4.2.1 Operational design	36
4.2.2 DW1000 calibration	37
4.3 Ranging test	38
4.4 Simulation & evaluation	39
4.4.1 Simulated signal	40

4.4.2	Choice of anchors	41
4.5	Filter evaluation	41
4.5.1	Extended Kalman Filter	42
4.5.2	EKF and UKF	45
5	Results	47
6	Discussion	53
7	Conclusion	59
8	Future work and remarks	61
8.1	NLOS	61
8.2	Antenna	62
8.3	Sensors	62
8.4	Dead reckoning model	62
8.5	Choice of hardware	62
8.6	Path planning algorithm	63
	Bibliography	65
	A Unscented Kalman Filter	I
	B Software Flowcharts	III
	C Angle of rotation using UWB	V
	D Distance measurements	VII
	E Results appendix	XI
	F Schematics and circuit boards	XV
	G Contributions	XXI
	H Code	XXIII

List of Figures

2.1	Comparison between range measurements that uses UWB (left: Ubisense, middle: BeSpoon and right: Decawave)[60].	7
2.2	Comparison between Bespoon (top and bottom left) and Decawave (top and bottom right) in an outdoor environment [34].	8
2.3	Results for indoor localization using UWB [19].	9
2.4	Anchor configurations from [40].	9
2.5	Mean error of different configurations from [40] with respect to distance.	10
3.1	Differential drive model.	15
3.2	Frequency chart of UWB compared to other radio communication protocols [49].	18
3.3	IR-UWB signal example.	18
3.4	Foci of hyperbola from measurements using TDoA.	20
3.5	Different two-way ranging methods.	20
3.6	Two cases a and b for the geometric algorithm.	22
3.7	Multilateration case for the rover.	23
3.8	Kalman phases.	26
3.9	Graphic representation of the error.	30
3.10	Navigation frame and rover frame.	30
3.11	Two cases for the geometric algorithm, a and b.	31
3.12	Geometry used to solve the orientation angle.	32
3.13	Navigation frame & rover frame.	32
4.1	Raspberry Pi 3.	35
4.2	Arduino Mini Pro 3.3V.	36
4.3	DecaWave DWM1000 module.	36
4.4	Transmit and receive antenna delay.	38
4.6	Comparison of simulated signal and measured signal at 43.4 m.	40
4.7	Empirical cumulative distributive function of the error at a range of 43.4 m.	40
4.8	Placement of the UWB-transmitters on the robot.	41
4.9	Position estimated by proposed filters.	42
5.1	Comparison of estimated position through UWB and dead reckoning system in the 56.5x56.5m square scenario.	48
5.2	Dimensions of the arbitrary environment and estimated position of the rover moving inside the said area.	49

5.3	Comparison of position estimate of rover when travelling randomly in an arbitrary environment.	49
5.4	Comparison of position estimate of rover when travelling in large circle, with and without encoder input.	50
5.5	Comparison of estimated position through UWB and dead reckoning system in the 30x30m square scenario.	51
5.6	Estimation of position in 56.5x56.5m square scenario using UWB as rotation angle input.	51
5.7	Cumulative distribution function of position estimate error with standard deviation 0.027 m signal.	52
5.8	Cumulative distribution function of position estimate error with standard deviation 0.046 m signal.	52
6.1	Estimated position through UWB and dead reckoning system.	55
6.2	Zoomed view of Figure 5.1a.	56
6.3	Position estimate in the arbitrary environment.	57
B.1	Flowchart of anchor software	III
B.2	Flowchart of tag software	IV
D.2	Histogram of measurements made at 8.7 m	VIII
D.3	Range measurements at various distances	IX
D.4	Histogram of measurements made at various ranges displayed in Figure D.3	IX
F.1	DWM1000 breakout board schematic	XVI
F.2	Arduino tag schematic	XVII
F.3	Module connector board schematics	XVIII
F.4	Arduino tag PCB	XIX
F.5	Connectorboard PCB	XIX
F.6	DWM1000 breakoutboard PCB	XX

Nomenclature

Explanation of the used abbreviations

Abbreviation	Explanation
RF	Radio Frequency
GNSS	Global Navigation Satellite Systems
GPS	Global Positioning System
LPS	Local Position System
LoS	Line of Sight
NLoS	No Line of Sight
RTK	Real Time Kinematic
ToF	Time of Flight
ToA	Time of Arrival
TDoA	Time Difference of Arrival
AoA	Angle of Arrival
RSS	Received Signal Strength
SLAM	Simultaneous Localization and Mapping
EKF	Extended Kalman Filter
LLS	Linear Least Square
LIDAR	Light Detection And Ranging
RFID	Radio-Frequency Identification
IMU	Inertial Measurement Unit
UWB	Ultra Wide-Band
UAV	Unmanned Aerial Vehicle
ROS	Robotic Operating System
ICC	Instantaneous Center of Curvature
SNR	Signal to Noise Ratio
IR-UWB	Impulse Radio Ultra Wide-band
PL	Path Loss
TWR	Two-Way Ranging
SDS-TWR	Symmetrical Double Sided Two-Way Ranging
ADS-TWR	Asymmetrical Double Sided Two-Way Ranging
D-TWR	Double Two-Way Ranging
NLLS	Non-Linear Least Squares
UKF	Unscented Kalman Filter
SPI	Serial Peripheral Interface

Explanation of the used abbreviations (cont.)

Abbreviation	Explanation
MCU	Microcontroller Unit
RPi	Raspberry Pi
RTLS	Real-Time Locating System
PRF	Pulse Repetition Frequency
AWGN	Additive White Gaussian Noise

1

Introduction

A trend of consumer devices that interact with the environment and moving objects can be observed, not the least in the vehicle industry and self-driving cars [27]. One of the autonomous applications that are moving into the consumer market is autonomous lawn mowers, robots with the assignment of cutting the lawns of public and private gardens.

The Husqvarna Automower, which is the platform used for this MSc thesis project is an autonomous lawn mower developed by Husqvarna. The Automower of today applies crash detection and magnetic sensors to navigate through the garden. By making use of a boundary wire dug down along the perimeter of the garden and the built-in obstacle detection it makes sure the Automower doesn't leave the specified area. This is not sufficient to localize the Automower as it has no perception of its position within the area. The Automower moves in a random pattern across the garden, choosing a random direction when the robot passes the boundary wire or hits an obstacle [30]. Given enough time the whole area will be covered.

If the Automower could position itself relative to a known landmark, the charging station for instance, a map of the area could be created. It would then be possible to implement a full coverage path planning algorithm and in that fashion make sure that the lawnmower passes all points of the area to be cut in a shorter amount of time while also save energy and resources. The Automower would therefore benefit from using a positioning system in form of a global positioning system or a local positioning system.

The goal of this project is to develop a positioning system for autonomous robots such as the Husqvarna Automower which shall cope with an arbitrary environment without any requirement of visual landmarks and intervention of the existing infrastructure. This thesis explores the possibility of using classic multilateration techniques with a new approach. Instead of having stationary reference nodes placed at strategic positions, the reference anchors are placed on the mobile target and pinpoints the location of one single node located at the known base station. This could be of use when the possibility of placing the reference anchors in the area is limited or not possible as for instance consumer products that must work *out of the box* or when the environment can't be tampered with. This method requires high precision transceivers as the distance between each of these anchors are very narrow. That is why this thesis will focus on multilateration using ultra wide-band technique.

1. Introduction

2

Background

This chapter discusses the foundations of the positioning problem and presents previous work done in this field. Additionally, the scope of the project is presented and a more in-depth analysis of the work done regarding Radio Frequency (RF) positioning systems.

2.1 Problem formulation

There are outdoor intermediate moving applications which have no localization system as for example the *Husqvarna Automower 430X*. A localization system is needed for mapping environments which gives the opportunity to apply a path covering algorithm. A compact localization system is desired so that the system can be applied to small and agile applications and to avoid or minimize changes in the pre-existing infrastructure.

2.2 The positioning problem

Positioning a moving object in an arbitrary environment is not a trivial task. There are several approaches available and they all have their advantages and disadvantages. Positioning techniques can be separated into two large subgroups; global and local positioning systems. The Global Navigation Satellite Systems (GNSS), usually referred as Global Positioning System (GPS) can be considered a global solution to the positioning problem as it is available worldwide, while the Local Positioning System (LPS) is for short range applications used to position an object relative to known reference points. Both of these approaches will be discussed in this chapter.

The GPS is extensively used for tracking a position or navigate in an outdoor environment. It has been in use since its development in the 1970's for military use but has after the release to the public in 1984 evolved into a system widely adapted and used by commercial grade products such as navigation for vehicles [8]. The system relies on 24 satellites orbiting the earth transmitting signals to the various GPS receivers on the surface. The method makes use of lateration, determining the distance between the receiver and four different satellites and thus being able to calculate an absolute position [7]. The drawback of this method is the signal attenuation due to the long distance, therefore the obstacle penetration is limited and Line of Sight (LoS) is more or less a requirement. It is also affected by scattering and multipathing, which leads to accuracy degradation in urban environments and

2. Background

is uncommonly used for indoor positioning. GPS is one of the most researched and used positioning systems in the world. There is a wide variety of available GNSS with various accuracy such as the real-time kinematic GPS (RTK-GPS), Differential GPS, GLONASS-M GPS, Galileo etc. The RTK-GPS is by far one of the most accurate, with an accuracy of $< 0.1m$ during good conditions. The RTK-GPS utilize one or more static reference stations on the ground with known positions. By combining the position from the satellites and the relative position from the reference stations a much higher accuracy than regular GPS can be achieved [55]. A study focused on positioning this type of application [44] showed that drift of the GPS signal is still an issue when high accuracy is required but can be enhanced with sensor fusion [42, 76]. A big drawback is the cost of this system which makes it unsuitable for this project.

LPS is used in a range of applications for military and civilian purposes to determine the relative position of an object or a person. Infrared light, radio, laser, cameras etc. are all different technologies used for LPS [5]. These technologies can be used with different types of techniques to determine the position of an object or person. There are three fundamental principles used to localize an object; triangulation, scene analysis and proximity measures [29]. Triangulation can be divided into two separate subgroups, *angulation* and *lateration*. Angulation make use of measured angles to known reference points and lateration use distance measurements to known reference points to compute the position. Different techniques can be used to determine the distance between transmitter and receiver, this is referred to as ranging. One technique to derive the distance is Time of Flight (ToF), which is the time it takes for the signal to travel from the transmitter to the receiver. By knowing the velocity of the signal, the distance between nodes can be calculated. Techniques that uses ToF are Time of Arrival (ToA), Time Difference of Arrival (TDoA), Two-Way Ranging (TWR) and Angle of Arrival (AoA) [77]. Another approach is Received Signal Strength (RSS) [49] which measures the strength of the received signal from the transmitter rather than the travel time for the signal. It makes use of the received signal strength and by knowing the signal strength from the transmitter to the receiver and the propagation of the signal in the medium it travels in, it is possible to determine the distance.

Scene analysis includes visual examinations to create a positioning system. This includes comparing pictures and features to known datasets and newer techniques that can make use of visual aid such as the popular *simultaneous localization and mapping* (SLAM). These systems could utilize images of the environment from cameras to distinguish landmarks, colours or shapes using machine vision algorithms, to then position the robot with the regards of the environment. This technique is highly reliant on processing heavy algorithms which require the prior pose of the robot and a large set of observations of the environment. A solution to this kind of mapping and localization is often referred as solving the SLAM problem. SLAM has been a hot topic since the entry of mobile robotic systems in the 1980's. Something as teaching a robot what the world looks while also positioning the robot relative its surroundings using only onboard sensors is not a simple task but is however, a very

researched topic due to opportunities within the consumer market. One approach to solve this problem is, as stated above, to use images of the environment. Combined with a wide group of algorithms such Extended Kalman Filter (EKF) and Linear Least Squares (LLS) it is possible to estimate a map of the environment and the pose of the robot using the inputs from the camera and the control signals used to move the robot in a certain direction [10]. Stereo-cameras can be used to add some depth of the to the observations. As early as 2005 it was possible to successfully implement SLAM and full path coverage algorithms for a robotic vacuum cleaner using camera images of the ceiling [32]. Other approaches to classify the environment are using some kind of laser since it has long range capability and high precision. The Laser Imaging Detection And Ranging (LIDAR) is a popular choice of range measuring device where distance measurements are used to create a grid map of the surroundings such as in [50]. 3D mappings can also be made by creating a point cloud from the laser scans such as in [54] using a mobile robot. SLAM algorithms usually assume a static environment but with novel algorithms such as proposed by [38] it is possible to adapt to non-stationary changes such as moving humans or objects in the vicinity. Especially important for robots operating in urban environment. This type of system is however very reliant on visual landmarks which is why it isn't an ample method for all applications.

Proximity systems utilize known locations and senses when the object is near one of these known positions. An example connected to the lawn mower would be that a known position is the charging station which is detected through the dug down boundary wire. However as both the proximity sensors and optical systems require some kind of landmarks to create reference points in the environment this solutions might not be applicable for a mobile robot in an ambiguous environment such as an open field.

The techniques introduced above that are used to determine a distance to an object can all be considered to belong to the *geometrically driven* framework where the geometric link (distance, angle, view, etc) are used to estimate a objects position.

Radio is a commonly used technology when deriving the distance in an LPS system. The various radio technologies use different bandwidth and protocols to communicate and are therefor suitable for different applications. RFID is mostly used to fetch data from transponders and memories at a short range. Applicable to car tolls and credit cards, the receiver retrieves information on the RFID-tag using a large frequency range up to 5.8 Ghz depending on the protocol. Positioning systems using RFID has been successfully implemented in short range such as in [70] where RSS is used to correlate the position of the tag using an artificial neural network. However the range for these systems are rather limited [12], if not the more expensive and complex active tags operating in the ultra high frequency range are used.

Wi-Fi and its subgroups most commonly solve the positioning problem by measuring the RSS but can also be incorporated with ToF techniques. RSS localization techniques are inherently difficult to implement with high accuracy due to the prop-

2. Background

agation of the signal when traveling through obstacles and drift of signal strength over time. Using the Wi-Fi infrastructure it has been proven to be difficult to implement a positioning system with an accuracy better than the magnitude of meters [47] but it is still popular due to the fact that the Wi-Fi structure is readily available in many indoor locations. WiFi localization systems that incorporate ToF technique have shown to give better results but also makes the implementation more difficult and increases computational complexity, the location performance is not better than in the order of one meter under optimal conditions [72, 63].

Bluetooth and its addition Bluetooth Low Energy are also candidates which most commonly, like the Wi-Fi approach, use RSS to estimate a range between transmitter and receiver. Studies such as [33] show accuracy similar to Wi-Fi networks, not much better than 1 m.

Wi-Fi can be considered to be within the ultra wide-band (UWB) frequency scope but the protocol limits the usage to a narrow bandwidth. If the open regulated frequency range is used without protocol delimitations UWB has a large bandwidth which results in a capability of high transfer rate of data. The frequency band for UWB is between 3.1–10.6 GHz and due to the wide bandwidth the signal has robust multi-path propagation, obstacle penetration [74] and fine accurate ranging [16]. The transmission power is however limited to -41.3 dBm/MHz since the high frequencies can interfere with other radio equipment. The range of UWB systems have been proved to work to ranges up to $>100 \text{ m}$ [34] even with this low transmit power.

UWB is therefore used for short range communication with high data rates, such as sensor networks and radar systems. As with all RF technologies the measurements are noisy by nature. To deploy a working positioning system using UWB, sophisticated filtering algorithms are usually employed by combining several measurements, usually the EKF as [51] or non-linear filtering techniques such as a particle filter is applied like in [25].

No single positioning system provides very good performance in all attributes such as accuracy, complexity, scalability, cost and robustness, and so forth. Therefore a conjunction of several sensors or inputs, *sensor fusion*, are usually utilized when developing a navigation system for a mobile robot, such as odometry, visual aid and inertial measurement units (IMU) to add redundancy and improve the overall performance beyond what one individual sensor can achieve. Together with filter algorithms the accuracy of the navigation system can be further improved [36]. This thesis has chosen to focus on UWB with sensor fusion since the UWB is by far the most accurate of the radio technologies which don't require any visual landmarks, and the range limitations are ample for this application.

2.3 Previous work

There are no specific techniques to be used for a given positioning problem. In this section previous research and applications of this are presented. The accuracy, coverage, transmit power and complexity of the technologies presented in the previous section 2.2 is summarized in Table. 2.1.

Table 2.1: Comparison of position technologies [15, 49, 78].

Technology	Typical accuracy [m]	Typical coverage [m]	Transmit power [W]	Complexity
GPS	0.1-20	global	500	High
RFID	1	1-50	0.02-0.3	Low
Wi-Fi	1-5	<100	0.5-1	High
UWB	<0.3	<300	0.03	Low-Medium
Bluetooth	1	<10	0.001	Medium
Zigbee	1-5	<30	0.02-0.04	Low

As previously mentioned they all have their advantages and disadvantages but it is obvious that the UWB technology outperforms its competitors regarding accuracy which in this project is an important factor.

There are several UWB products on the market that offer ranging capabilities at a low cost such as Ubisense, BeSpoon and DecaWave. A comparison between these systems was carried out by [60]. The test was performed in a indoor environment with disturbing objects. The results can be seen in Figure 2.1 where the modules from DecaWave performed the best with lowest scattering from the true value.

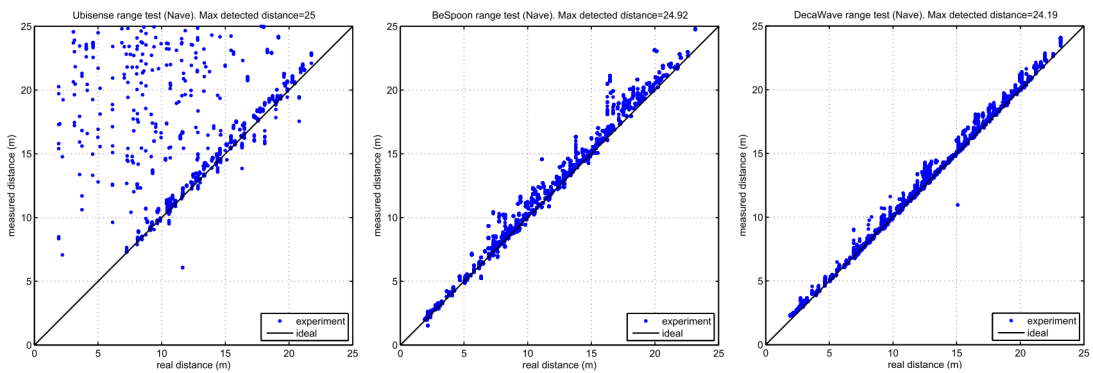


Figure 2.1: Comparison between range measurements that uses UWB (left: Ubisense, middle: BeSpoon and right: Decawave)[60].

There is also a test performed by [34] which compares DecaWave and Bespoon in a outdoor environment and in line of sight. The nodes were placed on 2.1 m high posts and on a private road with no obstacles. The measured distances were from 0-100 m separated by different discrete steps. The standard deviation for Bespoon was

2. Background

0.11 m and for DecaWave 0.055 m. In Figure 2.2 the measured distance is compared to the real distance and the precision of the measured distances is presented in histograms. These two studies indicate that the modules from DecaWave outperform its competitors in the same price range.

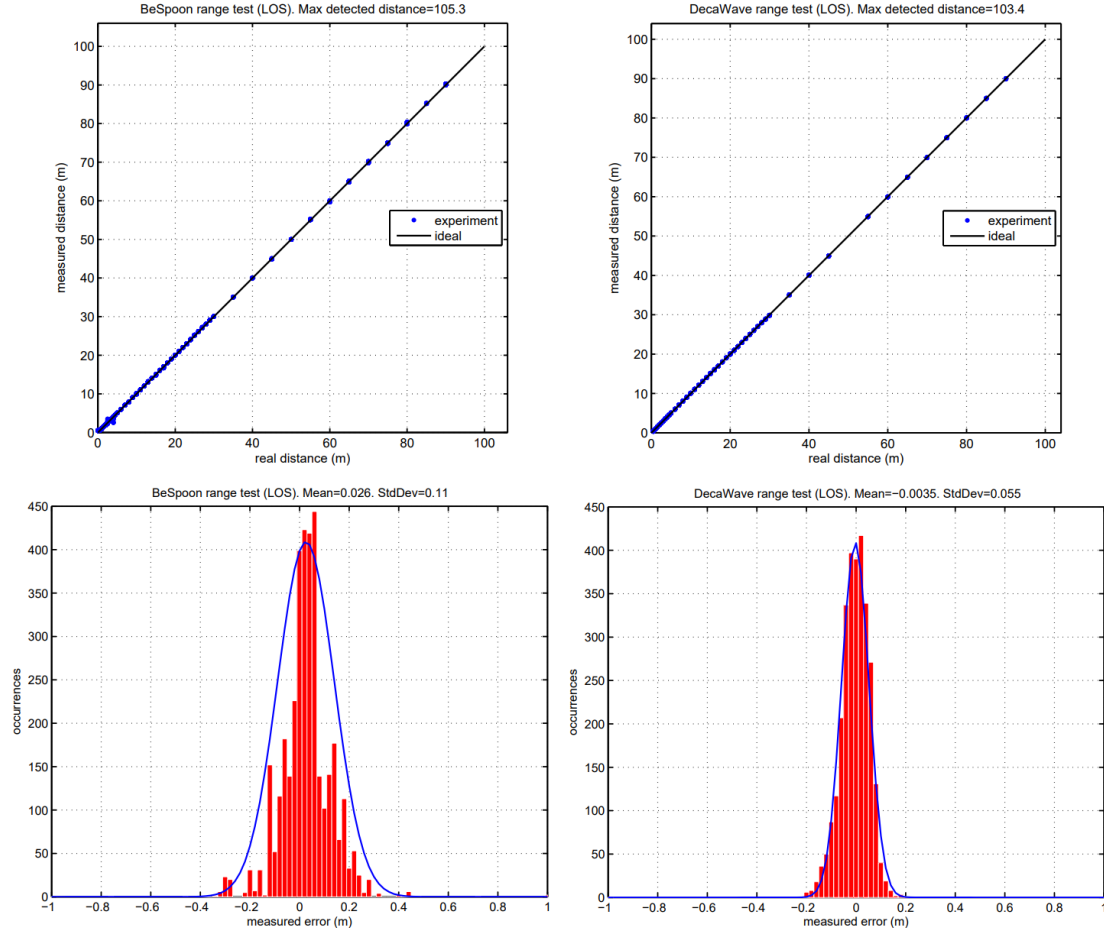


Figure 2.2: Comparison between Bespoon (top and bottom left) and Decawave (top and bottom right) in an outdoor environment [34].

There are many studies on positioning with small UWB modules. A positioning system for elderly persons to ensure their safety was developed and tested by [19] with DWM1000-modules. This particular study showed that it was possible to position a moving target with a standard deviation of 0.4 m for 90% of the test points. The tests were performed in an indoor environment for both a stationary and a moving target. The results of the data points taken during the test with a moving target can be seen in Figure 2.3. The study used multiple stationary anchors and a reference node to synchronize the anchor-nodes and an Extended Kalman Filter based algorithm was used for tracking the tag. The explanation for the deviation in ranging for some areas in the test environment was multipath-propagation due to the thick concrete walls.

An interesting numerical study of a UWB localization technique for tracking an

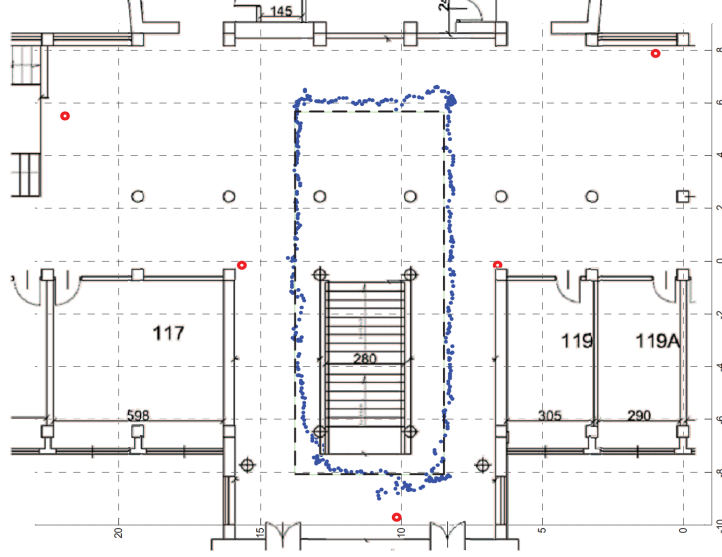


Figure 2.3: Results for indoor localization using UWB [19].

unmanned aerial vehicle (UAV) was performed by [40]. The anchors in this study were placed on a moving platform and in different constellations to investigate the difference in performance depending on how the anchors were placed. A sketch of the ground station equipped with four UWB nodes in different configurations and the UAV flying in front of it equipped with one UWB node can be seen in Figure 2.4 [40].

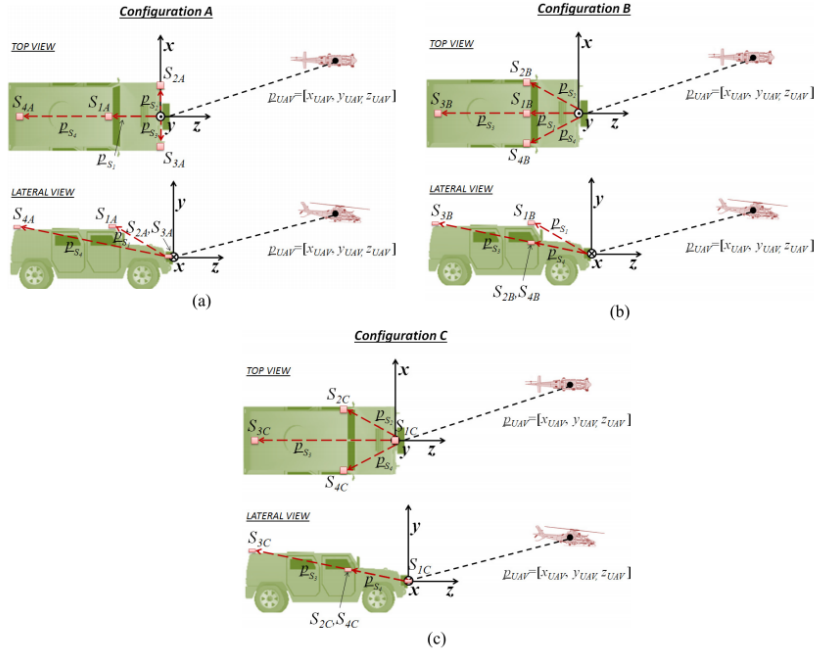


Figure 2.4: Anchor configurations from [40].

The setup of the anchors were similar to the setup approached in this thesis, with the tracking node always outside the area spanned by the ranging anchors.

2. Background

This study used TDoA for ranging and since the performance of the system was simulated the ranging precision was derived by testing UWB PulsON 400 nodes from TimeDomain[20]. The performance of the system depended on the constellation of the anchor nodes where the best performing was the one with the anchor nodes placed further apart spanning up a larger area. In this case Configuration A. The performance of the system in x-, and y-coordinates can be seen in Figure 2.5

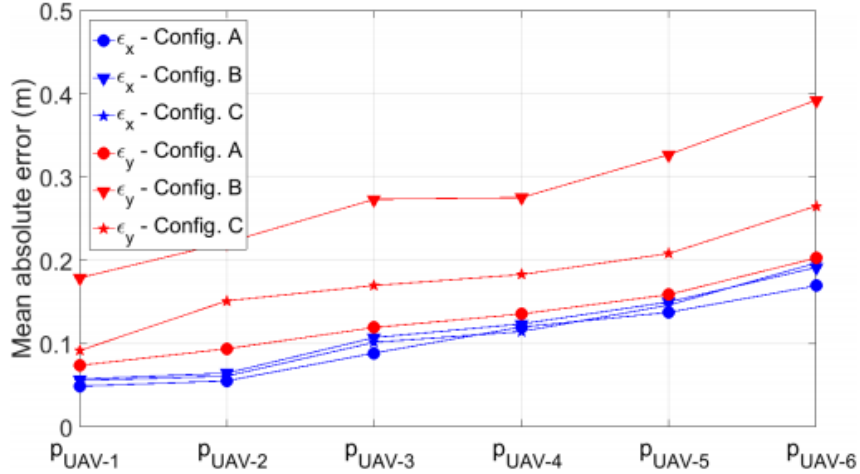


Figure 2.5: Mean error of different configurations from [40] with respect to distance.

A common method when applying positioning systems with UWB technology is to incorporate other sensors to improve the results. The radio technology is usually sufficient in terms of an absolute position sensor but the inherent noise of radio signals can be mitigated by adding other relative sensors such as encoders or IMU. In [51] UWB was fused with inertial measurements to localize a moving quadrocopter. By fusing these two inputs in an EKF it was possible to achieve an accurate position estimate with a mean accuracy of 0.041 m during fast horizontal manoeuvres along a 4 m × 3 m square.

The authors in [71] incorporate all of the above said, inertial sensors and visual odometry with a UWB multilateration scheme in a non-iterative SLAM method to localize and map the surroundings of a moving object. The UWB system was set up in a classical way using stationary reference anchors and was able to perform with an average mean accuracy of 0.06 m. The tests were however conducted in a small room of 6x6m which is why the visual odometry is applicable.

Most applications using UWB as the central input to the system are focused on short range operations or indoor conditions due to the obstacle penetration abilities. There are however tests on outdoor applications such as localization of parked electric vehicles as to be able to align and select dug down coils in the ground to charge the vehicles with inductive charging pads. Using two base nodes on the end of the parking square the alignment accuracy was as good as 0.1 m in 95% of the cases using an EKF state estimator [67].

A study [26] using UWB modules P410 from TimeDomain showed that it was possible to localize a moving quadrocopter at longer ranges with very high accuracy. By placing four anchors in an open field and flying the quadrocopter equipped with one ranging tag along a rectangle of roughly 60x30m it was possible to estimate the drone's position with an average accuracy of 0.175 m using an EKF estimator without any additional sensor input.

The majority of the work done within this field of radio positioning systems utilize static anchors placed in the environment and a single tag is localized within the area spanned of these anchors. This thesis explores the possibilities of placing the reference anchors within a small constricted area of a mobile object while localizing a static tag outside the area of reference nodes, a kind of inverse multilateration. This area could be considered relatively unexplored where three studies (including the UAV study by [40]) have been found to use a similar topology.

In [14] the authors managed to track the position of a small moving robot using UWB multilateration and sensor fusion where the reference anchors were fixated to a movable and adjustable basestation while the rover equipped with a single tag was tracked outside the area of the reference nodes. The results were verified by video recordings and indicated that this kind of topology is capable of position a moving robot. Here the reference anchors are stationary which isn't the case for this thesis but they are spaced very close to each other which is the case for this study.

An application with similar setup as proposed in this work with movable reference points has been found used for a following quadrocopter. In [28] the authors managed to create a system that was capable of following a single node with an average accuracy of 0.1 m at a range of 4 m. The similarities with this project is the distance between each anchor node as they both are small applications and the continuous movement of the robot but the derived position is only in a coordinate system relative the robot whereas in this project the position has to be projected onto the coordinate system relative the tag node or basestation.

2.4 Research question

The focus of this thesis will be to evaluate whether it is possible to develop a positioning system with sufficient accuracy by using multilateration and arranging the reference nodes in an unconventional way where they are all placed on a medium sized moving robot while tracking a single static tag node. The narrow placement of the anchors demand high precision with regards to range measurements and the orientation of the robot is required as to map the position back into a coordinate relative the basestation. The research questions that are being answered in this project are as follows:

Is reversed multilateration using UWB a viable technical solution for positioning a small and agile intermediate moving outdoor robot?

How much is the positioning performance improved when combining the system with odometry data?

2.5 Scope

The focus in this MSc thesis project will be UWB-positioning systems for small and agile intermediate moving outdoor robots. The platform used in this project is a Husqvarna Automower 430X, this to give a concrete example of an application that could benefit of or use a localization system.

The requirements are set to match a typical operating environment for the Husqvarna Automower 430X. The delimitations for the project are:

- The operation area is 2D static.
- The operation area is a flat, smooth surface containing no moving objects.
- The small and agile intermediate moving outdoor robot is in line of sight of the tag node.

Constraints to take into consideration is time since the project will be conducted over 20 weeks and cost due to the budget of 5000 SEK.

The project will result in evaluating the capability and possibility of inverted multilateration using UWB-ranging.

2.6 Requirements

The requirements that are taken into consideration when designing the localization positioning system are set to meet the customers expectations for the product and to meet the expectations of a ranging and localization system. The requirements are:

- **Range**

The cutting area of the Automower 430X is 3200 m². The range of the positioning system shall therefore be able to cover an area of 59x59m given that the stationary base station is located in the centre.

- **Accuracy**

The accuracy shall be <0.2 m in 95% of the positioning estimates as to be able to develop an adequate path coverage algorithm.

- **Cost**

The components should be consumer grade products and be kept under a total cost of 5000sek.

- **Size**

The localization system shall fit the already existing Automower 430X and not infer structural changes on the pre-existing infrastructure of which the robot is deployed.

2.7 Method

The application used as a small and agile intermediate moving outdoor robot in this project was an Husqvarna Automower 430X. The UWB-modules used were *DecaWave DWM1000*[17] and the microcontroller a *Raspberry Pi 3*[3]. The circuit boards used for connecting the different components were made with a *LPKF ProtoMat E34*[45] at the mechatronics department at the Royal Institute of Technology, in Stockholm, Sweden. The system was designed to fit *Husqvarna Automower 430X*, but the size and portability was taken into consideration so that the system could be used in other applications as well.

The scientific method implemented in this project was a deductive method which started with a state of the art research of technologies and techniques for positioning systems followed by a hypothesis of expected results. Observations of system behavior and performance was conducted and quantitative data were collected. The collected data were then used for a simulation in a robotic operating system (ROS)[4] and in Mathworks MATLAB 2017b[48]. The simulation results were then evaluated and a conclusion was drawn. Scrum was used as a framework for the project with weekly meetings and updates on the progress in the project.

As the work was made by two persons, the individual contributions to this project can be found in Appendix G.

2.8 Ethics

Possible impacts on personal integrity are of biggest concern when developing a positioning system. If the system is capable of tracking an object or person, who will supervise this system and have the rights to access it? If the system is able to map where the tracked object is and where it has been, how should this sensitive

2. Background

information be stored? These are questions that have to be reflected upon. If the system is made sufficiently small it might even be possible to track people unknowingly using small modules attached to the persons themselves. These are all scenarios that should be considered when developing new electronic devices in this field. However, as a research project and as the majority of the work will be focused towards simulation and evaluation, this project will have of low levels of influence in the issues mentioned above and no regard to these problems will be taken.

3

Theory

This chapter contains a theoretical model of a differentially steered system, it introduces relevant technologies for ultra wide-band (UWB) ranging, different techniques for trilateration and filtering methods.

3.1 Rover model

The Husqvarna Automower is a mobile robot propelled by two motors mounted along a single axis. This can be considered to be a *differentially steered system* as the wheels cannot pivot around its axis but the steering is done by adjusting the speed of each wheel individually. The robot have encoders fixed to each wheel and hence an estimated velocity can be calculated. The kinematics of the robot have been modeled in this section without taking into consideration the torque, friction and other physical implications.

A differential drive model estimates its pose by measuring the velocity or distance travelled of the two wheels independently and can be modeled as in Figure 3.1.

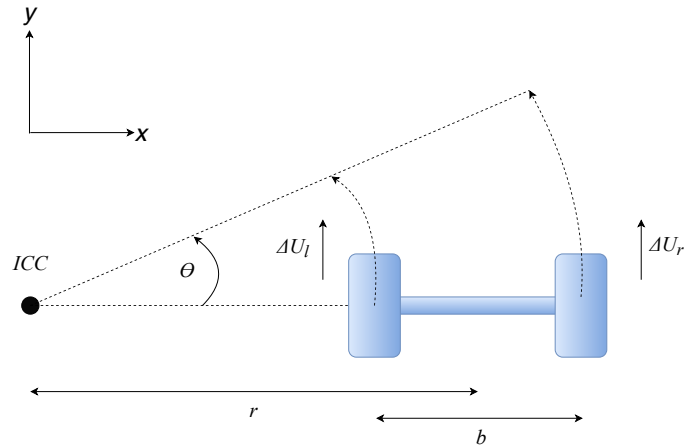


Figure 3.1: Differential drive model.

One way to estimate the rovers pose is to assume that it rotates around a point along the common axis of the wheels, referred to as the instantaneous center of curvature (ICC) [21] in Figure 3.1. By controlling the velocity of the wheels the trajectory and the point of this rotation is varied. This type of estimating the pose of the

3. Theory

robot is a form of dead reckoning, where the new pose is calculated by using the last known position and at the time estimated speed and course. There are however some considerations with this implementation. If the speed of each wheel are equal, $v_l = v_r$, i.e when traveling in a straight line, then the distance to the rotation point ICC becomes infinite and could be somewhat demanding on the Microcontroller Unit (MCU) in terms of floating point operations.

With a sufficient sampling rate a simpler method can be used as proposed by [31]. This method is mainly appropriate for robots with low computing power or when computing power is needed elsewhere which is mainly the case for this project.

By considering the amount of pulse increments of each wheel since the last sample, denoted N_l and N_r for the left and right wheel respectively. The translation from encoder pulses to wheel displacement constant c_m can be described as

$$c_m = \frac{\pi D_n}{C_e} \quad (3.1)$$

where D_n is the wheel diameter and C_e being the encoder resolution. The incremental travel distance for each wheel $\Delta U_l, \Delta U_r$ from Figure 3.1 can then be derived as

$$\Delta U_l = c_m N_l \quad (3.2)$$

$$\Delta U_r = c_m N_r. \quad (3.3)$$

The total incremental distance traveled with regards to the rovers center point ΔU is calculated by using each wheels cumulative change as

$$\Delta U = \frac{\Delta U_l + \Delta U_r}{2}. \quad (3.4)$$

The change of orientation $\Delta\theta$ and relative orientation θ_t at time t is then calculated as

$$\Delta\theta = \frac{\Delta U_r - \Delta U_l}{b} \quad (3.5)$$

$$\theta_t = \theta_{t-1} + \Delta\theta \quad (3.6)$$

with b being the wheelbase as denoted in Figure 3.1.

The estimated position x_t, y_t at time t from the dead reckoning system is then

$$x_t = x_{t-1} + \Delta U \cos \theta_t \quad (3.7)$$

$$y_t = y_{t-1} + \Delta U \sin \theta_t. \quad (3.8)$$

These types of dead reckoning methods always contain errors and inaccuracies, some easier than others to correct. The systematic errors can be easy to predict, such as unequal wheel diameters or incorrect wheelbase. The non-systematic, random

errors are however more difficult to model. These could be wheel slippage because of slippery surfaces or external forces applied to the rover but also instances when the rover travels over uneven terrain [31]. There are several ways of modelling instances that violate the pure rolling constraints that induce stochastic errors such as proposed by [6, 35, 66]. These models however require additional sensors such as torque sensors for each wheel or large datasets of the robot motion to make an accurate statistic model. This is considered outside the scope of this project as it is assumed that the rover moves over a relatively flat surface and the goal ultimately is to evaluate the possibility to use multilateration in this reversed fashion as proposed. Instead, in the simulation environment a Poisson distributed error is induced on each of the two encoders of the rover to simulate stochastic events to infer large errors on the readings. All of these errors makes the dead reckoning model inadequate as an exclusive positioning system. However it makes up a prediction of how the rover could be moving and is used to improve the proposed positioning system.

3.2 Radio

Radio communication use radio waves to transfer information. By modulating electromagnetic energy waves it is possible to wirelessly send large amounts of data. Different technologies are operating at different frequency spans and have various capacity and bandwidth. There is a relationship between capacity and bandwidth, according to the Shannon-Hartley theorem [59], the capacity can be calculated by

$$C = B \cdot \log_2 \left(1 + \frac{S}{N} \right) \quad (3.9)$$

with C being the capacity in bits/second, B the bandwidth, S the signal power and N being the noise. The $\frac{S}{N}$ component in the logarithm is usually referred to as the Signal to Noise Ratio (SNR). It can be observed in Equation (3.9) that increasing the bandwidth will impact the capacity more than increasing the SNR indicating one of the many perks of the ultra wide-band technology.

An ultra wide-band transmitter is defined by the Federal Communications Commission as a device that radiates a signal with a fractional bandwidth B_{frac} greater than 0.2 as defined in Equation (3.10) with f_h and f_l being the highest and lowest frequencies transmitted or transmitting with a bandwidth of at least 500 MHz at all times[9].

$$B_{frac} = \frac{2(f_h - f_l)}{f_h + f_l}. \quad (3.10)$$

The usable frequency range spans 3.1 GHz to 10.6 GHz and varies due to national regulations. This large bandwidth has realized very fast data transmission as according to the Shannon-Hartley theorem in Equation (3.9) with speeds up to >100 Mbit/s. It also has the ability to make use of a very fine time resolution due to the high data rates which can be used in applications such as localization.

3. Theory

This large bandwidth has a tendency to disturb existing wireless narrow-band communications so the signal power of the UWB application has to be considered. That is why commercial use of UWB communication has to follow strict limits regulating the total transmitted power to 0.56 mW, or a limit of -41.3 dBm/MHz for the 3.1 to 10.6 GHz frequency range [57]. A power spectral density graph of how UWB is compared to some of the commercially available radio technologies can be seen in Figure 3.2. Due to the power limitations, the range of applicable positioning systems have been shown to drop rapidly after ~ 100 meters [14, 37, 34].

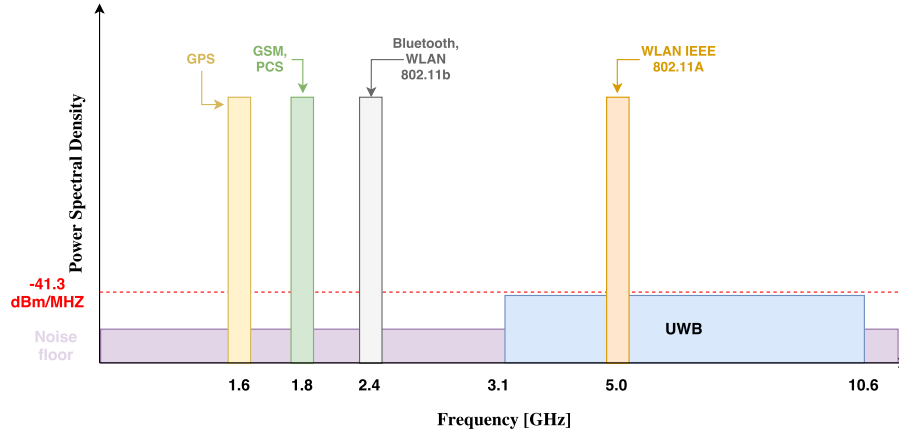


Figure 3.2: Frequency chart of UWB compared to other radio communication protocols [49].

Impulse Radio Ultra Wide-Band (IR-UWB) is used to exploit the possibilities of UWB while meeting the emission regulations. The impulse radio transmit data with pulses (a very short Gaussian pulse with a large bandwidth hence the name *impulse* radio), usually in the order of a fraction of a nanoseconds. Information is commonly sent using a time-hopping impulse radio signal, see Figure 3.3 where one pulse is sent in each frame (T_f).

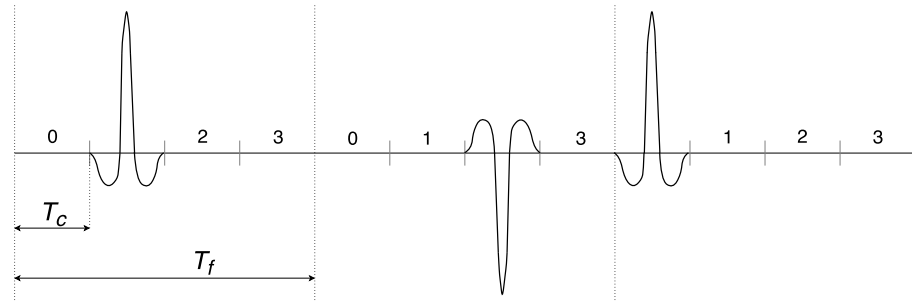


Figure 3.3: IR-UWB signal example.

The frame is divided into parts, chip-intervals (T_c) that resides in the frame. To decrease risk of interference of different UWB systems a time-hopping code is usually used as to denote at which T_c the signal is read. Information of the bit symbol can be sent either by the position within the frame or as polarity of the signal. As for the example in Figure 3.3 the polarity of the signal specifies the symbol of the bit. With

a time-hopping code of {1,2,0} the stream can be interpreted as 101. This method is called time-hopping binary phase-shift keying and is a robust way of sending data through IR signals. There are more methods to convey messages in terms of sending several consecutive signals to retrieve one bit or using the position of the signal within the timeframe to determine the symbol of the bit sent [79]. Most of the consumer grade IR-UWB devices do not use a carrier wave, which implies that it can be manufactured inexpensively and broadcasted from simpler components, further decreasing the complexity of the system [73]. There are also other UWB devices that utilize this kind of time-hopping on to a carrier frequency, such as the DecaWave DWM1000. In this fashion it is possible to increase the propagation robustness of the radio signal [18].

3.3 Ranging methods

There are two main ranging categories. The first one is Received Signal Strength (RSS) which measure the strength of the received signal. The strength of a signal propagated through a medium is decreased by its Path Loss (PL) which in an ideal case is proportional to the distance between the transmitter and receiver. The received power $\bar{P}(d)$ at a distance d is given by

$$\bar{P}(d) = P_0 - 10n \cdot \log_{10} \left(\frac{d}{d_0} \right) \quad (3.11)$$

where P_0 is the received power at the reference distance d_0 and n is the PL exponent [79]. RSS is one of the simplest distance measuring approaches in theory but there are several things that affect the PL making this method difficult to implement. The distance estimation algorithm needs to consider multi-path phenomena where the signal propagates and is diffracted on obstacles along the path from the transmitter to the receiver. Another difficulty is noise when the signal is sent over longer distances.

The second ranging category is Time of Flight (ToF) which measures the time it takes for the signal to travel from the transmitter to the receiver. The messages sent between nodes contains time-stamps of when the message was sent. ToF is multiplied with the speed of light $c \approx 3 \times 10^8$ m/s to acquire the distance between transmitter and receiver. There are several methods to calculate ToF, one is Time of Arrival (ToA) which simply subtract the time of when the message was sent, t_{sent} from the time the message was received, $t_{arrival}$ as in Equation (3.12).

$$ToF = t_{arrival} - t_{sent}. \quad (3.12)$$

This seems straightforward, but ToA requires synchronized clocks for both the transmitter and receiver nodes which will increase the complexity of the system.

Time Difference of Arrival (TDoA) is another subcategory of ToF that uses two or more base stations and one tracking node to estimate the position by calculating the time difference of arrival between the base stations using the same calculations as in

ToA. The benefit of using TDoA is that synchronization is only needed for the base stations which facilitate the implementation compared to ToA. The calculation of ToA for each node will include a timing offset since the base stations and the target node are not synchronized, this timing offset will be the same in TDoA for every estimation since the base stations are synchronized [24]. The calculation defines a hyperbola with a foci at the position of the target node. This can be seen in Figure 3.4.

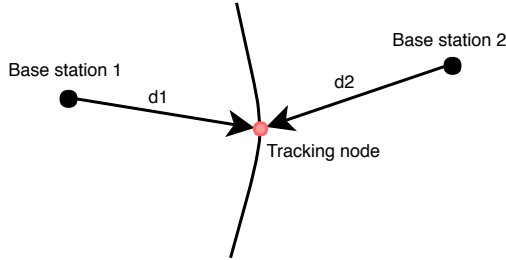


Figure 3.4: Foci of hyperbola from measurements using TDoA.

Precise time-stampings are crucial for incoming and outgoing messages for both of these ToF categories since the velocity of radio waves are $\approx 3 \times 10^8$ m/s. A time-stamp error in the order of a nano-second will result in a positioning error of ≈ 0.3 m. Synchronization of clocks with this precision are often not possible for consumer electronics as it usually require high precision clocks or intricate synchronization methods. To resolve this a Two-Way Ranging method can be used.

3.3.1 Two-Way Ranging

The difference between ToA, TDoA and Two-Way Ranging (TWR) is that TWR does not require synchronized clocks. In Figure 3.5 three TWR methods are shown graphically. These TWR methods are Symmetrical-Double-Sided Two-Way Ranging (SDS-TWR, Figure 3.5a), Asymmetrical-Double-Sided Two-Way (ADS-TWR, Figure 3.5b) and Double Two-Way Ranging (D-TWR, Figure 3.5c). Just as in ToA and TDoA the ToF between two nodes are estimated in TWR.

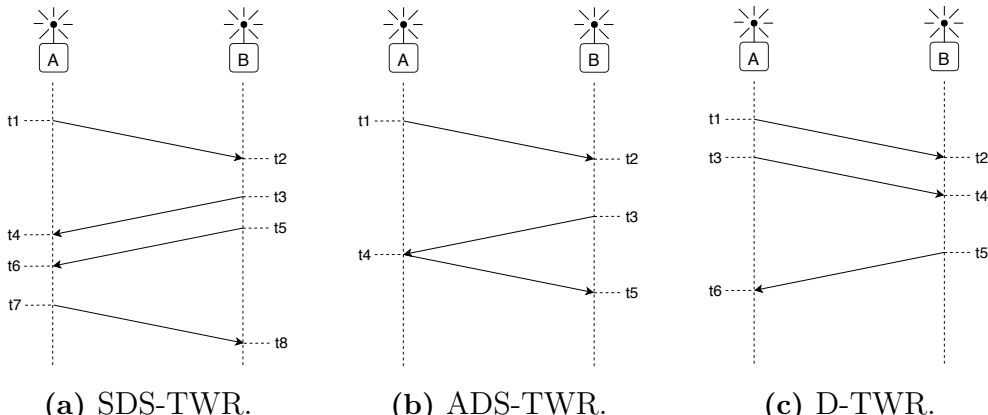


Figure 3.5: Different two-way ranging methods.

The ranging process of SDS-TWR is shown in Figure 3.5a. This method sends four messages to estimate the ToF. The first process is initialized from device A at time t_1 and the second process is initialized from device B at time t_5 . ToF for SDS-TWR is calculated with [56]:

$$ToF_{SDS-TWR} = \frac{(t_4 - t_1) - (t_3 - t_2) + (t_8 - t_5) - (t_7 - t_4)}{4} \quad (3.13)$$

where $t_i, i = 1, 2, \dots, 8$ are the time-stamps of when the signal is sent and received. There are disadvantages with SDS-TWR such as decreased measurement frequency due to that four messages that are sent and it is difficult to accomplish true symmetry since the ranging processes are done in software. The maximal error in ToF for SDS-TWR is given in [56] as

$$\varepsilon_{SDS-TWR} = \frac{1}{2}t_{ToF}(e_A + e_B) + \frac{1}{4}(e_A - e_B)((t_7 - t_4) - (t_3 - t_2)) \quad (3.14)$$

where e_A and e_B are the clock drift in parts per million (10^{-6}) of a second for node A and B respectively and t_i is the time-stamps.

The ADS-TWR will transmit a message to node B when it receives the message from node B at t_4 (shown in Figure 3.5b). The ToF for ADS-TWR is [56] as follows:

$$ToF_{ADS-TWR} = \frac{(t_4 - t_1) - (t_5 - t_3)] + [(t_3 - t_2)}{4} \quad (3.15)$$

The assumption of immediate reply is not achievable since device A will process the received data from node B before sending a message. The maximal error in ToF for ADS-TWR [56] is:

$$\varepsilon_{ADS-TWR} = \frac{1}{4}(t_3 - t_2)(e_A + e_B) \quad (3.16)$$

D-TWR is a ranging method that can be used to decrease run time and has the corresponding precision as SDS-TWR. Device A initiates the process and instead of waiting for a reply from node B, A will send a second message and the calculation for ToF is therefore given by [56]:

$$ToF_{D-TWR} = \frac{2(t_6 - t_5) - t_3 + t_4 - t_1 + t_2}{4} \quad (3.17)$$

and the maximal error is given by Equation (3.18), it can thus be seen that the error does not depend on the clock error of B. This method can therefore be used when low cost is an important factor.

$$\varepsilon_{D-TWR} = t_{ToF}e_A \quad (3.18)$$

A comparison between the different TWR methods were performed by [56], using the same hardware for all tests, the result of the test can be found in Table 3.1.

The conclusion is that the ADS-TWR has the smallest max error. Of the introduced ranging methods, RSS indicates least promising precision while both TDoA and ToA are superior to TWR. However, of the found UWB modules in this project's price range the DWM1000 from DecaWave showed best performance of them all. This

Table 3.1: Results from various protocols.

	SDS-TWR	ADS-TWR	D-TWR
Mean Error [m]	0.00	0.00	0.00
Max Error [m]	4.78	2.50	16.6
Standard Deviation [m]	0.07	0.08	0.16
95 Percentile $p_{95}[\text{m}]$	0.07	0.07	0.08
Robustness [%]	99.8	99.8	99.9

device does as of today not have a clock synchronization feature as to why the chosen method to derive a range between base station and tracking node is ADS-TWR.

3.4 Positioning techniques

Lateration or multilateration is used to calculate the position of an object using the distance to multiple stationary ground references. How the distances are estimated is discussed in section 3.3.1.

Equation (3.19) is used to estimate the position of the tracking node relative the base stations [11]. In the ideal case there will be exactly one point where the distance from each base station will intersect each other. This is usually not the case since there is always noise and fluctuations in the system. The circles intersection tend to construct an area which will contain the position of the tag node as demonstrated in Figure 3.6a and 3.6b. The radius of the circles can be described using Equation (3.19).

$$r_i = \sqrt{(x - x_i)^2 + (y - y_i)^2}, \quad i = 1, 2, \dots, n \quad (3.19)$$

were x, y are the coordinates of the tag node, denoted x in Figure 3.6 and x_i, y_i are the coordinates of the base stations.

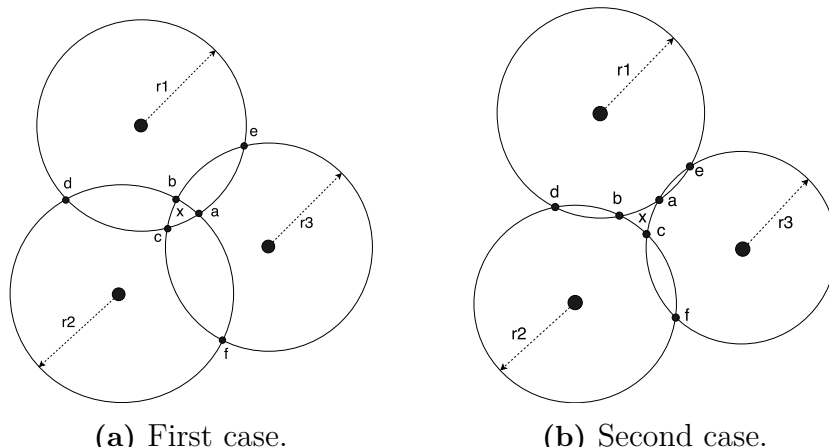


Figure 3.6: Two cases a and b for the geometric algorithm.

Note that not all intersections are relevant, this can be seen in Figure 3.6. The relevant intersections a, b and c can be determined by the geometrical properties of the system.

The UWB setup for the small and agile intermediate moving outdoor robot will be a type of reversed multilateration, meaning only one stationary base station will be used denoted as *tracking node* and four mobile anchor nodes placed on the robot. The reversed multilateration will use the same Equation (3.19) as the traditional multilateration. The base station will however always be placed outside the area covered by the anchor nodes as in Figure 3.7. In [41] the variance of the position estimate was evaluated depending on where the tracking node was located relative the anchor nodes. The ranging method used was ToA with synchronized anchors and tracking node. The results shows that the variance is 3-5 times larger outside the area covered by the anchor nodes which will always be the case in reversed multilateration meaning that the variance can be expected to be larger in this setup than the classical method.

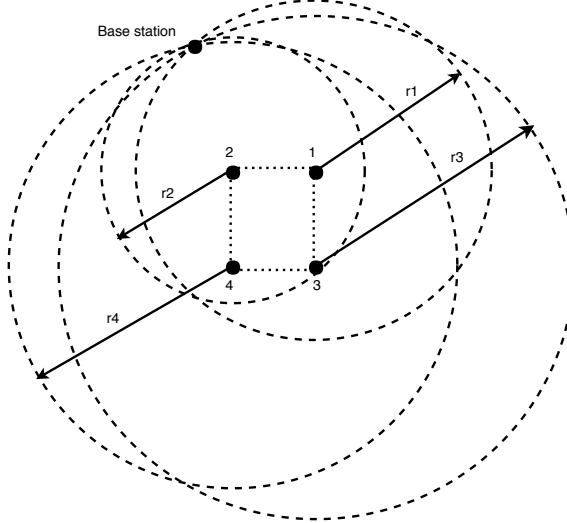


Figure 3.7: Multilateration case for the rover.

3.4.1 Linear Least squares and Non-linear least square

If the geometric algorithm (3.19) is linearized the Linear Least Squares (LLS) method can be used to solve the set of equations (r_1, r_2, \dots, r_n) as to derive the position of the tracking node in coordinates x, y and in the same time minimizing the residual error the ranging noise infers. If the n^{th} equation in the set of geometric algorithms is subtracted from r_1, r_2, \dots, r_{n-1} the equation is linearized [61], this gives

$$r_i^2 - r_n^2 = (x - x_i)^2 + (y - y_i)^2 - (x - x_n)^2 + (y - y_n)^2. \quad (3.20)$$

If expanded, the quadratic terms of x and y will be negated which after rearranging gives the equation:

$$\frac{1}{2}[r_n^2 + x_i^2 + x_n^2 - r_i^2 - x_n^2 - y_n^2] = (x_i - x_n)x + (y_i - y_n)y. \quad (3.21)$$

3. Theory

The linear system of equations on matrix form can be written as

$$\mathbf{Ax} = \mathbf{b} \quad (3.22)$$

were

$$\mathbf{A} = \begin{bmatrix} x_1 - x_n & y_1 - y_n \\ x_2 - x_n & y_2 - y_n \\ \vdots & \vdots \\ x_{n-1} - x_n & y_{n-1} - y_n \end{bmatrix}, \quad \mathbf{x} = \begin{bmatrix} x \\ y \end{bmatrix} \quad (3.23)$$

and

$$\mathbf{b} = \frac{1}{2} \begin{bmatrix} r_n^2 + x_1^2 + y_n^2 - r_1^2 - x_n^2 - y_n^2 \\ r_n^2 + x_2^2 + y_n^2 - r_2^2 - x_n^2 - y_n^2 \\ \vdots \\ r_n^2 + x_{n-1}^2 + y_n^2 - r_{n-1}^2 - x_{n-1}^2 - y_{n-1}^2 \end{bmatrix}. \quad (3.24)$$

If the unknowns are equal to the number of equations, the solution to the Equation (3.22) becomes:

$$\mathbf{x} = \mathbf{A}^{-1}\mathbf{b}. \quad (3.25)$$

If the system is overdetermined i.e. more equations than unknowns, the inverse of \mathbf{A} does not exist, but it is still possible to find a solution. This is done by solving the pseudo-inverse in Equation (3.26).

$$\mathbf{x} = (\mathbf{A}^T\mathbf{A})^{-1}\mathbf{A}^T\mathbf{b}. \quad (3.26)$$

When the linearization is done one measured range is lost which is sometimes undesirable. An option to LLS is Non-Linear Least Squares (NLLS) where there is no need for linearization. The error that is being minimized is the error between the actual distance \hat{r}_i and the measured distance r_i . This is achieved using Equation (3.19) and subtracting the real distance from the measured distance:

$$f_i(x, y) = r_i - \hat{r}_i = \sqrt{(x - x_i)^2 + (y - y_i)^2} - \hat{r}_i, \quad i = 1, 2, \dots, n \quad (3.27)$$

The sum of all square errors is the function that is being minimized:

$$F_i(x, y) = \sum_{i=1}^n (r_i(k) - \hat{r}_i)^2 = \sum_{i=1}^n f_i(x, y)^2. \quad (3.28)$$

Newton iteration is used as the algorithm for minimizing the square error [61]. The Jacobian in Equation (3.29) for the set of equations is determined from partial differentiating Equation (3.28) with respect to x and y . The vector \mathbf{f} and \mathbf{r} are introduced as:

$$\mathbf{J} = 2 \begin{bmatrix} \frac{\partial f_1}{\partial x} & \frac{\partial f_1}{\partial y} \\ \frac{\partial f_2}{\partial x} & \frac{\partial f_2}{\partial y} \\ \vdots & \vdots \\ \frac{\partial f_n}{\partial x} & \frac{\partial f_n}{\partial y} \end{bmatrix}, \quad \mathbf{f} = \begin{bmatrix} f_1 \\ f_2 \\ \vdots \\ f_n \end{bmatrix}, \quad \mathbf{r} = \begin{bmatrix} x \\ y \end{bmatrix}. \quad (3.29)$$

Newton iteration gives [61],

$$\mathbf{r}_{k+1} = \mathbf{r}_k - (\mathbf{J}_k^T \mathbf{J}_k)^{-1} \mathbf{J}_k^T \mathbf{f}_k. \quad (3.30)$$

where \mathbf{r}_{k+1} is the current position, \mathbf{r}_k the last approximated position. An estimated guess of the initial position can be obtained by using LLS. Since this is a iterative process the algorithm will terminate when the difference between the k and $k + 1$ iteration converges to an acceptable value.

3.5 Filtering

The position estimated by the techniques introduced in section 3.4 will contain noise and erroneous data that result in unsatisfactory positioning if not filtered properly. The accuracy of the estimated position is highly dependent on treatment of the signal and thus this has to be designed with much thought. Pose approximation using methods like LLS can be filtered with simple means such as moving average or exponential smoothing. Another approach is to use something like a Kalman filter, a recursive filter that is capable of solving the least squares problem which effectively accounts for the sensor and process noises in the system.

3.5.1 Discrete Kalman filter

A Kalman filter is a Bayesian estimator, a probabilistic approach which is composed by a group of mathematical operations to minimize the mean square error of a linear problem. It is an estimation algorithm most commonly used to estimate a state of the system by making use of uncertain and indirect measurements. Given that the noise and disturbance of the process and measurements are Gaussian the Kalman filter can be considered an optimal estimator as it accounts for properties of the Gaussian uncertainties in the signals. It is a recursive process which means that new measurements are processed when they arrive which can further improve the estimations [64].

The Kalman process is described in Figure 3.8. The iterative process is composed by two steps, a prediction phase and one update phase. The *prediction phase* predicts what the next state will be based on the previous state and eventual command inputs. This is then compared to a generally noisy measurement in the *update phase* to correct the prediction made earlier. Depending on how trustworthy the measurement and prediction is the state is updated. From this it is then possible to make an adequate estimation of the state, the process is then repeated with a new prediction of the next state and so forth.

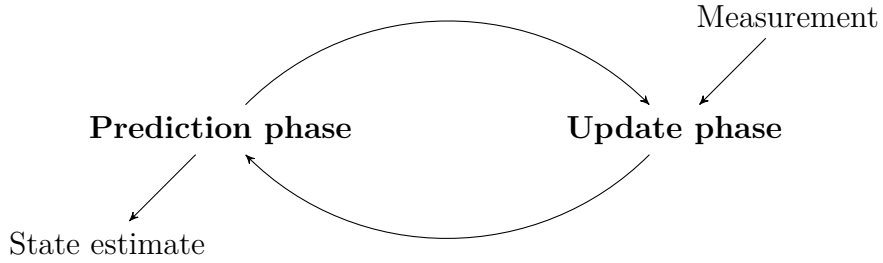


Figure 3.8: Kalman phases.

A dynamic model which changes over time assumes that a new state linearly relates to the previous state and any eventual inputs to the system. The equation for the process can then be described as

$$\mathbf{x}_k = \mathbf{F}\mathbf{x}_{k-1} + \mathbf{B}\mathbf{u}_{k-1} + \mathbf{w}_{k-1}, \quad \mathbf{w}_{k-1} \sim \mathcal{N}(0, \mathbf{Q}_{k-1}) \quad (3.31)$$

where the state at time k is depicted as \mathbf{x}_k , \mathbf{F} is the transition matrix from the previous state, the control model \mathbf{B} represent the effects of each input from the control input \mathbf{u}_{k-1} and the process noise \mathbf{w}_{k-1} is assumed to be white Gaussian noise with zero mean and covariance \mathbf{Q}_{k-1} .

The measurements of the system are an observation of the current state but also inflicted by measurement noise

$$\mathbf{z}_k = \mathbf{H}\mathbf{x}_k + \mathbf{v}_k, \quad \mathbf{v}_k \sim \mathcal{N}(0, \mathbf{R}_k) \quad (3.32)$$

where \mathbf{z}_k is the set of observations made at time k , \mathbf{H} the matrix that maps the true state to the observed state and \mathbf{v}_k is the measurement noise and similar to the process noise, assumed to be zero mean white Gaussian noise with the covariance \mathbf{R}_k .

To be noted is that the Kalman filter provides an estimate of the state at time k , $\hat{\mathbf{x}}_k$, by making use of the models of the inherently noisy system- and measurement models. As the noise is assumed Gaussian the system- and measurement models can be described by their variance and mean parameters. One can say that the Kalman filter outputs two important parameters

- The updated, *a posteriori* state estimate $\hat{\mathbf{x}}_k$ given the measurement \mathbf{z}_k and old state $\hat{\mathbf{x}}_{k-1}$
- The updated, *a posteriori* error covariance matrix \mathbf{P}_k indicating how accurate the state estimate $\hat{\mathbf{x}}_k$ is

Looking back at the Kalman phases in Figure 3.8, the prediction phase performs two operations. It calculates the predicted *a priori* state $\hat{\mathbf{x}}_k^-$ and the *a priori* estimate covariance \mathbf{P}_k^-

$$\hat{\mathbf{x}}_k^- = \mathbf{F}\hat{\mathbf{x}}_{k-1} + \mathbf{B}\mathbf{u}_k \quad (3.33)$$

$$\mathbf{P}_k^- = \mathbf{F}\mathbf{P}_{k-1}^-\mathbf{F}^T + \mathbf{Q}_k. \quad (3.34)$$

In the update phase, the measurements from the system are taken into account and a Kalman gain is calculated as to define how much the new information of the state can be trusted

$$\mathbf{y}_k = \mathbf{z}_k - \mathbf{H}\hat{\mathbf{x}}_k^- \quad (3.35)$$

$$\mathbf{S}_k = \mathbf{H}\mathbf{P}_k^-\mathbf{H}^T + \mathbf{R}_k \quad (3.36)$$

$$\mathbf{K}_k = \mathbf{P}_k^-\mathbf{H}^T\mathbf{S}_k^{-1} \quad (3.37)$$

$$\hat{\mathbf{x}}_k = \hat{\mathbf{x}}_k^- + \mathbf{K}_k\mathbf{y}_k \quad (3.38)$$

$$\mathbf{P}_k = (\mathbf{I} - \mathbf{K}_k\mathbf{H})\mathbf{P}_k^- \quad (3.39)$$

where \mathbf{y}_k is the innovation matrix; the difference between the predicted state and the measured state. \mathbf{S}_k the innovation covariance, which depicts how trustworthy the innovation is. \mathbf{K}_k the Kalman gain as explained above. The result of the Kalman filter is a new state estimate that is somewhere in between the predicted state and the measured state with a lower uncertainty than any of the states alone[22, 64].

As mentioned, the Kalman filter is a linear estimator. As a Bayesian filter, one of the key exploits of the filter is that the product of two Gaussian functions is another Gaussian. This does not hold for a non-linear function and thus the Gaussian covariance matrices would not behave as expected. If the process is of non-linear behavior it needs to be linearized if the regular Kalman filter is to be applied. This is known as the Extended Kalman Filter (EKF) [64] where the process is linearized around an operating point through a Taylor expansion to be able to apply the regular Kalman process.

The general equations for this model is expressed as

$$\mathbf{x}_k = \mathbf{f}(\mathbf{x}_{k-1}, \mathbf{u}_{k-1}, \mathbf{w}_{k-1}) \quad (3.40)$$

$$\mathbf{z}_k = \mathbf{h}(\mathbf{x}_k, \mathbf{v}_k). \quad (3.41)$$

With the same annotation as the standard kalman filter where the noise \mathbf{w}, \mathbf{v} is represented by the covariance matrices \mathbf{Q}, \mathbf{R} respectively.

To be able to apply the regular Kalman filter, each non-linear function is linearized around a specific point and can be approximated as

$$\mathbf{x}_k \approx \tilde{\mathbf{x}}_{k-1} + \mathbf{A}(\mathbf{x}_{k-1} - \tilde{\mathbf{x}}_{k-1}) + \mathbf{w}_k \quad (3.42)$$

$$\mathbf{z}_k \approx \tilde{\mathbf{z}}_k + \mathbf{H}(\mathbf{x}_k - \tilde{\mathbf{x}}_k) + \mathbf{v}_k. \quad (3.43)$$

Where the state vector $\tilde{\mathbf{x}}$ and measurement vector $\tilde{\mathbf{z}}$ are approximated without using their respective noise as

$$\tilde{\mathbf{x}}_k = \mathbf{f}(\tilde{\mathbf{x}}_{k-1}, \mathbf{u}_k, \mathbf{0}) \quad (3.44)$$

$$\tilde{\mathbf{z}}_k = \mathbf{h}(\tilde{\mathbf{x}}_k, \mathbf{0}). \quad (3.45)$$

Here the observed measurements and actual state are once again represented as \mathbf{z}_k and \mathbf{x}_k . \mathbf{H} and \mathbf{A} are the Jacobian matrices of the functions \mathbf{h} and \mathbf{f} defined as

$$\mathbf{A}_{[i,j]} = \frac{\partial \mathbf{f}_{[i]}}{\partial \mathbf{x}_{[j]}}(\tilde{\mathbf{x}}_{k-1}, \mathbf{u}_{k-1}, \mathbf{0}) \quad (3.46)$$

$$\mathbf{H}_{[i,j]} = \frac{\partial \mathbf{h}_{[i]}}{\partial \mathbf{x}_{[j]}}(\tilde{\mathbf{x}}_k, \mathbf{0}). \quad (3.47)$$

With these definitions it is possible to linearize the process and measurement models hence be able to apply the Kalman filter introduced earlier. The process of doing so for this specific multilateration problem is specified in section 4.5.1.

There are also other variants of Kalman filters such as the unscented Kalman filter (UKF) [69] which samples the non-linear functions at strategically chosen points to create a Gaussian from that. This can then be used on the motion and measurement models. The UKF has the benefit of making a better approximation of the state as it is able to capture the *3rd* order Taylor approximation in contrast to the extended that approximates the state using the *1st* order. All with the same computational complexity [69] which should deem the UKF a superior solution. The unscented transformation is used to calculate *sigma points* to sample the non-linear functions and in that fashion better capture the posterior mean pose and covariance matrices instead of linearizing around the mean as EKF does. The theory of the applied unscented Kalman filter in this thesis can be found in appendix A.

Other non-linear state estimators can also be used when the problem is not linear. They are more complex and computationally more intensive [69], such as Monte Carlo particle filters, globally iterated Kalman filtering and moving horizon estimation. Generally speaking these techniques are not ample for small MCUs and are thus not within the scope of this project.

3.6 Performance evaluation

The performance of the positioning system was evaluated using three measurements. These three are:

- Mean error in position, which is the average euclidean error of the position estimate.
- Position error as a cumulative distributed function where the position estimate could be described as a radius of a circle of which the rover is located in with a probability of 95%.
- Standard deviation for the position estimate error.

The positioning error for coordinates x and y of every sample is expressed as

$$\varepsilon_x = x_{actual} - x_{estimate} \quad (3.48)$$

$$\varepsilon_y = y_{actual} - y_{estimate} \quad (3.49)$$

Where x_{actual} and y_{actual} are the true coordinates of the rover at the given sample. $x_{estimate}$ and $y_{estimate}$ is the estimated position of the rover at the same instance. The euclidean distance error at sample i is

$$\varepsilon_{x,y,[i]} = \sqrt{\varepsilon_{x,[i]}^2 + \varepsilon_{y,[i]}^2} \quad (3.50)$$

The average error is described as

$$\varepsilon_{average} = \frac{\sum_{i=1}^n \varepsilon_{x,y,[i]}}{n} \quad (3.51)$$

where n is the number of sampled points.

The cumulative distribution of the position error can be graphically explained by Figure 3.9. The circle represent an cumulative distribution where 95% of the samples are within the radius of 0.5m.

The standard deviation σ is presented as to give a measurement of how the error deviates from the mean error.

3.7 Reference frame

As the transceivers on the rover are used as reference and *static* anchors, the position retrieved (x'_k, y'_k) is the position of the base station in a coordinate system relative to the rover, depicted in Figure 3.10.

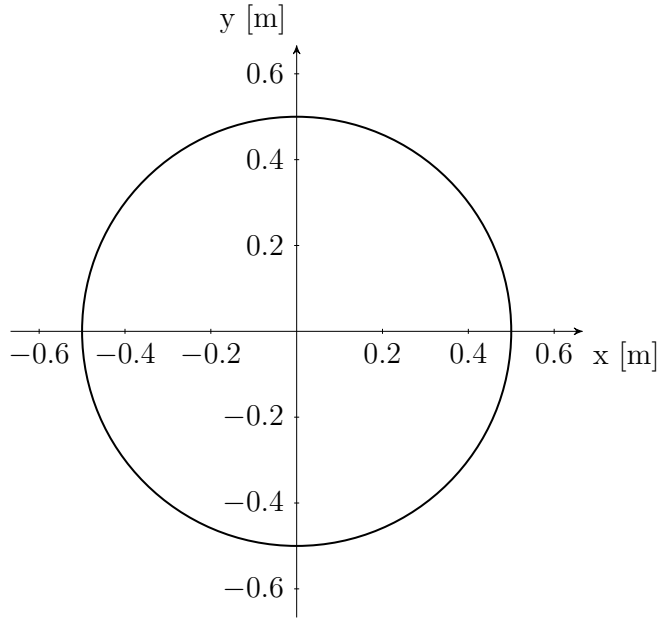


Figure 3.9: Graphic representation of the error.

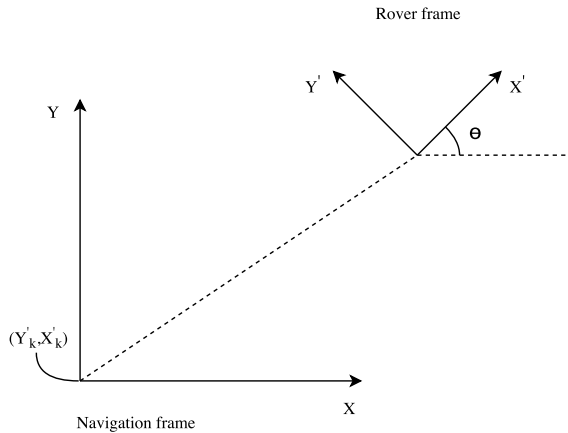


Figure 3.10: Navigation frame and rover frame.

The navigation frame is used to represent the final results of the positioning system in coordinates (x, y) . The position retrieved however is in the rover frame with coordinates (x'_k, y'_k) in the Figure 3.10. To rotate these coordinates in the navigation frame, the yaw of the rover relative to the navigation frame θ is required. The rover frame $\mathbf{p}' = [x', y']^T$ can be represented in the navigation frame $\mathbf{p} = [x, y]^T$ using the rotational matrix Γ as in Equation (3.52).

$$\mathbf{p} = \mathbf{p}'\Gamma \quad (3.52)$$

where the rotational matrix Γ is

$$\Gamma = \begin{bmatrix} \cos \theta & \sin \theta \\ -\sin \theta & \cos \theta \end{bmatrix} \quad (3.53)$$

3.8 Orientation angle

The orientation angle or yaw is an important variable in this project due to the need of rotation of the rovers frame as stated in the previous section 3.7.

If the ranging precision is in the order of 0.1 m the error induced by the rotational matrix can be no greater than 0.1 m to stay within the requirements of 0.2 m. And thus at a range of ≈ 40 m which is defined as the scope of this project the yaw error can be no larger than 0.143° as the error propagated through the rotational matrix at that range would infer errors larger than 0.1 m.

It is possible to make use of the UWB system to calculate the yaw of the rover by using the measured distances. However, a single base station node is not sufficient to derive the yaw angle since the measured distances from the nodes to the base station can be identical in infinite occasions around a circle of the base station. Different cases of this are shown in Figure 3.11a where it is impossible to derive in which of the positions the rover is located since the measurements from each node to the base station is equal. A solution to this problem would be to place an additional node on the base station which will give the system geometrical properties to derive the yaw angle of the rover. A Figure of how this would be implemented is shown in Figure 3.11b and calculations of how to derive the yaw angle can be found in appendix C. A solution with two base station nodes will require a case solution to determine which of the nodes on the rover to use for calculation of the angle.

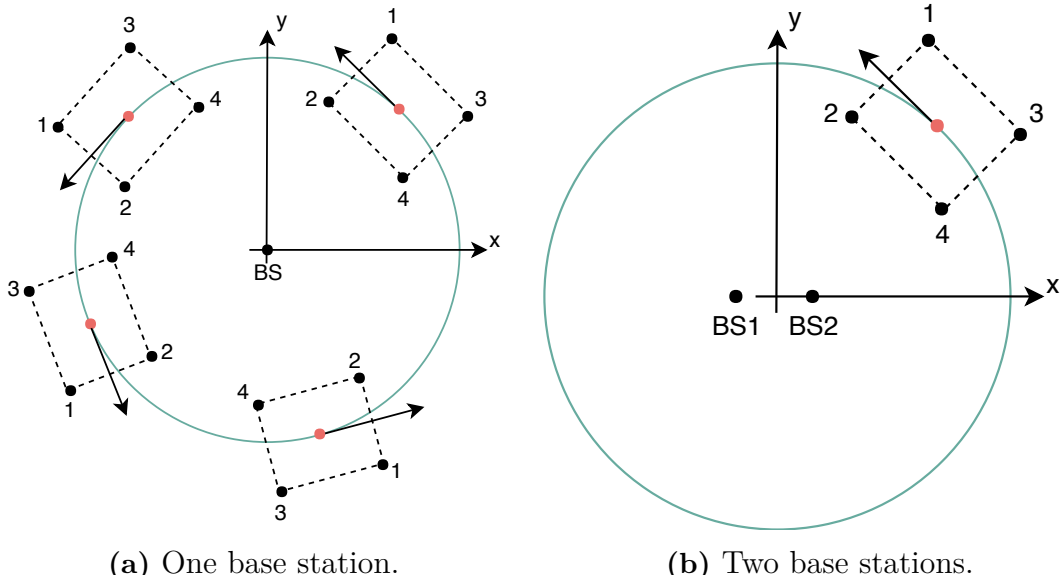


Figure 3.11: Two cases for the geometric algorithm, a and b.

The manufacturer of the DW1000 module state that the precision in ranging measurements are ± 0.10 m. The derived Equation (C.7) from appendix C is used to calculate the maximal error in yaw. The angle α in Figure 3.12 is the yaw angle and is equal to the sum of ϕ , ϕ_1 and ϕ_2 . As can be seen this angle sum will increase

3. Theory

rapidly if the measurements of r_1, r_2 and r_3 has an error $\pm 0.10\text{m}$. Calculations were made to estimate how the error in yaw will vary depending on the error in ranging for ε_{r_1} and $\varepsilon_{r_2}, \varepsilon_{r_3}$ the estimation can be seen in Figure 3.13

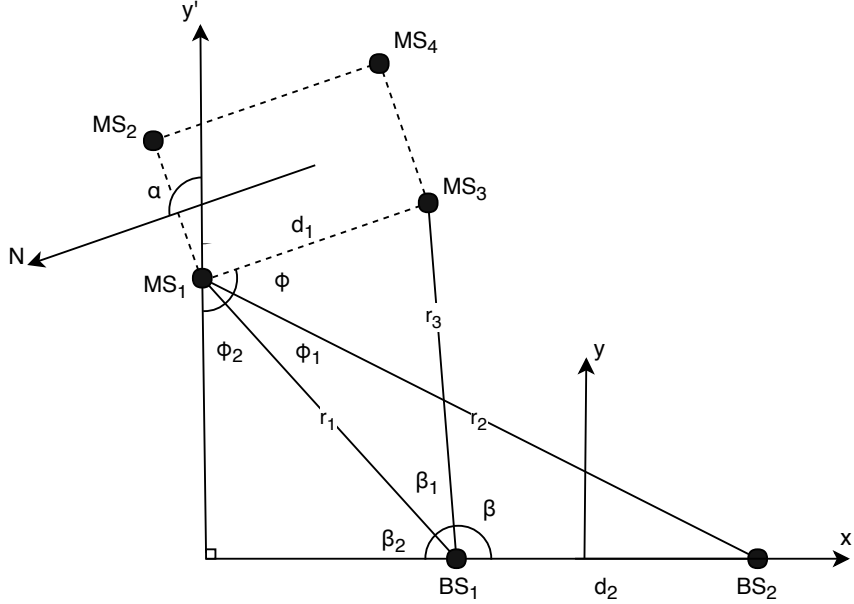


Figure 3.12: Geometry used to solve the orientation angle.

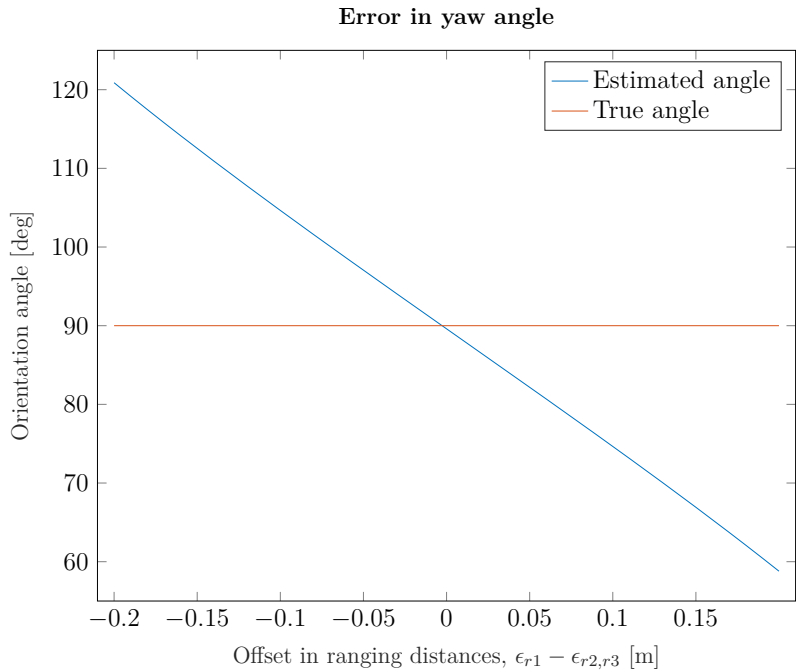


Figure 3.13: Navigation frame & rover frame.

Considering the yaw error in Figure 3.13, the measured UWB-ranges are not suitable to use for calculating the yaw angle since the error quickly exceeds the limit of 0.143° .

A measurement error of 0.05 m would induce a yaw error of 10° . An additional solution would be to use a digital compass. As pose estimation of the robot is relative the base station the important factor of the compass is not the accuracy with regards to the true cardinal direction but rather the repeatability and resolution of the measured or calculated yaw angle. An example of a compass that fulfills these conditions and that would be suitable for this project is the *HMR3200* from Honeywell [2]. This compass has a typical repeatability of 0.1° and a resolution of 0.1° .

3. Theory

4

Unit tests & Simulation

The chapter reviews implementation details as well as evaluation of the introduced positioning techniques. Also some configurations and tests of the proposed topology of ultra wide-band (UWB) ranging anchors. The hardware presented in this section are the appliances needed for unit tests of the UWB-modules.

4.1 Micro controllers

The chosen Microcontroller Unit used for processing and collecting data was a Raspberry Pi 3 (RPi) [3], see Figure 4.1. This small unit has a high clock frequency of 1.2 GHz and a WiFi module for sending data to a laptop computer for further analysis which makes it a good candidate for this project. This was used to read the Serial Peripheral Interface (SPI) bus from the *UWB anchors* and collect the ranging data.

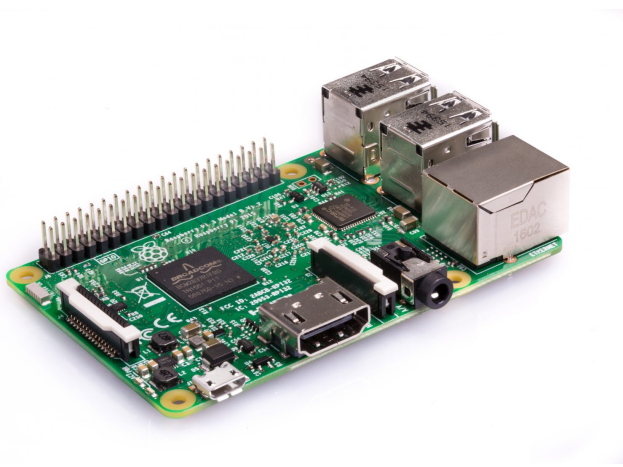


Figure 4.1: Raspberry Pi 3.

An Arduino Mini PRO 3.3V (see Figure 4.2) was chosen to run the *UWB-tag* protocol. The Arduino Mini PRO has a clock frequency of 8 MHz



Figure 4.2: Arduino Mini Pro 3.3V.

Since the unit tests was performed outdoors the 18V battery from the Automover was used in collaboration with a 5 volt step down regulator to power the RPi and a 3.3 V regulator was used to power the UWB anchors. The Arduino Mini PRO was powered by a 5V battery with a 3.3V step down regulator. The schematics and circuit boards can be seen in appendix F.

4.2 DWM1000

The UWB-modules used for ranging was the DecaWave DWM1000 [1] transceiver seen in Figure 4.3. This small module has proven to be accurate as discussed in chapter 2 and also a low cost option as fit for this application.



Figure 4.3: DecaWave DWM1000 module.

The transceivers used in this project had to be adjusted and calibrated for its application. As in this specific case, the modules was set up with the focus as a medium range Real-Time Locating System (RTLS) discussed further in the next section.

4.2.1 Operational design

The DW1000 chip has some operational settings that are stored in its internal memory, such as frame data rate, preamble length, channel selection and Pulse Repetition Frequency (PRF) [23]. These settings impact the operating range as well as the propagation of the signal during Line of Sight (LOS) and Non Line of Sight

(NLOS) conditions. For this research project, channel 4 was chosen with a centre frequency of 3993.6 MHz and an increased bandwidth of 900 MHz instead of the regular bandwidth of 500 MHz. This channel works on a wider bandwidth than the others as mentioned, which allows more energy to be sent out according to the regulatory limit and would also increase the capacity of the signal according to the Shannon theorem introduced in Equation (3.9). The choice of a lower centre frequency than for example channel 5 with a centre frequency of 6489.6 MHz was made because a lower frequency would in theory infer a longer operating range as the range performance is decreased with an increasing channel frequency as per Friis transmission equation [62]. However, for industrial and consumer applications, the choice of channel needs to be reconsidered to comply with the European regulations.

The lowest data rate of 110 kbit/s was chosen as the sensitivity of the receiver increases with decreasing data rate according to [17]. The disadvantage with a lower data rate is the fact that each frame sent takes longer time to be transmitted and as such the power consumption is increased to send each frame. The PRF was set to the higher limit 64 MHz instead of 16 MHz due to the increase in precision but once again at a cost of power consumption. As for this specific application the tag will be deployed on the charging station of the mover and hence will have a constant power supply while the reference anchors will be placed on the rover which is equipped with a large battery pack and as such the power consumption is not considered a problem. The length of the preamble determines the receivers ability to detect an incoming signal and in general a longer preamble increases the operating range of the modules. In general there is no benefit of choosing a longer preamble than necessary as long as the receiver is able to detect the signal and as such the preamble length was set to 2048 bit which proved to work sufficiently during testing.

With this setup, a tag scheme was set to run on the Arduino, constantly sending a poll message until an acknowledge is received. As the four anchors are connected to the RPi, the software has to loop all the modules to retrieve a range to each of them. A flowchart of how the DWM software operates can be seen in appendix B. The protocol used to derive the range from the sent signals is the asymmetrical-double sided two-way ranging since it was confirmed in section 3.3.1 that this was the superior protocol of the two-way ranging methods.

4.2.2 DW1000 calibration

Before any statistics can be determined for the ranging performance the chip has to be calibrated. As mentioned earlier the DWM1000 modules make use of timestamps to calculate the range between the two transceivers. To measure this range accurately, the delay induced by the antenna, fabrication uncertainties, external components and PCB has to be compensated for [23] as depicted in Figure 4.4.

4. Unit tests & Simulation

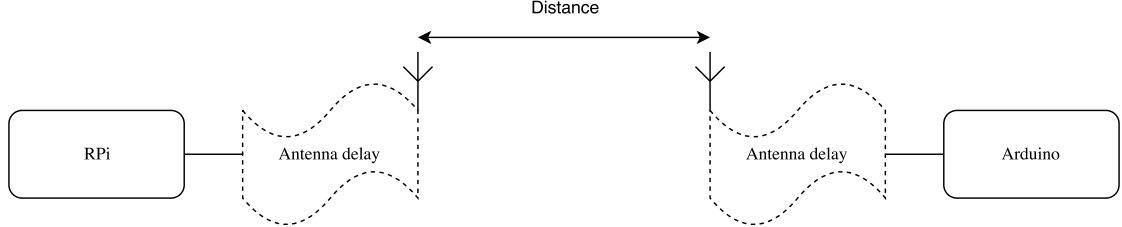


Figure 4.4: Transmit and receive antenna delay.

To compensate these errors, an offline calibration was performed. The range was sampled 1000 times at a distance of 8.68 m according to [23] between the anchor-and tag module and then the antenna delay is adjusted so that the measured range and known distance agree. A snippet of this measurement can be seen in Figure 4.5a. The calibration was made in a outdoor environment with no disturbing objects between the two nodes.

4.3 Ranging test

Ranging tests of the DWM1000 module was performed to observe the performance and variance of the measured distance. The test was carried out in LoS and in an outdoor environment with the settings that are mentioned in section 4.2.1. Different distances were tested, results can be seen in Figures 4.5a, 4.5b for 8.68 m and 43.4 m. The distribution of the measured distances can be seen in Figures 4.5c, 4.5d. 300 measurements were made for each test.

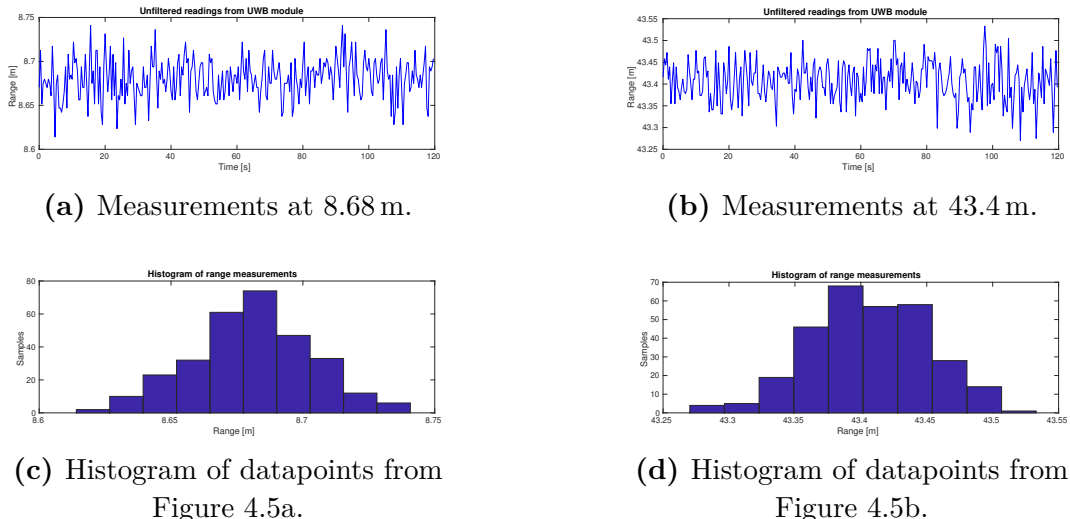


Figure 4.5: Measurement readings from UWB modules

As can be seen in the histogram the distribution can be considered a Gaussian with a mean at the true value which confirms the assumption that the simulated signal takes the form of the true value with an Additive White Gaussian Noise (AWGN).

Measurement data from all the modules at the range of 8.68 m can be seen in Appendix D as well as measurements made at longer ranges.

At medium to long ranges >2 m the mean value of all tests were ± 0.02 m from the "true" value which most likely is due to erroneous measurement of the true value which was made with a long measuring tape. As such it is assumed that the raw signal from the modules has a mean of the true value and the most important characteristic is the standard deviation, the amount of noise in the signal. Attributes from the measurements made can be seen in Table 4.1 where the the standard deviation and average true value offset can be seen from a minimum of 300 samples for each range.

Table 4.1: Range measurements.

Range [m]	σ [m]	Mean true value offset [m]
43.4	0.046	0.006
34.72	0.042	0.005
26.04	0.040	0.005
17.36	0.027	0.016
8.68	0.023	0.0007
4.34	0.037	0.02
2.17	0.071	0.32
1	0.063	0.51

The largest standard deviation can be noted from distances of ≈ 2 m and shorter where also the true offset started to grow making this method unsuitable for shorter distances. As such the UWB system would need to be disregarded at these short ranges. Instead the positioning system will be designed to work at longer range where the largest standard deviation noted was 0.046 m at 43.4 m.

4.4 Simulation & evaluation

The Robotic Operating System (ROS) compatible environment Gazebo was used to graphically present the small and agile intermediate moving robot in its outdoor environment. The Gazebo node subscribes and listens to sensors such as the encoder readings from each wheel as well the true position of the robot. The node then publishes the output from the sensors which Matlab subscribes to as a topic. With Matlab the data can be post processed to test filtering and lateration techniques. At this point it is possible to induce errors to the already existing sensors to better mimic the real environment but also simulate new data such as the UWB signals. As the true position of the robot is available in the simulation environment it is possible to unit test various models and implementations and compare it to ground truth. With this method it is possible to improve and test conditions in an iterative process as well as test the required characteristics of the sensors.

4.4.1 Simulated signal

After measuring the real signals in field tests, a simulated signal for the UWB-modules was reconstructed to fit the actual signal. As an example, the measurement with the largest noises, the measurement at 43.4 m is mimicked; the measured signal as shown in Figure 4.5b has a mean of the true value +0.006 m with an AWGN with boundaries of roughly ± 0.06 m. A model was made for the simulated signal as to catch the characteristics and disturbances of the real signal. It was assumed that the real signal had a mean of the true value at all times with an AWGN. A comparison between the two signals at 43.4 m can be seen in Figure 4.6.

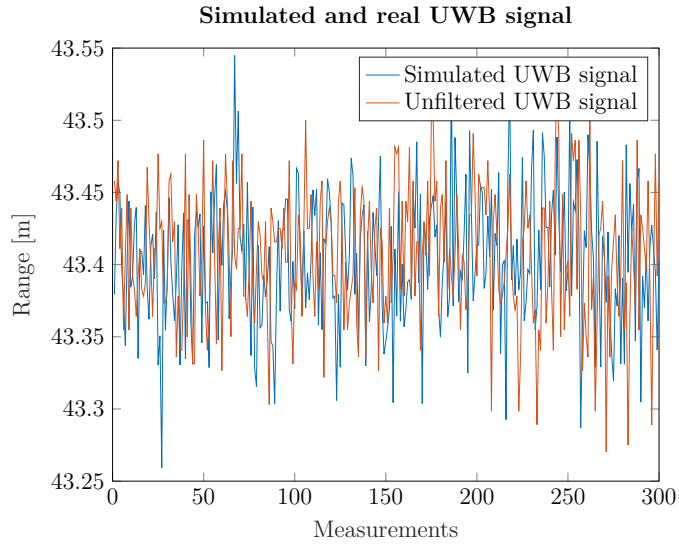


Figure 4.6: Comparison of simulated signal and measured signal at 43.4 m.

Furthermore the mean value and a confidence interval for each signal was calculated to confirm that the signals are similar to each other. An empirical Cumulative Distributive Function (CDF) of the error from the mean at 43.4 m of the two signals can be seen in Figure 4.7 which indicates that the two signals are equivalent to each other. The same analysis was made for all simulated signals.

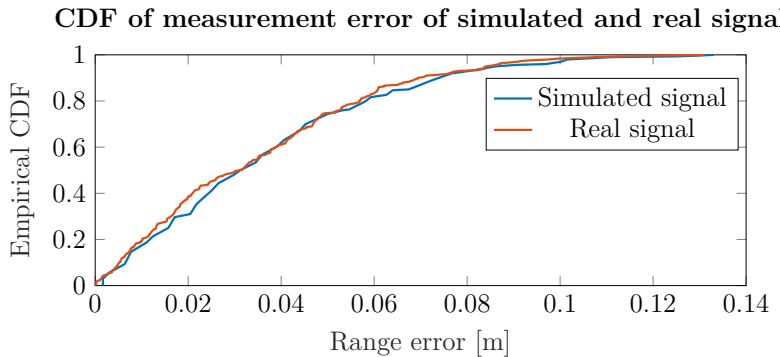


Figure 4.7: Empirical cumulative distributive function of the error at a range of 43.4 m.

4.4.2 Choice of anchors

The number reference nodes placed on the rover can theoretically be chosen to any number above two to derive a position through triangulation in a 2D environment. As per the study in [40] there seemed to be a correlation between the area spanned by the anchor nodes and positioning accuracy. Initially three anchors was tested in the simulation environment set up in a triangle topology (Figure 4.8, Placement a) and then letting the robot move around in an arbitrary fashion for 30 seconds and then estimating a position through the Extended Kalman Filter (EKF) with only UWB signals as input for 10 runs. The same conditions were tested for four (Figure 4.8, Placement b) and five (Figure 4.8, Placement c) anchors with them placed in a square topology and the fifth in the center of the rover. The results showed that the mean error showed an improvement of roughly 14 % when using four transceivers over three whilst no improvement was seen with five modules. To create some margin for implementation errors while still keeping to a low cost solution it was settled for four anchors on the actual platform.

Best results with regards to positioning accuracy were not surprisingly found with the reference anchors spaced as far apart as possible. Thus the placement of the modules were setup in a fashion where the distance was as large as possible while still being within the boundaries of the physical rover.

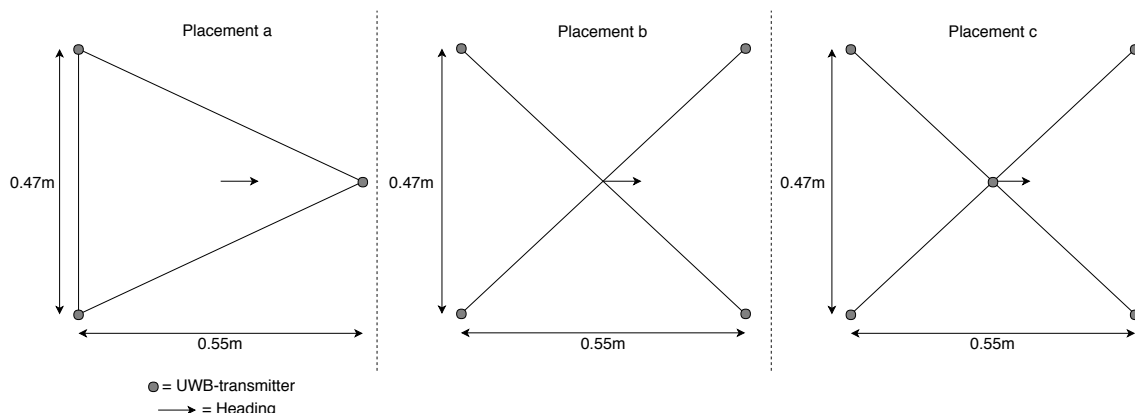


Figure 4.8: Placement of the UWB-transmitters on the robot.

4.5 Filter evaluation

The filters proposed in the theory chapter 3.4 had to be evaluated to determine which is suitable for this implementation. Using the simulation environment with the simulated UWB signal as found in the previous section the performance of the three filters was investigated. The rover was made to travel in a square-like pattern in a speed of 0.3 m/s which is the same conditions as the real application. The estimated position using Linear Least Squares (LLS), Non-Linear Least Squares (NLLS) and EKF can be seen in Figure 4.9.

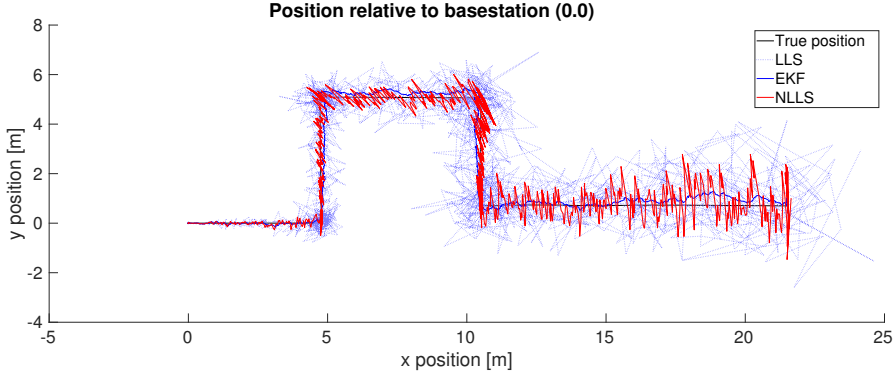


Figure 4.9: Position estimated by proposed filters.

The position estimates are made with UWB signals solely as input, without using any control inputs such as encoders. The rotation matrix to fit the position of the rover onto the real coordinate system use the true rotation as to only consider the performance of each filter. The performance in terms of mean error can be seen in Table 4.2.

Table 4.2: RMSE of tested filters in Figure 4.9.

Method	Mean error [m]
LLS	1.42
NLLS	0.75
EKF	0.47

The NLLS and EKF methods outperform the simple LLS technique and similar results were achieved for several simulations. The performance of both the non-linear filter and EKF are of the same magnitude while the LLS filter is much more noisy and showed to be unstable at longer ranges. This and the consideration that EKF performs better made the decision of choosing a Kalman filter as the positioning algorithm. To be noted here is that the performance of the EKF filter is still outside the bounds of the requirements, and would need further calibration and inputs to improve the performance such as sensor fusion of the encoder readings. A detailed implementation of this filter is followed in the next section.

4.5.1 Extended Kalman Filter

To retrieve any kind of position from the measured ranges, the signals need to be filtered and processed through some kind of state estimator. As mentioned earlier, of the introduced filters a Kalman filter was the most promising. However as discussed in section 3.5.1, the Kalman filter is a linear filter hence the standard filter cannot be used but rather the extended filter was used. Consider the Kalman process- and measurement models introduced in section 3.5.1. For this scenario the state vector of the Kalman filter was chosen as to only consider the coordinates of the rover. The distance measured is the distance from the base station to each of the anchor nodes on the rover. The state vector can be represented as

$$\mathbf{x} = \begin{bmatrix} x \\ y \end{bmatrix} \quad (4.1)$$

and measurement vector as

$$\mathbf{z} = \begin{bmatrix} r_1 \\ r_2 \\ r_3 \\ r_4 \end{bmatrix}. \quad (4.2)$$

Where the state vector $[x, y]^T$ is the position of the rover relative the base station and measurement vector $[r_1, r_2, r_3, r_4]^T$ being the retrieved distances from the modules. To infer the observation equation as a function of the rover states the equation becomes non-linear and defined as

$$\mathbf{z}_k = \mathbf{h}(\mathbf{x}'_k) + \mathbf{v}_k \quad (4.3)$$

with

$$\mathbf{h}(\mathbf{x}'_k) = \begin{bmatrix} \sqrt{(x'_k - s_{x,1})^2 + (y'_k - s_{y,1})^2} \\ \sqrt{(x'_k - s_{x,2})^2 + (y'_k - s_{y,2})^2} \\ \sqrt{(x'_k - s_{x,3})^2 + (y'_k - s_{y,3})^2} \\ \sqrt{(x'_k - s_{x,4})^2 + (y'_k - s_{y,4})^2} \end{bmatrix}. \quad (4.4)$$

With $\mathbf{s}_i = [s_{x,i}, s_{y,i}]$ being the position of the stationary nodes on the rover and the $[x', y']$ coordinates of the basestation relative to the moving rover. The observed measurement Jacobian is then computed as follows

$$\mathbf{H}_k = \frac{\partial \mathbf{h}(\tilde{\mathbf{x}}_k)}{\partial \mathbf{x}_k} \begin{bmatrix} \frac{\tilde{x}'_k - s_{x,1}}{\sqrt{(\tilde{x}'_k - s_{x,1})^2 + (\tilde{y}'_k - s_{y,1})^2}} & \frac{\tilde{y}'_k - s_{x,1}}{\sqrt{(\tilde{x}'_k - s_{x,1})^2 + (\tilde{y}'_k - s_{y,1})^2}} \\ \frac{\tilde{x}'_k - s_{x,2}}{\sqrt{(\tilde{x}'_k - s_{x,2})^2 + (\tilde{y}'_k - s_{y,2})^2}} & \frac{\tilde{y}'_k - s_{x,2}}{\sqrt{(\tilde{x}'_k - s_{x,2})^2 + (\tilde{y}'_k - s_{y,2})^2}} \\ \frac{\tilde{x}'_k - s_{x,3}}{\sqrt{(\tilde{x}'_k - s_{x,3})^2 + (\tilde{y}'_k - s_{y,3})^2}} & \frac{\tilde{y}'_k - s_{x,3}}{\sqrt{(\tilde{x}'_k - s_{x,3})^2 + (\tilde{y}'_k - s_{y,3})^2}} \\ \frac{\tilde{x}'_k - s_{x,4}}{\sqrt{(\tilde{x}'_k - s_{x,4})^2 + (\tilde{y}'_k - s_{y,4})^2}} & \frac{\tilde{y}'_k - s_{x,4}}{\sqrt{(\tilde{x}'_k - s_{x,4})^2 + (\tilde{y}'_k - s_{y,4})^2}} \end{bmatrix}. \quad (4.5)$$

Now the regular Kalman filter can be applied with the transition matrix \mathbf{F} from the process model from Equation (3.31) defined as a 2x2 identity matrix.

The transition matrix \mathbf{F} was defined as \mathcal{I} because the only states of the rover considered was it's position and it was assumed that no external forces were applied to the rover. The *a priori* prediction input was set to predict movement when encoder rotations were measured. As such the control matrix was defined to translate the encoder readings into translational movement as

$$\mathbf{B} = \begin{bmatrix} \frac{c_m}{2} \cos \theta & 0 \\ 0 & \frac{c_m}{2} \sin \theta \end{bmatrix} \quad (4.6)$$

With c_m as defined in Equation (3.1). The control input \mathbf{u}_k takes into account the encoder readings from each wheel N_l and N_r

$$\mathbf{u}_k = \begin{bmatrix} N_l + N_r \\ N_l + N_r \end{bmatrix} \quad (4.7)$$

This model assumes that the rover is moving in a straight path in between every sample but with ample sampling time the approximation can be sufficient. Experimental tests were made on the dead reckoning position estimate on a flat grass surface which indicated that the wheels had little to none slippage and made a very accurate position estimate when travelling around the surface. Nonetheless a Poisson distributed error was included on the encoder pulse readings in the simulation as to mimic inferior conditions, such as wet and uneven surfaces where more slippage could occur.

To be noted here is that the states of the *a priori* prediction are coordinates of the rover relative the base station while the states in the measurement Equation (4.3) are coordinates of the base station relative the rover. As such the *a priori* prediction needs to be passed through the rotation matrix in Equation (3.53) to be compared to the innovation matrix in Equation (3.38). Ultimately the coordinates retrieved are rotated once more to capture the coordinates in the final state space.

The Unscented Kalman Filter (UKF) application was set up with the same states and measurements as the EKF with some modifications as described in appendix A and using Equation (4.4) to create the sigmapoints in the measurement domain.

The filters have two more important parameters that need to be defined, \mathbf{Q} and \mathbf{R} . As mentioned earlier, \mathbf{R} represents the measurement noise covariance which can be determined empirically from the measurement devices used, in this case the UWB modules. The process noise matrix represented by \mathbf{Q} is the error and variance of the process model. Briefly described, the values of \mathbf{Q} indicates the confidence of the *a priori* prediction.

Experiments on the modules showed a maximum standard deviation of $\sigma = 4.6 \times 10^{-3}$ m which corresponds to the following measurement noise matrix

$$\mathbf{R} = \begin{bmatrix} \sigma^2 & 0 & 0 & 0 \\ 0 & \sigma^2 & 0 & 0 \\ 0 & 0 & \sigma^2 & 0 \\ 0 & 0 & 0 & \sigma^2 \end{bmatrix}. \quad (4.8)$$

The process noise is more difficult to estimate. The *correctness* of the prediction will vary depending on random errors from the encoders such as slippage. There are sophisticated ways to estimate this matrix in discrete time as according to [52]. However as this model only accounts for the static coordinates x, y of the rover the matrix was initially set as a diagonal matrix as Equation (4.9).

$$\mathbf{Q} = \begin{bmatrix} Q & 0 \\ 0 & Q \end{bmatrix} \quad (4.9)$$

These values were experimentally settled to 1.2×10^{-3} when the Kalman filter took into consideration the encoder control inputs for the *a priori* estimate and increased to 9×10^{-2} when the encoders were neglected, i.e. when the prediction assumed the last state.

4.5.2 EKF and UKF

Of the introduced filtering techniques, UKF and EKF showed the most promising results where UKF had to be investigated further as it had been praised to perform equally if not better than EKF.

To evaluate which of these two that are most suitable for this application the Gazebo simulation environment and Matlab was once again used. The results showed that these two filters behaved very similar with marginal difference in terms of mean error and cumulative distributive function and no noteworthy improvement was achieved by the UKF. It was chosen not to investigate this further as it was discovered that the computational burden of the UKF was significant higher. The runtime of the EKF filter was close to 80% faster using a simple timing scheme in Matlab.

4. Unit tests & Simulation

5

Results

The positioning system was evaluated in different scenarios through simulation. Performance evaluation of the positioning system was done with simulated ultra wideband (UWB) signals with varying standard deviation depending on which scenario that was evaluated. The accuracy of the digital compass was used for the rotational matrix and set as discussed earlier in section 3.7. The rover was made to travel along the edges along the explored area since that would induce the largest errors due to the compass and rotation of the reference frame. The dynamic behaviour was also investigated when travelling in a circle. Lastly a scenario mimicking a garden more applicable for this specific application on the Automover where the rover travelled in an arbitrary fashion was tested. The performance of all tests was measured in mean error and the positioning error is presented as the upper limit of 95% of the Cumulative Distributive Function (CDF) as well as the standard deviation. As the performance varies with every simulation due to variations of errors in ranging and encoder inaccuracies, 11 simulations were conducted to show the difference of the results in each scenario. These results can be found in appendix E. The median of each of the scenarios is displayed in Table 5.1.

Table 5.1: Position estimate performance

Scenario	Mean error [m]	95 Percentile [m]
Arbitrary environment, σ_{low}	0.106	0.253
Arbitrary environment, σ_{high} , no encoder	0.386	1.01
Arbitrary environment, σ_{low}	0.079	0.198
Arbitrary environment, σ_{low} no encoder	0.272	0.702
Square 56.5x56.5m	0.199	0.469
Square 56.5x56.5m, no encoder	0.551	1.38
Square 30x30m	0.097	0.246
Square 30x30m, no encoder	0.274	0.712
Circle 47m diameter	0.209	0.549
Circle 47m diameter, no encoder	0.537	1.40

The largest standard deviation of the measured UWB signal at 43.4 m was used for exploring the perimeters of a fictive area equal the size of the requirement of 3200 m^2 , a square of roughly $56.5 \text{ m} \times 56.5 \text{ m}$ which implies that the longest rangevector measured across the diagonal is 40 m. A plot of the rover moving along this perimeter can be seen in Figure 5.1a where the estimated position of the dead reckoning system is included as well. This is the same data used as control input for the Kalman

5. Results

filter. The performance was evaluated as introduced earlier, the mean error was 0.199 m and according to the cumulative distribution function the estimated position accuracy was <0.469 m with 95% probability. The same conditions were tested without using input from the encoders. The results are shown in Figure 5.1b which indicated a larger error since increased oscillations can be seen. The mean error was 0.551 m and the estimated positioning accuracy was <1.382 m with 95% probability.

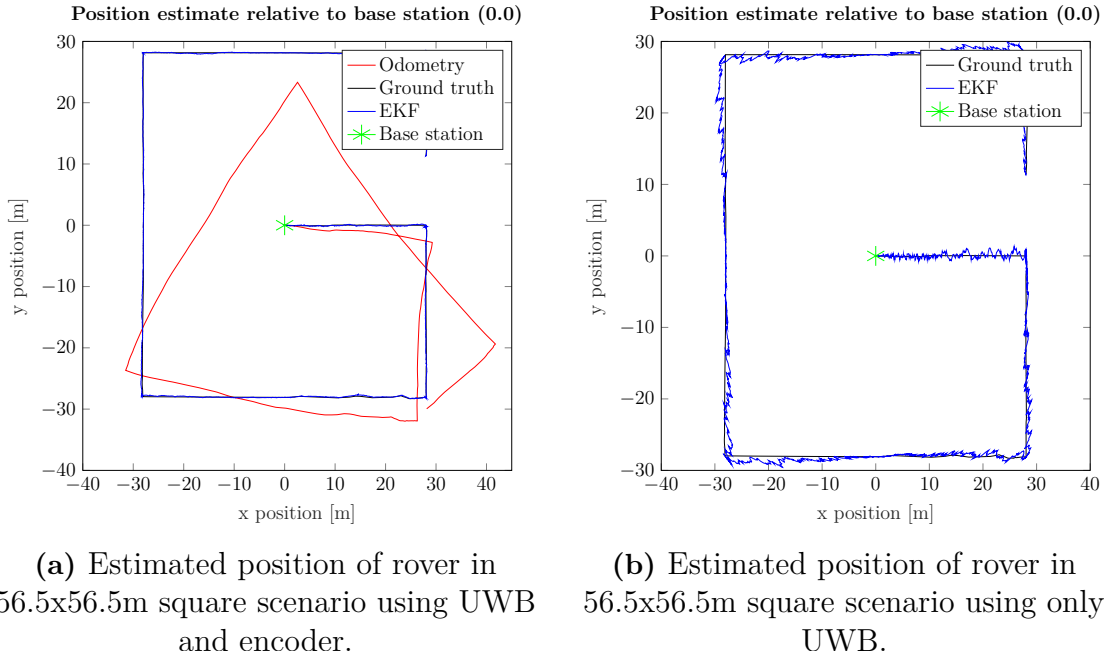


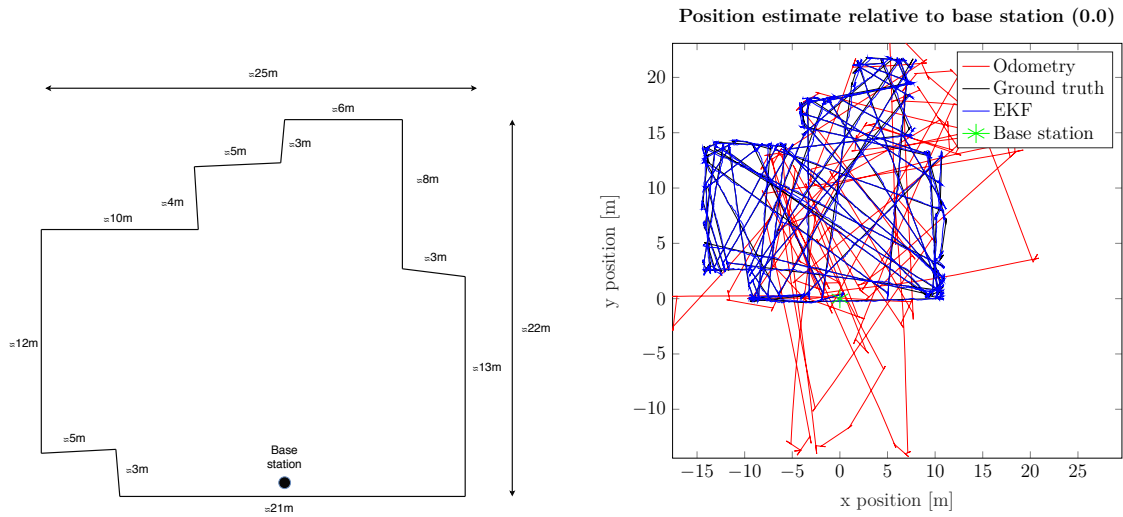
Figure 5.1: Comparison of estimated position through UWB and dead reckoning system in the 56.5x56.5m square scenario.

With an UWB signal with the same characteristics as above, the rover was set to travel in the same fashion it would do in a regular garden as to mimic the real behavior of the Automover. A "garden" was built in the Gazebo environment and the layout of the area can be seen in Figure 5.2a. The estimated position from the system as well as the dead reckoning is displayed in Figure 5.2b.

The estimated position with and without encoder input can be seen in Figure 5.3a and 5.3b. The mean error of a simulation with and without encoders in the arbitrary environment was 0.106 m and 0.386 m respectively. The estimated position accuracy was with 95% probability <0.253 m with encoders and <1.01 m without encoders.

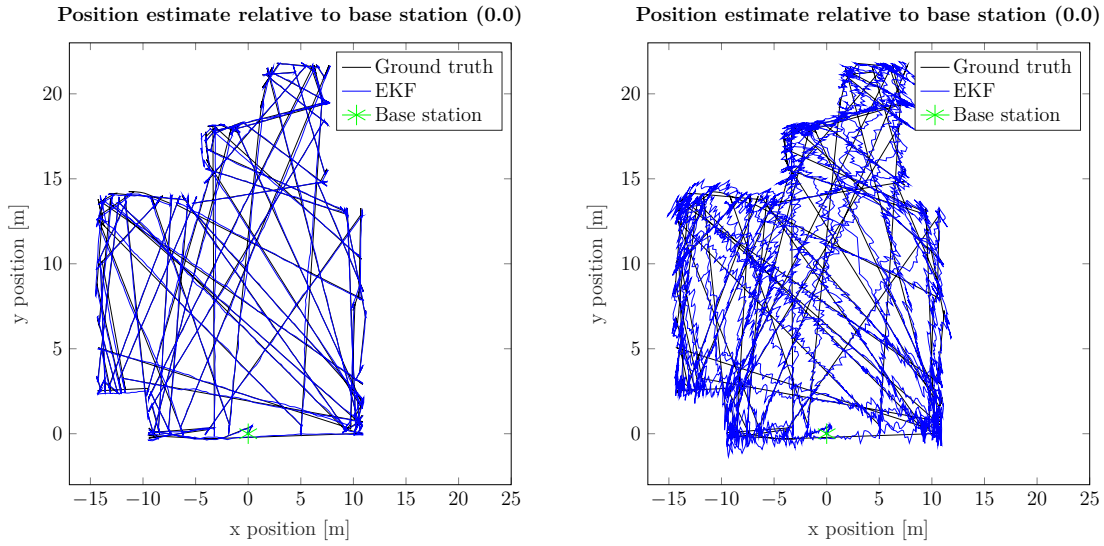
Furthermore, using the same signal, the position estimate was evaluated when traveling in a large circle as to see how the system behaves when the robot moves in an dynamic pattern without any natural stops. The track can be seen in Figure 5.4a.

This scenario with encoders had similar performance as the rectangle pattern, an estimated accuracy of <0.549 m with 95% probability and a mean error of 0.209 m. The behavior without encoders is displayed in Figure 5.4b with an accuracy of



(a) Outer dimensions of simulated area. (b) Estimated position through dead reckoning and UWB.

Figure 5.2: Dimensions of the arbitrary environment and estimated position of the rover moving inside the said area.



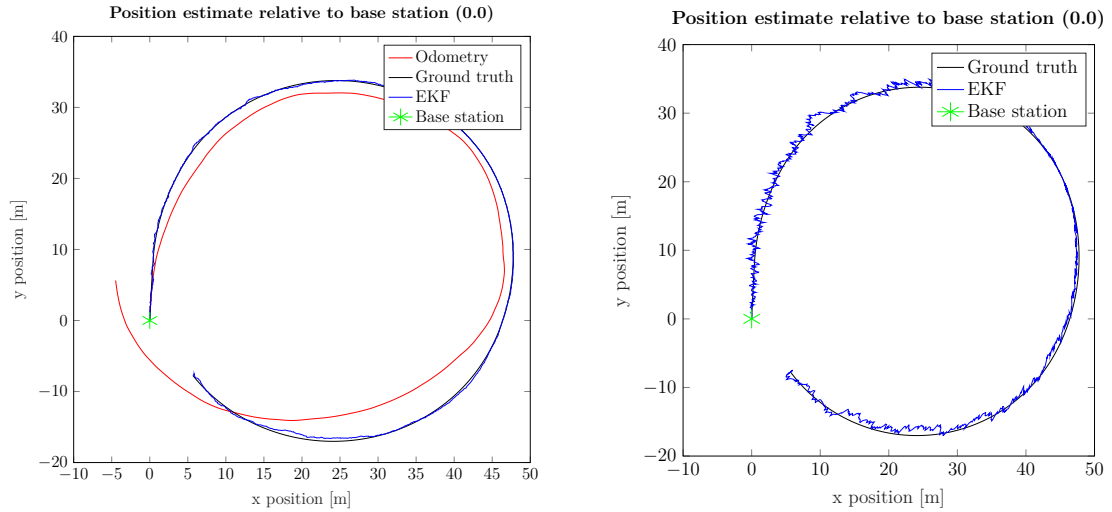
(a) Position estimate of the rover when moving in an arbitrary environment using UWB and encoder input. (b) Position estimate of the rover when moving in an arbitrary environment using only UWB input.

Figure 5.3: Comparison of position estimate of rover when travelling randomly in an arbitrary environment.

<0.140 m with 95% probability and a mean error of 0.537 m.

As the noise of the signal declined when the range shortened, a smaller area was simulated as well, $\approx 30 \times 30$ meters. For this scenario the simulated signal were set to have the characteristics of the measured signal made at 17.34 m, a signal

5. Results



(a) Position estimate when travelling in circle, 47m diameter, using UWB and encoder input.

(b) Position estimate when travelling in circle, 47m diameter, using only UWB input.

Figure 5.4: Comparison of position estimate of rover when travelling in large circle, with and without encoder input.

with standard deviation of 0.027 m. With these properties of the simulated signal the positioning estimate had an accuracy of <0.097 m with 95% probability for the simulation with encoders. The path followed can be seen in Figure 5.5a. When neglecting the input from the encoders and only using input from the UWB-modules the position estimate had an accuracy of <0.274 m with 95% probability and a mean error of 0.712 m. The position estimates can be seen in Figure 5.5b.

A simulation was performed not using the compass for orientation. This to test the performance of the system using UWB-ranging measurements to determine the rotational angle as described in section 3.8. The test was performed with and without encoder. The simulations results with encoders had a mean error of 0.274 m and a estimated position accuracy of <0.583 m. Without the encoder as seen before the accuracy decreased and had a mean error of 0.633 m and a estimated position accuracy of <1.58 m. The track of the estimated position for these two scenarios can be seen in Figure 5.6.

The cumulative distributive function of the errors for all position estimates are displayed in Figure 5.7 and 5.8 where they have been plotted separately depending on the standard deviation of the signal. In Figure 5.7 the CDF of the scenarios using a signal standard deviation of 0.027 m can be seen while in 5.8 the scenarios using the larger standard deviation of 0.046 m is plotted.

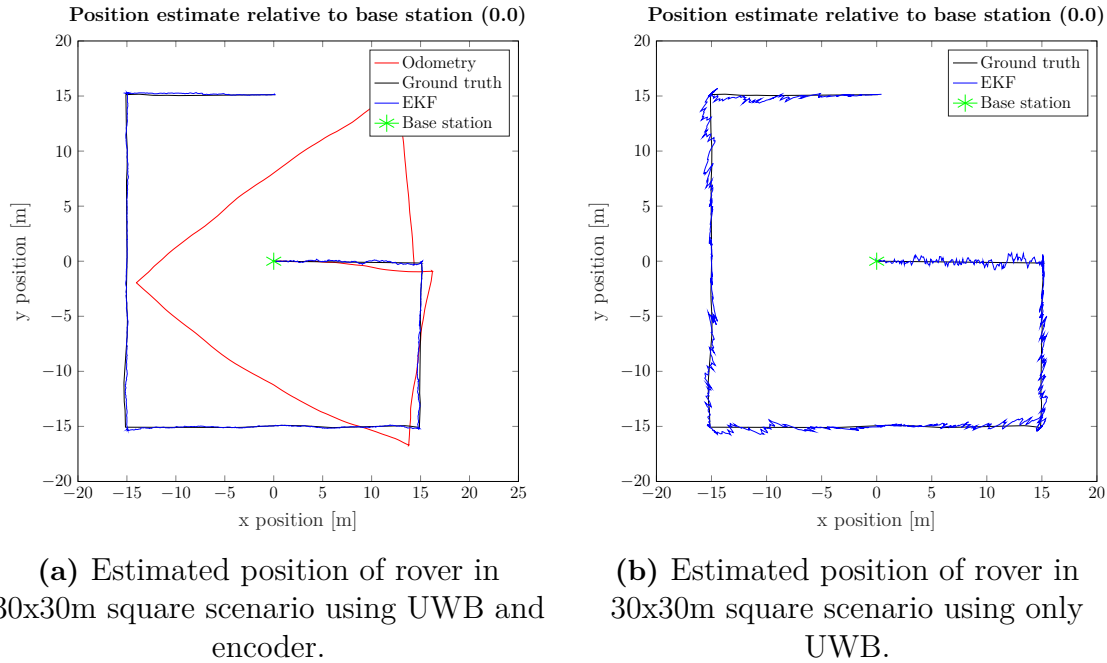


Figure 5.5: Comparison of estimated position through UWB and dead reckoning system in the 30x30m square scenario.

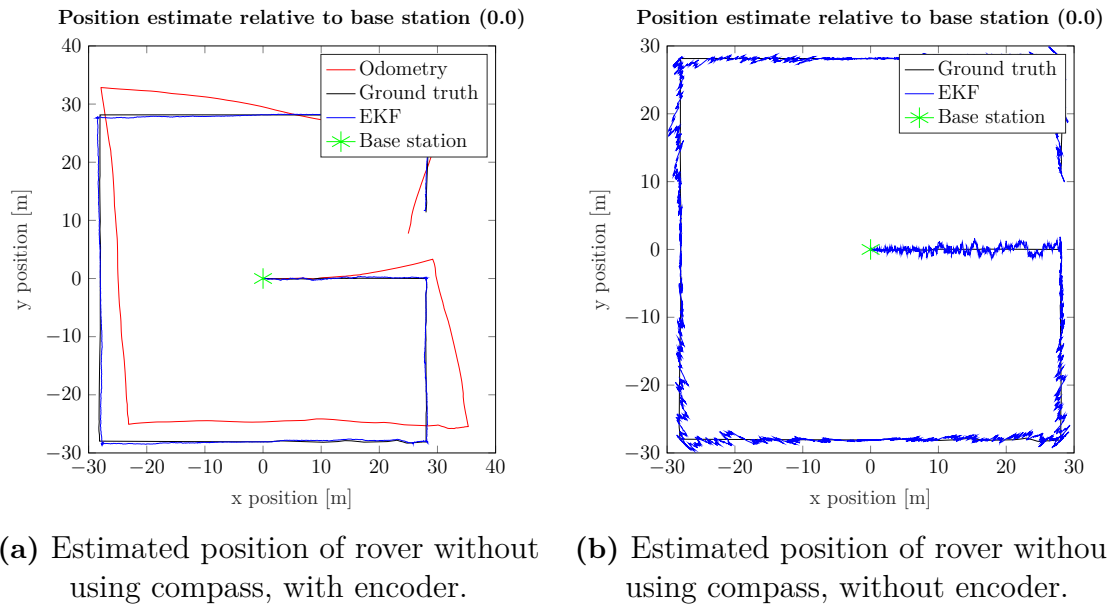


Figure 5.6: Estimation of position in 56.5x56.5m square scenario using UWB as rotation angle input.

5. Results

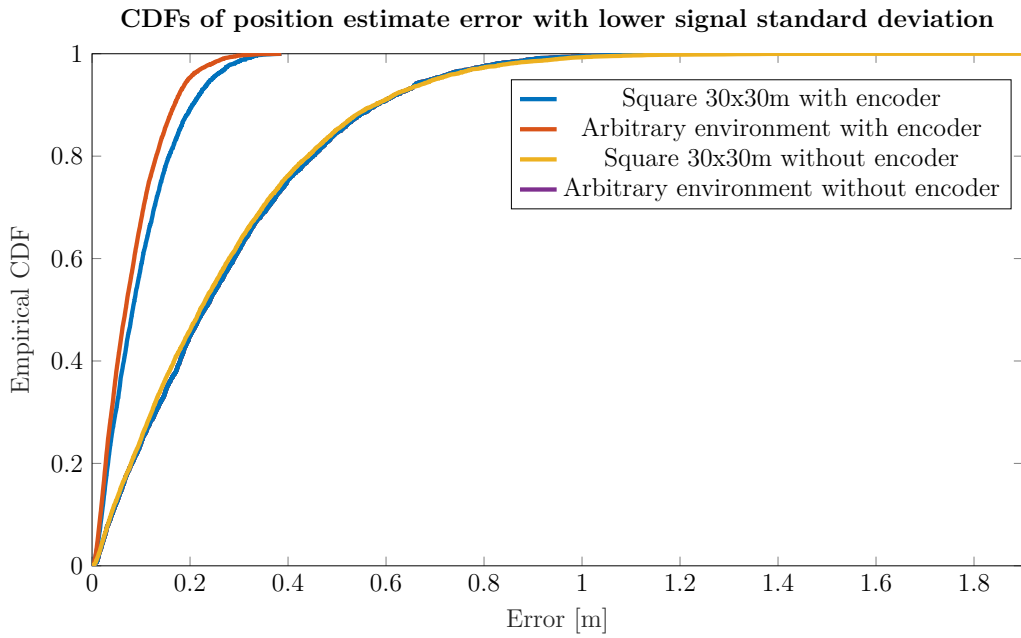


Figure 5.7: Cumulative distribution function of position estimate error with standard deviation 0.027 m signal.

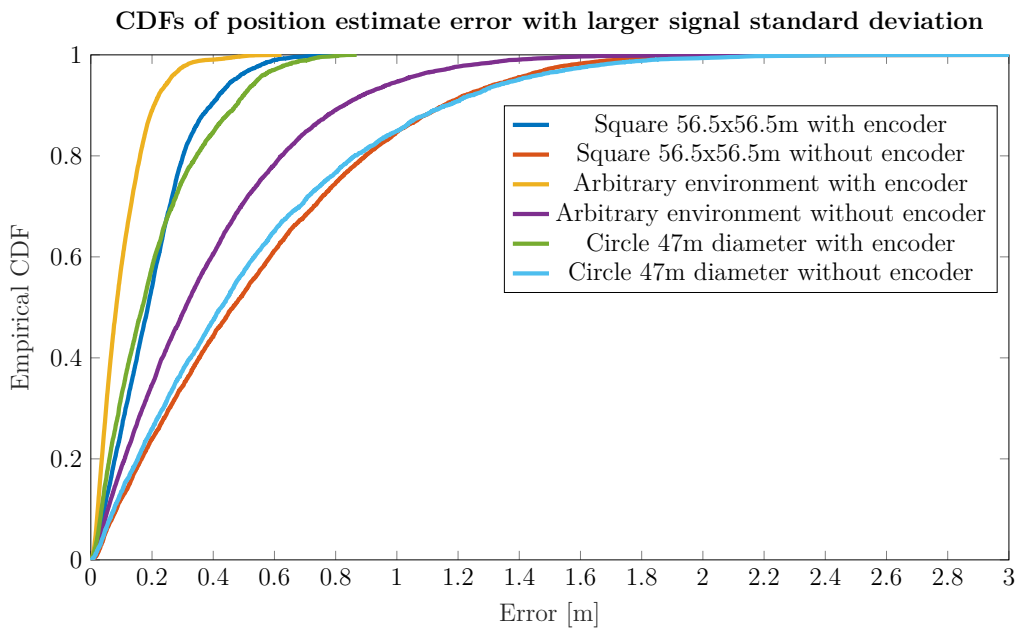


Figure 5.8: Cumulative distribution function of position estimate error with standard deviation 0.046 m signal.

6

Discussion

The evaluation of the Ultra Wide-Band (UWB) modules in Subsection 4.3 Figure 4.5d displays that the precision is ≈ 0.1 m at a distance of 43.4 m. The precision stated from the manufacturer is 0.1 m meaning that the UWB-modules work as expected. However constructing a 95% confidence interval shows a precision of 0.084 m at 43.4 m and 0.054 m at 17.4 m with 95% probability respectively which indicates that the modules perform better than expected at these ranges.

Further, the distance between the anchors had a large impact on the positioning results. Reducing the distance between the four anchors on the rover to span a square of 0.3 m \times 0.3 m compared to the full dimensions of the Automover of 0.47 m \times 0.55 m, resulted in an increase in error of the position estimation by almost 100% on all parameters during simulations. Pointing to that this multilateration topology cannot be decreased in size for much smaller application if not better ranging accuracy is achieved or if lower precision is acceptable. As a test to see how large the platform would have to be as to meet the internal requirements setup early in the project it was quickly concluded that a high accuracy is difficult to achieve with a small device. To meet the requirements of 0.2 m accuracy with 95% certainty in all simulated scenarios the size of the area covered by the modules would have to be roughly 2.5 m \times 2.5 m.

The result in Figure 5.1b shows that the estimated position using only UWB tends to oscillate in the area close to the ground truth. An important notification is that the range measurements did not drift from the ground truth in position estimations between 4-43m but the oscillation indicates that the UWB would benefit of an additional sensor input to stabilize the position estimate due to the inherent noise in the distance measurements. It also indicated that a UWB system might not be ample on its own. A standalone positioning system using only four UWB modules would probably be feasible with modules such as the PulseOn from TimeDomain because of the ranging performance but due to the price range of these devices they are mostly applicable for more expensive solutions.

The results pointed to that a fusion of UWB and encoder readings dramatically increased the performance of the system. An examination of Table 5.1 indicates that the position estimate was improved with a threefold when sensor fusion is incorporated. The position estimated by the dead reckoning system, i.e. the encoder, is not accurate enough due to systematic and random errors but if the predicted movement is used as input to the Kalman filter the position estimate is improved.

6. Discussion

The result of this is that the position estimate is less affected by the noise in the distance measurements.

The position retrieved by this reversed multilateration topology is the position of the base station relative the moving robot. The coordinate system has to constantly be rotated to create a static map of the rovers position. As a test to evaluate the influence of the compass inaccuracies, the true rotation of the rover was used for the large square simulation. With this it was possible to estimate the position with an error of $<0.404\text{ m}$ with 95% probability, a mean error of 0.159 m and standard deviation of 0.126 m . This can be considered as the limit of the system as it is of today. It was thought that a highly accurate digital compass was required to meet the requirements set up early in the project and that calculating the angle using the UWB ranging measurements was not possible due to the large estimation error generated by ranging errors. To confirm this a positioning estimate was conducted as can be seen in Figure 5.6. The simulation showed that the estimated positioning accuracy was 1.58 m with 95% probability and had a mean error of 0.633 m without the encoder input and with the encoder input the positioning system performed with a mean error of 0.274 m and an estimated accuracy of 0.583 m with 95% probability. However the angle estimation using UWB ranging calculations was far more accurate than expected. A reason for this is that the Kalman filter uses the angle retrieved by the compass or calculations as input for rotating the *a priori* prediction. It is here able to mitigate the effects of yaw error to some degree. This mitigation can visually be seen when inspecting Figure 5.1 where the position estimate without encoder with a larger process noise covariance matrix \mathbf{Q} is more inflicted by the compass as it moves further away from the base station. The performance of the calculated angle through UWB is however not sufficient to achieve results wanted.

A magnification of the results with the true rotation position estimate can be seen in Figure 6.1a which can be put in comparison with the estimated position with the calculated rotation angle Figure 6.1b where the same magnification can be seen. When applying the true rotation the position estimate converges towards the true position given enough time and the overall performance was improved. When the calculated rotation angle is used it so happens that the estimate sometimes converge a slight offset which corresponds to several faulty calculations or readings, seen in Figure 6.1b.

The results varied depending on the distance to the base station which was expected as the ranging performance of the UWB modules declined with the longer distances (see Figure 5.5). The results of the mean error at shorter ranges ($30\text{ m} \times 30\text{ m}$) was 0.097 m which is in line with the previous studies found in [40] and [28] which managed to get an accuracy of better than 0.2 m at ranges up to 20 meters and 0.1 m at a range of 4 meters respectively with the same topology.

As the rover moves, the estimated position through the Kalman filter oscillates around the true value as mentioned above. When the rover stops to turn the Kalman filter propagates to the true position given that the digital compass is accurate. This

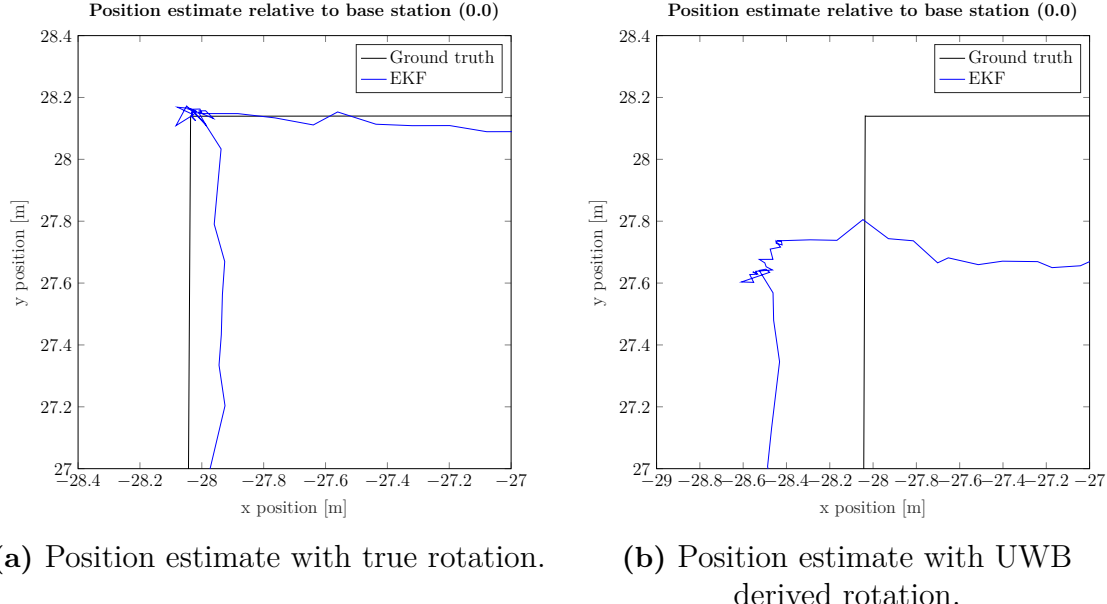


Figure 6.1: Estimated position through UWB and dead reckoning system.

and the oscillating behaviour can be seen in Figure 6.2 which is a zoomed view of Figure 5.1a.

An arbitrary scenario where the rover traveled randomly over an simulated area (Figure 5.2a) with outer constraints was conducted. This was done to evaluate the performance of the system when the robot required short stops to change directions which gives the Kalman filter time to propagate to the ground truth. The result shows that the accuracy is enhanced, with a decreased mean and positioning estimation error. With this knowledge, it would be beneficial to have constraints of how far the rover is allowed to travel before stopping and/or obstacles that require the robot to change direction. This results also shows that it is possible to create a very accurate map of the area, especially if it is done in smaller iterations. The map can be used for further exploitation of for example a path coverage algorithm. However this requires the encoder input as mentioned before.

In Figure 5.4 a test of continuous movement and turning was performed. The result shows that even if no stops are required the mean error was 0.209 m with encoder and a position estimation accuracy of <0.549 m is not far from the simulation results from the square 56.5 m × 56.5 m test.

Early in the project it was thought that the Unscented Kalman Filter (UKF) would outperform the Extended Kalman Filter (EKF) in terms of accuracy performance since the UKF would be able to linearize the system to the third order Taylor expansion while EKF only captured the first order expansion. This was not the case. The improvement was little to none while the computational burden was almost doubled even though the filters in theory have roughly the same computational complexity. A reason for the low improvement of accuracy could be that the measurement equa-

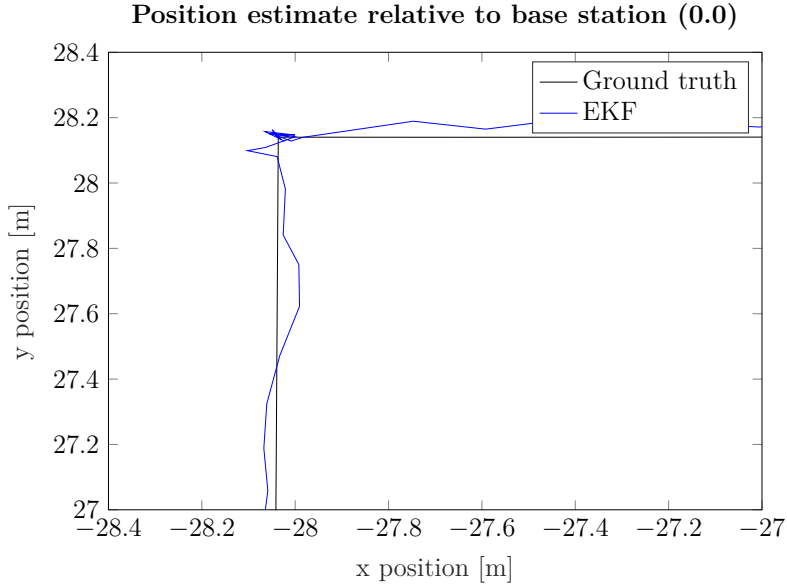


Figure 6.2: Zoomed view of Figure 5.1a.

tion that maps the measured values into the state space (Equation (4.4)) is close to quadratic making the first order Taylor expansion a very good estimator which could be a reason as to why the extended performed so well compared to the unscented.

The total sampling frequency of all the modules used for the positioning system was set to 10 Hz since it was found manageable to sample one module with the Raspberry Pi (RPI) at a rate faster than 40 Hz. This was deemed sufficient as the rover moves at a speed of 0.3 m/s and thus only capable of moving 0.03 m between each sample. However there has been reports that a tag polling rate of more than 200 Hz is achievable which means that frequency of 50 Hz is doable for the whole control loop. This does however require one Microcontroller Unit (MCU) per anchor as the RPi displayed limitations at frequencies above the one specified due to the serial bus being occupied with the DW1000 chip communication. To increase the tag polling frequency the ranging scheme has to either be changed from Asymmetric Double-Sided Two-Way Ranging (ADS-TWR) or change the operational setting of the DWM1000 chip, either shortening the preamble or increasing the bitrate. The influence of these changes are discussed in section 4.2.1 This however could have a negative impact on the accuracy of the range performance. Increasing the loop frequency means that smaller iterations can be made by the Kalman filter and since the measurement errors of the UWB modules have been found to have a normal distribution the Kalman filter should converge faster to the true position. This makes the position estimate of the multilateration slightly better when a higher sampling rate is utilized. Different sampling frequencies were tested on the various scenarios and a higher frequency did not exclusively outperform the one suggested at 10 Hz. The variation of performance was more stable at higher frequencies while not improving the system noteworthy. A lower sampling frequency than 5 Hz induced a divergent behaviour of the performance as the mean error varied between 0.18-0.6 m for the 58x58m square scenario.

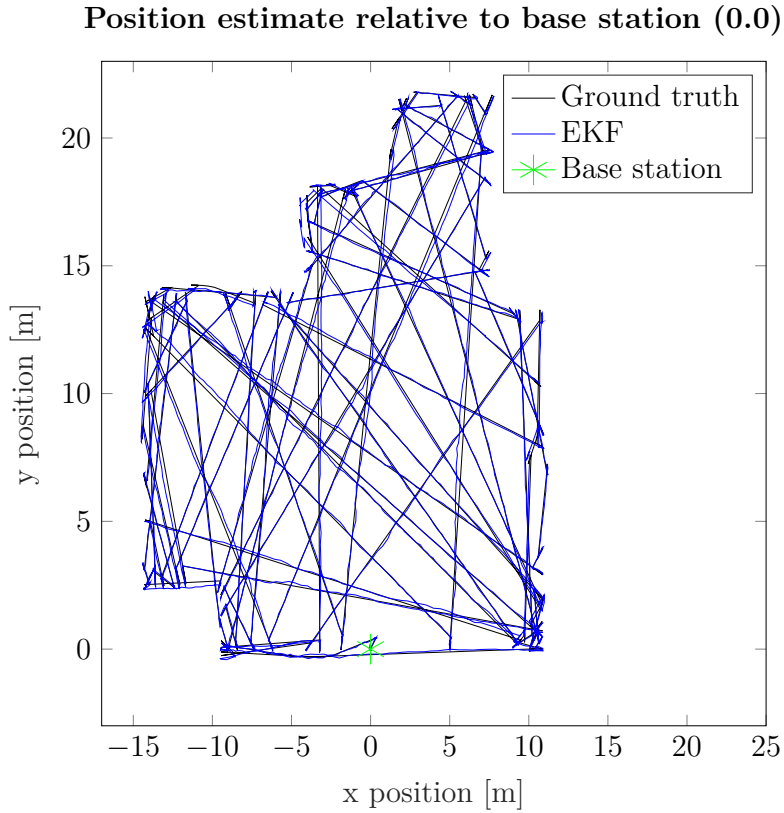


Figure 6.3: Position estimate in the arbitrary environment.

As with all simulations, assumptions and simplifications of the real world have been made. The simulated environment is a 2D static map which corresponds to the defined scope. Of biggest importance is that the simulated UWB signals are equivalent to the real world measurements. The measurements made on the UWB-modules in section 4.3 were made several times and the behaviour of the recorded signal was the same for all instances which strengthen the assumptions made of the UWB signals. These measurements are made during full Line of Sight (LoS) conditions. It was discovered that the radio range measurements was easily corrupted by objects reflecting signals as well as attenuation effects when the signal is propagated through different mediums or obstacles in the way as discussed by [65]. The distribution of the measurements changed to a skewed Gaussian distribution during these Non Line of Sight (NLoS) conditions with a tail of overestimated range measurements. As the scope of this thesis is defined as in LoS conditions this is of no concern for this model. A field test with Automover was made on a flat grass surface as to evaluate the performance of the dead reckoning system. On this surface with very good conditions the slippage of the wheels was close to none and the dead reckoning system performed better than expected. This however was during optimal conditions and as to not produce results non-applicable for inferior situations a disturbance to the encoder readings was inferred. With a better model of the dead reckoning system and the erroneous behaviour of the wheels it would be possible to further improve the a priori prediction of the Kalman filter and in that way improve the position

6. Discussion

estimate from the system.

7

Conclusion

Is reversed multilateration using UWB a viable technical solution for positioning a small and agile intermediate moving outdoor robot?

The results show that ultra wide-band radio frequency modules with reversed multilateration topology is a viable technical solution to localize a small and agile intermediate moving outdoor robot. Depending on the accuracy required for the robot it might not be a feasible choice. Using this ultra wide-band technique merged with encoder and compass input the mean error and the 95% percentile does not meet the internal requirements of an 0.2 m accuracy at a range of 40 m.

How much is the positioning performance improved when combining the system with odometry data?

Due to the noisy nature of radio signals and the fact that the variance of the measured signal grows with the distance measured, the results were vastly improved when fused with another sensor input. The results showed that if the multilateration was combined with an encoder input the position estimate error was improved with a threefold. Thus a sensor fusion is required to realize an ultra wide-band positioning system at longer ranges if high accuracy is required.

7. Conclusion

8

Future work and remarks

In this chapter suggestions for future work and recommendations are presented.

8.1 NLOS

The ultra wide-band signals have properties that make them adequate for usage in environments where obstacles are in the way but there will still be some accuracy loss during these scenarios. It can be improved by using intricate methods to identify these scenarios when a very high accuracy is required. To cope with the error propagation during Non Line of Sight (NLoS) conditions there are several approaches to mitigate these errors to create a more robust positioning system. Some of them are

1. Create a robust filter by making use of a redundant number of anchors for trilateration such as the Residual weighting algorithm where the residual of every combination of anchors is calculated and the solutions that coheres the best is chosen. This method assumes however that the number of Line of Sight (LoS) measurements are higher than the number of NLoS measurements which might not be ample for the topology proposed because if one anchor is in NLoS then all of them probably are. [13]
2. A second approach is to assume that it is possible to discriminate between NLoS and LoS measurements as the distribution and standard deviation will fluctuate more during NLoS. These readings can then be rejected or under-estimated during the positioning phase much like putting weights on signals during LoS and NLoS situation. [75]
3. Another method is to apply probability distributions that can model the NLoS conditions in a more appropriate way than the standard Gaussian assumptions. Such as a skew- t Bayes filter that is able to model the error distribution better as the range measurements are overestimated during NLoS. [53]
4. There are approaches that include analyzing the energy of the received signal and travel delay to extinguish NLoS to LoS situations and the error are then mitigated through for example using maximum likelihood (ML) to estimate the range [58] but also more novel methods that incorporate Support Vector Machine (SVM), machine learning to reduce the ranging errors [46].

8.2 Antenna

The antenna on the DWM1000 module is *omni-directional*, meaning that the signal from the antenna is not equally distributed along all coordinate axes. This will result in loss of communication in certain angles between the anchor-, and tracking-node which was experienced during testing. To avoid this an *isotropic* extension antenna can be fitted to the module to assure that the signal is distributed equally in all coordinate axes. An isotropic antenna will improve the performance when the surface of the area incorporates hills and unevenness and will also be required in a 3D-environment. Adding more sensors will however increase the complexity and cost for the system.

8.3 Sensors

The accurate digital compass in this project [2] uses three magnetoresistive sensors to determine the orientation of the robot and will only work in a 2D-plane. The compass was not tested during this project. To assure that the electrical components such as DC-motors not will effect the accuracy or repeatability of the compass it should be tested with the robot that it is implemented with. To further improve the accuracy of the local positioning system additional sensors can be implemented such as Inertial Measurement Unit (IMU) or choose an digital compass that uses both magnetoresistive sensors, gyroscope and accelerometer. This to get more input regarding the movement of the robot to the Kalman Filter to improve the position estimation. However in a 3D-environment this will not only increase the complexity of the system but also the cost.

8.4 Dead reckoning model

In this thesis an inferior model of the encoder readings is assumed where a stochastic error is added to the readings. With a better model of the dead reckoning system the trustworthiness of the *a priori* prediction phase of the Kalman filter can be improved and as such this input to the filter will have higher significance and be able to mitigate the noise in the radio signals even further. The development of this model would either require a large dataset of the motion of the rover as to properly make a statistical model of how the rover should be moving given the readings from the encoder or add additional torque sensors and in such a way detect if slippage occurs.

8.5 Choice of hardware

It was discovered that when all four UWB modules communicated with the Micro-Controller Unit (MCU) on the same bus the total sampling time was rather limited. The setup in this thesis with a Raspberry Pi connected to four DWM1000 modules was able to sample one single anchor at rates up to 50 Hz but dropped rapidly when

several anchors were sampled to test the positioning algorithm due to the long wake-up time of each chip when they were cycled. This made the sample rate of the four DWM1000 modules drop down to rates of roughly 1 Hz which is why the positioning system was not tested on the physical rover in practice. The recommendation would be to equip each of the anchors on the rover with a separate MCU which then passes the retrieved range to a main MCU which does the post processing and positioning algorithms.

To further improve the accuracy of the range measurements a Time Difference of Arrival (TDoA) protocol can be used. As mentioned earlier in this thesis, this requires synchronized clocks among the anchors. The module used, DWM1000 from Decawave does as of today not support this but the internal chip DW1000 has the synchronization feature. As such, if a separate circuit is made for the DW1000 chip this feature could be utilized and a TDoA protocol can be used instead of the now tested two-way ranging protocol which should in theory increase the positioning accuracy.

8.6 Path planning algorithm

The next step for this specific application would be to develop a coverage planning algorithm as to minimize the total length travelled to cover the whole area of the garden. As of today the Automover uses a kind of random coverage method where it bounces around the garden. By decomposing the garden into smaller non overlapping segments and using tools such as the *Boustrophedon cellular decomposition* [68] it is possible to create online path planning algorithms to reduce the time and energy consumed by the Automover to cover the area, which finally is the ultimate goal.

8. Future work and remarks

Bibliography

- [1] DecaWave ScenSor DWM1000 Module. <https://www.decawave.com/products/dwm1000-module>. Accessed: 2018-02-23.
- [2] Digital Compass Solution, HMR3200/HMR3300. <https://media.digikey.com/pdf/Data%20Sheets/Honeywell%20PDFs/HMR3200,3300.pdf>. Accessed: 2018-04-12.
- [3] Raspberry Pi about us. <https://www.raspberrypi.org/about/>. Accessed: 2018-02-15.
- [4] Robotic Operating System about us. <http://www.ros.org/about-ros/>. Accessed: 2018-02-15.
- [5] A. Alarifi, A. S. Al-Salman, M. Alsaleh, A. Alnafessah, S. Alhadhrami, M. A. Al-Ammar, and H. S. Al-Khalifa. Ultra wideband indoor positioning technologies: Analysis and recent advances. In *Sensors*, May 2016.
- [6] R. Balakrishna and A. Ghosal. Modeling of slip for wheeled mobile robots. *IEEE Transactions on Robotics and Automation*, 11(1):126–132, Feb 1995.
- [7] T. Balbirnie. How it works: Global positioning system (GPS). *Electronics Education*, 1999(1):7–8, Spring 1999.
- [8] J. M. Brandon. The global positioning system: Global developments and opportunities, 5 2003. U.S. International Trade Commission.
- [9] G. Breed. A summary of FCC rules for ultra wideband communications. *High Frequency Electronics*, pages 42–44, Aug 2005.
- [10] G. Bresson, Z. Alsayed, L. Yu, and S. Glaser. Simultaneous localization and mapping: A survey of current trends in autonomous driving. *IEEE Transactions on Intelligent Vehicles*, 2(3):194–220, Sept 2017.
- [11] P. Brida and J. Machaj. A novel enhanced positioning trilateration algorithm implemented for medical implant in-body localization. *International Journal of Antennas and Propagation*, 2013(2):10, July 2013.
- [12] L. Chen, H. Ba, W. Heinzelman, and A. Cote. RFID range extension with low-power wireless edge devices. In *2013 International Conference on Computing, Networking and Communications (ICNC)*, pages 524–528, Jan 2013.
- [13] P.-C. Chen. A non-line-of-sight error mitigation algorithm in location estimation. In *WCNC. 1999 IEEE Wireless Communications and Networking Conference (Cat. No.99TH8466)*, pages 316–320 vol.1, 1999.
- [14] K. C. Cheok, M. Radovnikovich, P. Vempaty, G. R. Hudas, J. L. Overholt, and P. Fleck. Uwb tracking of mobile robots. In *21st Annual IEEE International Symposium on Personal, Indoor and Mobile Radio Communications*, pages 2615–2620, Sept 2010.

- [15] R. F. D. Seetharam. Battery-powered RFID. Technical report, TagSense Inc, 432 Columbia St, B13B, Cambridge, MA 02141.
- [16] D. Dardari, A. Conti, U. Ferner, A. Giorgetti, and M. Z. Win. Ranging with ultrawide bandwidth signals in multipath environments. *Proceedings of the IEEE*, 97(2):404–426, Feb 2009.
- [17] Decawave. DW1000 datasheet. <https://www.decawave.com/sites/default/files/resources/dw1000-datasheet-v2.09.pdf>, 2015. Version 2.09.
- [18] DecaWave. *Application Note: Wireless sensor networks and the DW1000*. DecaWave, 2017.
- [19] V. Djaja-Josko and J. Kolakowski. Uwb positioning system for elderly persons monitoring. In *2015 23rd Telecommunications Forum Telfor (TELFOR)*, pages 169–172, Nov 2015.
- [20] T. Domain. Pulson 400. <https://timedomain.com/products/pulson-440/>, June 2018. Accessed 1-March-2018.
- [21] G. Dudek and M. Jenkin. *Computational Principles of Mobile Robotics*. Cambridge University Press, New York, NY, USA, 2nd edition, 2010.
- [22] R. Faragher. Understanding the basis of the kalman filter via a simple and intuitive derivation [lecture notes]. *IEEE Signal Processing Magazine*, 29(5):128–132, Sept 2012.
- [23] M. A. Finlayson. *DW1000 User Manual. How to use, configure and program the DW1000 UWB transceiver*. Decawave, 2017.
- [24] S. Gezici. A survey on wireless position estimation. *Wireless Personal Communications*, 44(3):263–282, Feb 2008.
- [25] J. Gonzalez, J. L. Blanco, C. Galindo, A. O. de Galisteo, J. A. Fernandez-Madrigal, F. A. Moreno, and J. L. Martinez. Combination of UWB and GPS for indoor-outdoor vehicle localization. In *2007 IEEE International Symposium on Intelligent Signal Processing*, pages 1–6, Oct 2007.
- [26] K. Guo, Z. Qiu, C. Miao, A. H. Zaini, C.-L. Chen, W. Meng, and L. Xie. Ultra-wideband-based localization for quadcopter navigation. *Unmanned Systems*, 04(01):23–34, 2016.
- [27] E. A. Hans-Werner Kaas. Automotive revolution – perspective towards 2030. Advanced Industries, Copyright McKinsey & Company, 1 2017.
- [28] B. Hepp, T. Nägeli, and O. Hilliges. Omni-directional person tracking on a flying robot using occlusion-robust ultra-wideband signals. In *2016 IEEE/RSJ International Conference on Intelligent Robots and Systems (IROS)*, pages 189–194, Oct 2016.
- [29] J. Hightower and G. Borriello. Location systems for ubiquitous computing. *Computer*, 34(8):57–66, Aug 2001.
- [30] Husqvarna. Husqvarna automower 420/430x/450x operator’s manual, 2016.
- [31] H. R. E. J. Borenstein and L. Feng. Where am I? Sensors and Methods for Mobile Robot Positioning. Technical Report 1, University of Michigan, 3 1996.
- [32] W. Jeong and K. M. Lee. CV-SLAM: a new ceiling vision-based SLAM technique. In *2005 IEEE/RSJ International Conference on Intelligent Robots and Systems*, pages 3195–3200, Aug 2005.

- [33] Z. Jianyong, L. Haiyong, C. Zili, and L. Zhaojun. Rssi based bluetooth low energy indoor positioning. In *2014 International Conference on Indoor Positioning and Indoor Navigation (IPIN)*, pages 526–533, Oct 2014.
- [34] A. R. Jiménez and F. Seco. Comparing decawave and bespoon uwb location systems: Indoor/outdoor performance analysis. In *2016 International Conference on Indoor Positioning and Indoor Navigation (IPIN)*, pages 1–8, Oct 2016.
- [35] R. K. Sidhartan, R. Kannan, S. Srinivasan, and V. Balas. Stochastic wheel-slip compensation based robot localization and mapping. In *Advances in Electrical and Computer Engineering*, volume 16, pages 25–32, May 2016.
- [36] M. Kam, X. Zhu, and P. Kalata. Sensor fusion for mobile robot navigation. *Proceedings of the IEEE*, 85(1):108–119, Jan 1997.
- [37] M. J. Kuhn, M. R. Mahfouz, J. Turnmire, Y. Wang, and A. E. Fathy. A multi-tag access scheme for indoor uwb localization systems used in medical environments. In *2011 IEEE Topical Conference on Biomedical Wireless Technologies, Networks, and Sensing Systems*, pages 75–78, Jan 2011.
- [38] R. Kümmeler, G. Grisetti, C. Stachniss, and W. Burgard. Simultaneous parameter calibration, localization, and mapping for robust service robotics. In *Advanced Robotics and its Social Impacts*, pages 76–79, Oct 2011.
- [39] J. J. LaViola. A comparison of unscented and extended kalman filtering for estimating quaternion motion. In *Proceedings of the 2003 American Control Conference, 2003.*, volume 3, pages 2435–2440 vol.3, June 2003.
- [40] F. Lazzari, A. Buffi, P. Nepa, and S. Lazzari. Numerical investigation of an uwb localization technique for unmanned aerial vehicles in outdoor scenarios. *IEEE Sensors Journal*, 17(9):2896–2903, May 2017.
- [41] A. Ledergerber, M. Hamer, and R. D’Andrea. A robot self-localization system using one-way ultra-wideband communication. In *2015 IEEE/RSJ International Conference on Intelligent Robots and Systems (IROS)*, pages 3131–3137, Sept 2015.
- [42] Y. Lee, J. Yoon, H. Yang, C. Kim, and D. Lee. Camera-GPS-IMU sensor fusion for autonomous flying. In *2016 Eighth International Conference on Ubiquitous and Future Networks (ICUFN)*, pages 85–88, July 2016.
- [43] B. W. Lennart Råde. *Mathematics Handbook*. Studentlitteratur, Lund, Sweden, 5 edition, 1988.
- [44] O. Lobell and F. Stenbeck. Localization and mapping for outdoor mobile robots with RTK GPS and sensor fusion. Master’s thesis, KTH Royal Institute of Technology, 2017.
- [45] LPKF Laser Electronics AG. LPKF ProtoMat E34 / E44. <http://www.lpkf.com/products/rapid-pcb-prototyping/circuit-board-plotter/protomat-e44.htm>, 2018. Accessed 12-March-2018.
- [46] S. Marano, W. M. Gifford, H. Wymeersch, and M. Z. Win. Nlos identification and mitigation for localization based on uwb experimental data. *IEEE Journal on Selected Areas in Communications*, 28(7):1026–1035, September 2010.
- [47] A. Mathisen, S. K. Sørensen, A. Stisen, H. Blunck, and K. Grønbæk. A comparative analysis of indoor wifi positioning at a large building complex. In *2016*

- International Conference on Indoor Positioning and Indoor Navigation (IPIN)*, pages 1–8, Oct 2016.
- [48] Mathworks. Matlab R2017b. https://se.mathworks.com/products/new_products/release2017b.html, 2017. Accessed 12-March-2018.
 - [49] R. Mautz. *Indoor positioning technologies*. PhD thesis, ETH, Zürich, Schweiz, Feb 2012.
 - [50] A. Milstein. *Occupancy Grid Maps for Localization and Mapping, Motion Planning*. InTech, 1 edition, 6 2008.
 - [51] M. W. Mueller, M. Hamer, and R. D’Andrea. Fusing ultra-wideband range measurements with accelerometers and rate gyroscopes for quadrocopter state estimation. In *2015 IEEE International Conference on Robotics and Automation (ICRA)*, pages 1730–1736, May 2015.
 - [52] H. Musoff and P. Zarchan. *Fundamentals of Kalman Filtering: A Practical Approach, Progress in Astronautics and Aeronautics*. American Institute of Aeronautics and Astronautics, 3 edition, 2009.
 - [53] H. Nurminen, T. Ardestiri, R. Piché, and F. Gustafsson. A nlos-robust toa positioning filter based on a skew-t measurement noise model. In *2015 International Conference on Indoor Positioning and Indoor Navigation (IPIN)*, pages 1–7, Oct 2015.
 - [54] M. G. Ocando, N. Certad, S. Alvarado, and A. Terrones. Autonomous 2D SLAM and 3D mapping of an environment using a single 2D LIDAR and ROS. In *2017 Latin American Robotics Symposium (LARS) and 2017 Brazilian Symposium on Robotics (SBR)*, pages 1–6, Nov 2017.
 - [55] O. M. P. Teunissen. *Springer Handbook of Global Navigation Satellite Systems*. Springer International Publishing, 1 edition, 2017.
 - [56] M. Pelka, D. Amann, M. Cimdins, and H. Hellbriick. Evaluation of time-based ranging methods: Does the choice matter? In *2017 14th Workshop on Positioning, Navigation and Communications (WPNC)*, pages 1–6, Oct 2017.
 - [57] D. Porcino and W. Hirt. Ultra-wideband radio technology: potential and challenges ahead. *IEEE Communications Magazine*, 41(7):66–74, July 2003.
 - [58] A. Rabbachin, I. Oppermann, and B. Denis. Ml time-of-arrival estimation based on low complexity uwb energy detection. In *2006 IEEE International Conference on Ultra-Wideband*, pages 599–604, Sept 2006.
 - [59] S. O. Rice. Communication in the presence of noise; probability of error for two encoding schemes. *The Bell System Technical Journal*, 29(1):60–93, Jan 1950.
 - [60] A. R. J. Ruiz and F. S. Granja. Comparing ubisense, bespoon, and decawave uwb location systems: Indoor performance analysis. *IEEE Transactions on Instrumentation and Measurement*, 66(8):2106–2117, Aug 2017.
 - [61] W. S. Murphy Jr. and W. Hereman. Determination of a position in three dimensions using trilateration and approximate distances. Technical report, Colorado School of Mines, Department of Mathematical and Computer Sciences, 1999.
 - [62] H. Schantz and A. Nikravan. Simple formulas for near-field transmission, gain, and fields. In *Conference: 2013 Antennas Applications Symposium*, 09 2013.
 - [63] L. Schauer, F. Dorfmeister, and M. Maier. Potentials and limitations of wifi-positioning using time-of-flight. In *International Conference on Indoor Positioning and Indoor Navigation*, pages 1–9, Oct 2013.

- [64] D. Simon. *Optimal State Estimation: Kalman, H Infinity, and Nonlinear Approaches*. Wiley-Interscience, 2006.
- [65] V. S. Sonwalkar, A. Venkatasubramanian, J. G. Hawkins, B. Satavalekar, B. Johnson, and C. E. Mayer. Dependence of multipath propagation effects on the uwb pulse characteristics. In *2006 International Waveform Diversity Design Conference*, pages 1–7, Jan 2006.
- [66] Y. Tian, N. Sidek, and N. Sarkar. Modeling and control of a nonholonomic wheeled mobile robot with wheel slip dynamics. In *2009 IEEE Symposium on Computational Intelligence in Control and Automation*, pages 7–14, March 2009.
- [67] J. Tiemann, J. Pillmann, S. Bocker, and C. Wietfeld. Ultra-wideband aided precision parking for wireless power transfer to electric vehicles in real life scenarios. In *2016 IEEE 84th Vehicular Technology Conference (VTC-Fall)*, pages 1–5, Sept 2016.
- [68] M. Waanders. Coverage path planning for mobile cleaning robots. In *15th Twente Student Conference on IT*, pages 1–10, June 2011.
- [69] E. A. Wan and R. V. D. Merwe. The unscented kalman filter for nonlinear estimation. In *Proceedings of the IEEE 2000 Adaptive Systems for Signal Processing, Communications, and Control Symposium (Cat. No.00EX373)*, pages 153–158, 2000.
- [70] C. Wang, Z. Shi, F. Wu, and J. Zhang. An rfid indoor positioning system by using particle swarm optimization-based artificial neural network. In *2016 International Conference on Audio, Language and Image Processing (ICALIP)*, pages 738–742, July 2016.
- [71] C. Wang, H. Zhang, T. M. Nguyen, and L. Xie. Ultra-wideband aided fast localization and mapping system. In *2017 IEEE/RSJ International Conference on Intelligent Robots and Systems (IROS)*, pages 1602–1609, Sept 2017.
- [72] J. Wang, Q. Gao, Y. Yu, X. Zhang, and X. Feng. Time and energy efficient tof-based device-free wireless localization. *IEEE Transactions on Industrial Informatics*, 12(1):158–168, Feb 2016.
- [73] M. Z. Win and R. A. Scholtz. Impulse radio: how it works. *IEEE Communications Letters*, 2(2):36–38, Feb 1998.
- [74] M. Z. Win and R. A. Scholtz. On the robustness of ultra-wide bandwidth signals in dense multipath environments. *IEEE Communications Letters*, 2(2):51–53, Feb 1998.
- [75] M. P. Wylie and J. Holtzman. The non-line of sight problem in mobile location estimation. In *Proceedings of ICUPC - 5th International Conference on Universal Personal Communications*, volume 2, pages 827–831 vol.2, Sep 1996.
- [76] S. Yousuf and M. B. Kadri. Sensor fusion of ins, odometer and GPS for robot localization. In *2016 IEEE Conference on Systems, Process and Control (ICSPC)*, pages 118–123, Dec 2016.
- [77] D. M. C. e. a. Zain Bin Tariq. Non-gps positioning systems: A survey. *ACM Computing Surveys (CSUR)*, 50:34, November 2017.
- [78] J. Zhang, P. V. Orlik, Z. Sahinoglu, A. F. Molisch, and P. Kinney. Uwb systems for wireless sensor networks. *Proceedings of the IEEE*, 97(2):313–331, Feb 2009.

Bibliography

- [79] Z. Şahinoğlu, S. Gezici, and I. Güvenç. *Ultra-wideband Positioning Systems. Theoretical Limits, Ranging Algorithms, and Protocols*. Cambridge University Press, 3 edition, 7 2008.

A

Unscented Kalman Filter

Contemplate that a variable \mathbf{x} of dimension n is to propagate through a non-linear function $\mathbf{y} = g(\mathbf{x})$ with a mean μ and covariance \mathbf{P}_k . The unscented transform calculates the statistics of \mathbf{y} when the variable is passed through the function by first forming a matrix of sigma vectors $\boldsymbol{\chi}$ of size $2n + 1$ accordingly [39]

$$\chi^0 = \mu \quad (\text{A.1})$$

$$\chi^i = \mu + (\sqrt{(n + \lambda)\mathbf{P}_k})_i \quad i = 1, \dots, n \quad (\text{A.2})$$

$$\chi^i = \mu - (\sqrt{(n + \lambda)\mathbf{P}_k})_{i-n} \quad i = n + 1, \dots, 2n \quad (\text{A.3})$$

$$w_{(m)}^0 = \frac{\lambda}{n + \lambda} \quad (\text{A.4})$$

$$w_{(c)}^0 = \frac{\lambda}{n + \lambda} + 1 - \alpha^2 + \beta \quad (\text{A.5})$$

$$w_{(m)}^i = w_{(c)}^i = \frac{1}{2(n + \alpha)} \quad i = 1, \dots, 2n \quad (\text{A.6})$$

Where w^i is the weights corresponding to each sigma point χ_i which represents how *trustworthy* each sigma point is, the *power of*-index represents mean and covariance sigma points and the lambda $\lambda = \alpha^2(n + \kappa) - n$ is a scaling factor. β represents the prior knowledge of the distribution for \mathbf{x} where $\beta = 2$ is optimal for a Gaussian distribution. Note that due to the nature of the error covariance \mathbf{P} , the term $(\sqrt{(n + \lambda)\mathbf{P}_k})$ is assumed symmetric and positive definite [39] and thus the Cholesky decomposition can be used to efficiently find the square root.

These sigma points are then sent through the non-linear functions of both the process and the measurement as

$$\gamma^i = g(\chi^i) \quad i = 0, \dots, 2n \quad (\text{A.7})$$

As to create samples of the non-linear functions. These can then be used together with the weights to approximate the mean and the covariance. In the unscented Kalman filter this is done for both the process model $f(x)$ and the measurement model $h(x)$ as

$$x_k^i = f(\chi_{k-1}^i) \quad (\text{A.8})$$

$$\hat{x}_k = \sum_{i=0}^{2n} w_{(m)}^i x_k^i \quad (\text{A.9})$$

$$z_{k-1}^i = h(\chi_{k-1}^i) \quad (\text{A.10})$$

$$\hat{z}_{k-1} = \sum_{i=0}^{2n} w_{(m)}^i z_{k-1}^i \quad (\text{A.11})$$

Where the hat indicates the estimated mean. The covariance matrices of the *a priori* estimation, innovation covariance and cross covariance of the estimated values of the unscented transform has to be computed to calculate the Kalman gain as follows

$$\mathbf{P}_k^e = \sum_{i=0}^{2n} w_{(c)}^i (x_k^i - \hat{x}_k)(x_k^i - \hat{x}_k)^T + \mathbf{Q} \quad (\text{A.12})$$

$$\mathbf{P}_{zz} = \sum_{i=0}^{2n} w_{(c)}^i (z_{k-1}^i - \hat{z}_{k-1})(z_{k-1}^i - \hat{z}_{k-1})^T + \mathbf{R} \quad (\text{A.13})$$

$$\mathbf{P}_{xz} = \sum_{i=0}^{2n} w_{(c)}^i (x_k^i - \hat{x}_k)(z_{k-1}^i - \hat{z}_{k-1})^T \quad (\text{A.14})$$

With these equations, together with tuning the scaling factors it is possible to apply the UKF in a similar fashion as the EKF as demonstrated below with \mathbf{Z}_k being the real measurements.

$$\bar{\mathbf{x}}_k = \hat{\mathbf{x}}_k + \mathbf{K}_k (\mathbf{Z}_k - \hat{\mathbf{z}}_{k-1}) \quad (\text{A.15})$$

$$\mathbf{K}_k = \mathbf{P}_{xz} \mathbf{P}_{zz}^{-1} \quad (\text{A.16})$$

$$\mathbf{P}_k = \mathbf{P}_k^e - \mathbf{K}_k \mathbf{P}_{zz} \mathbf{K}_k^T \quad (\text{A.17})$$

B

Software Flowcharts

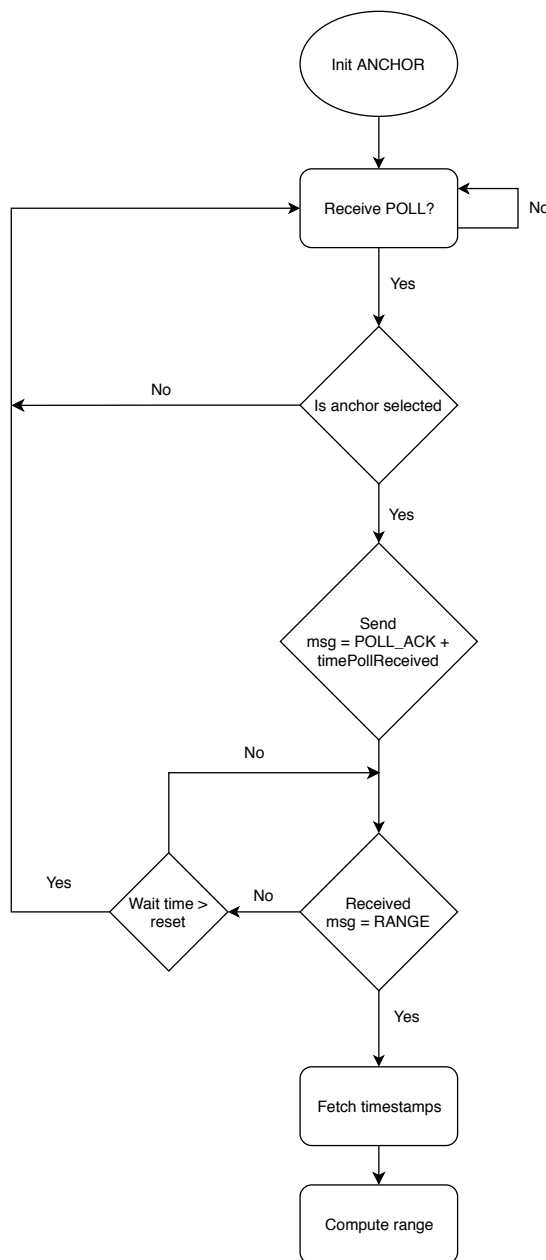


Figure B.1: Flowchart of anchor software

B. Software Flowcharts

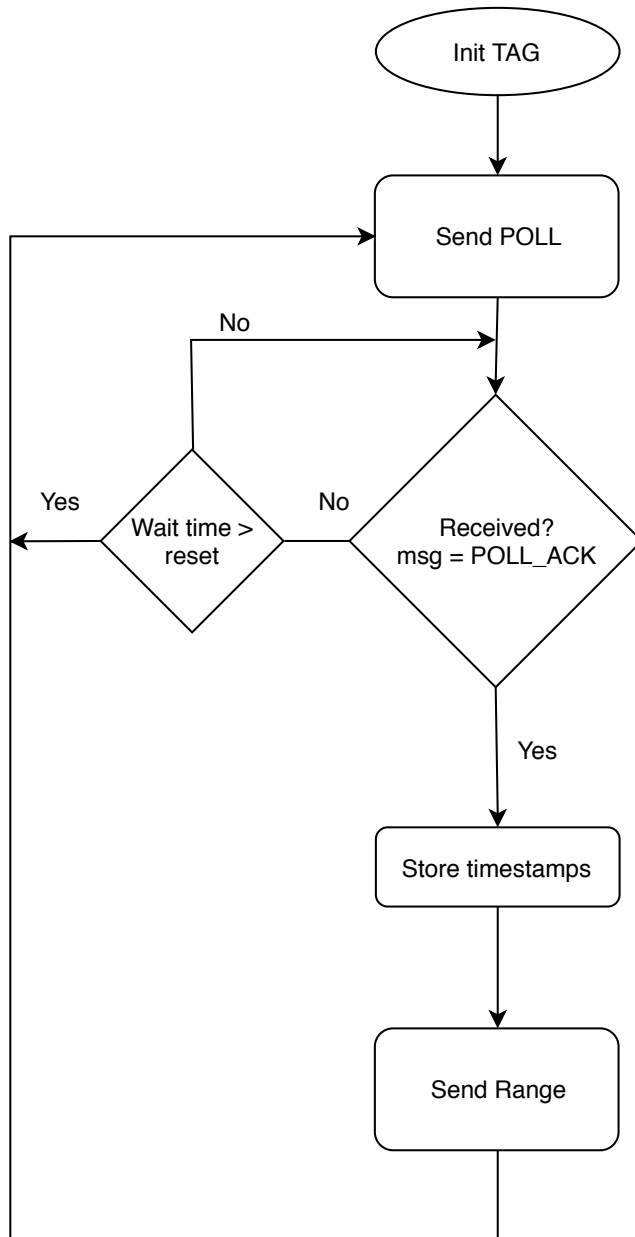


Figure B.2: Flowchart of tag software

C

Angle of rotation using UWB

The orientation angle is defined as the angle between the $y - axis$ and the lawn mowers direction vector defines as N in Figure 3.12. The distances that are needed to calculate the rotation angle can be seen in Figure 3.12. Where MS_1 , MS_2 , MS_3 and MS_4 are the nodes on the lawn mower and BS_1 and BS_2 are the two base station nodes. The distance between the nodes on the lawn mower d_1 and d_2 is the distance between the nodes on the base station. The ranging measured between the MS and BS nodes are defined as r_1 , r_2 and r_3 . As can be seen in the figure, $\alpha = \phi + \phi_1 + \phi_2$ which is the orientation angle from the $y' - axis$ which is parallel to the $y - axis$. Define $\gamma = \phi + \phi_1$ and $\gamma_1 = \beta + \beta_1$ then according to the law of cosines [43]:

$$\gamma = \cos \left(\frac{d_1^2 + r_1^2 - r_3^2}{2 \times d_1 \times r_1} \right)^{-1} \quad (C.1)$$

$$\gamma_1 = \cos \left(\frac{r_1^2 + d_2^2 - r_2^2}{2 \times r_1 \times r_2} \right)^{-1}. \quad (C.2)$$

To derive ϕ_2 , the angle β_2 needs to be calculated as:

$$\beta_2 = \pi - \gamma_1 \quad (C.3)$$

and ϕ_2 can be calculated with Equation (C.4) since the angular sum of a triangle is π :

$$\phi_2 = \pi - \frac{\pi}{2} - \beta_2 \quad (C.4)$$

using Equation (C.1) and (C.4) together, α can be defined as:

$$\alpha = \phi + \phi_1 + \phi_2 \Rightarrow \quad (C.5)$$

$$\alpha = \gamma + \phi_2 \Rightarrow \quad (C.6)$$

$$\alpha = \cos \left(\frac{d_1^2 + r_1^2 - r_3^2}{2 \times d_1 \times r_1} \right)^{-1} - \frac{\pi}{2} + \cos \left(\frac{r_1^2 + d_2^2 - r_2^2}{2 \times r_1 \times d_2} \right)^{-1} \quad (C.7)$$

When using this approach, cases are needed to decide which node pair to use when calculating the orientation angle, which case to use depends on the distances from each mobile station to the two base stations.

C. Angle of rotation using UWB

D

Distance measurements

Measurements on the modules were made at various distances to examine the behaviour of the signal as to confirm the assumption of a constant Gaussian noise. All the modules was tested at a range of 8.7 m as seen below with their correlating histograms. The mean value of each measurement was the true value ± 0.005 m.

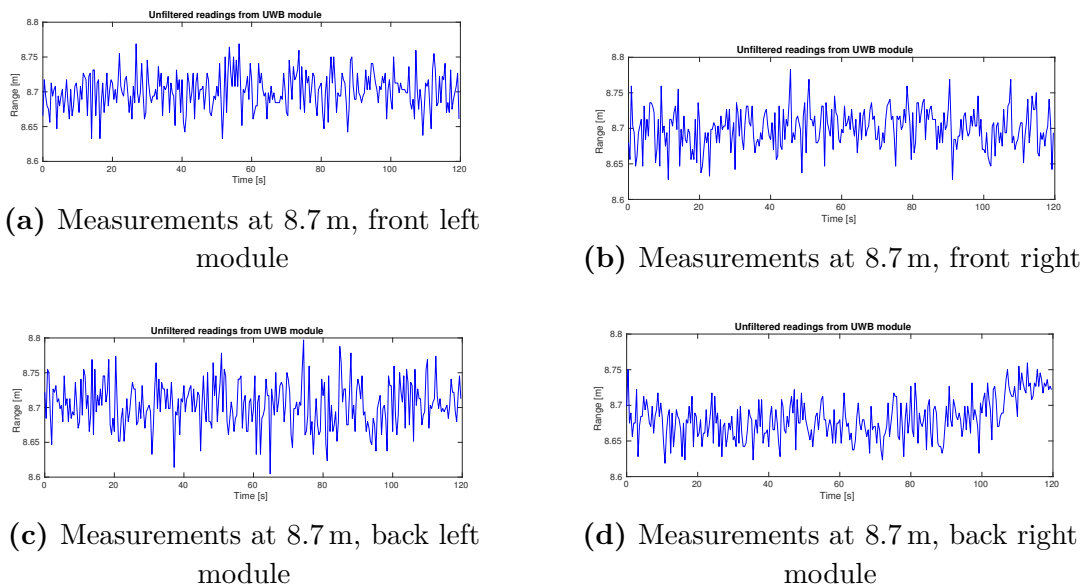
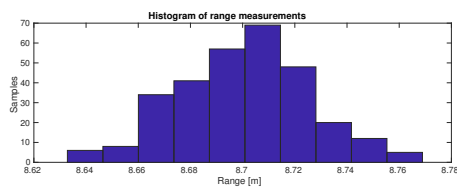


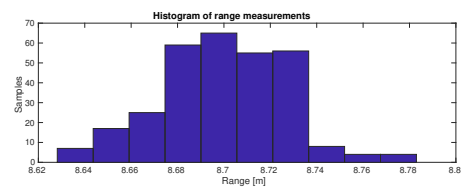
Figure D.1: Range measurements for all modules

D. Distance measurements

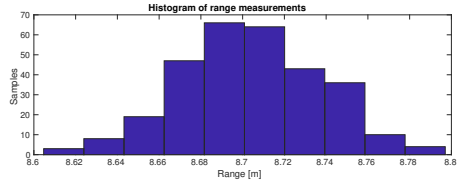
The histograms from the measurements depicted above can be seen in Figure D.2. They all indicate a Gaussian noise of ± 0.05 m.



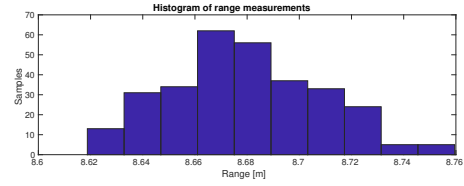
(a) Histogram of measurements in Figure D.1a



(b) Histogram of measurements in Figure D.1b



(c) Histogram of measurements in Figure D.1c



(d) Histogram of measurements in Figure D.1d

Figure D.2: Histogram of measurements made at 8.7 m

Furthermore, measurements were made at longer ranges to confirm the uniformity of the error. Range measurements from distances 2, 8.68, 17.36, 26.04, 34.72 and 43.4 meters can be seen below.

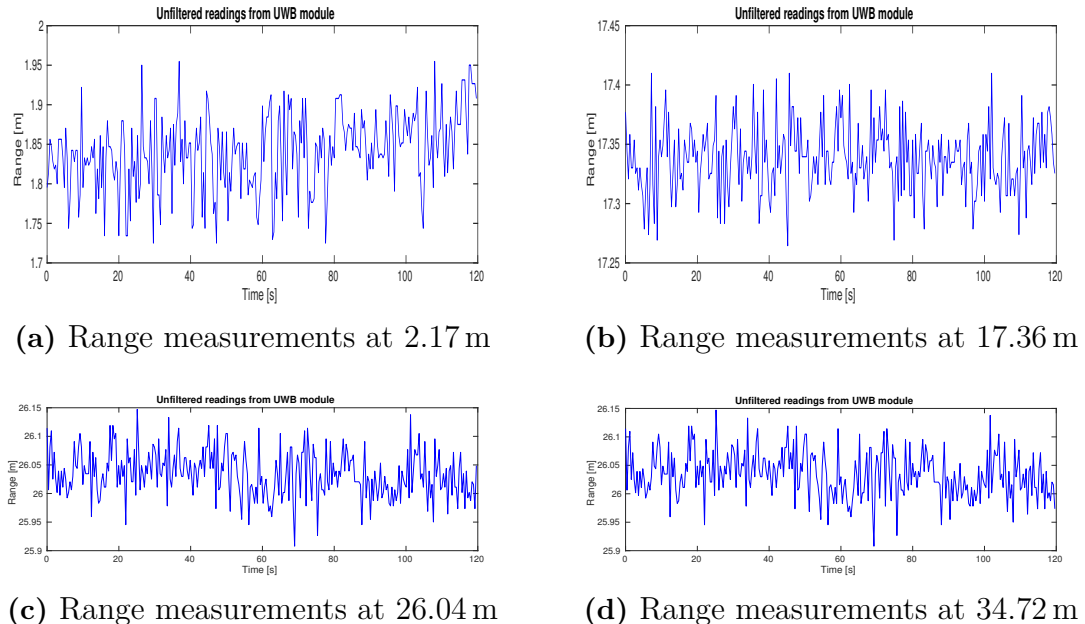


Figure D.3: Range measurements at various distances

The histograms for each of these measurements can be seen below

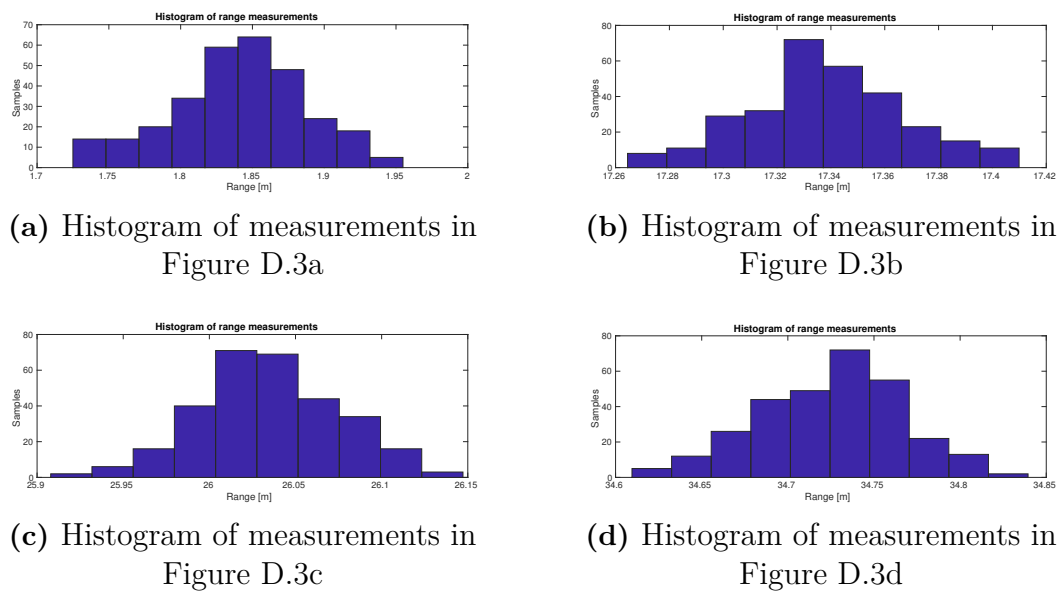


Figure D.4: Histogram of measurements made at various ranges displayed in Figure D.3

D. Distance measurements

E

Results appendix

The system was tested in several scenarios. A 56.5x56.5m square, 47m diameter circle, 30x30m square and an arbitrary garden environment for two different standard deviations of the signal. Tables for all simulation runs are displayed below

Arbitrary environment, signal standard deviation σ of 0.046 m with encoder input

Run	Mean error [m]	95 Percentile [m]	Standard deviation [m]
1	0.106	0.265	0.081
2	0.112	0.308	0.093
3	0.097	0.238	0.072
4	0.109	0.264	0.081
5	0.101	0.235	0.071
6	0.108	0.279	0.087
7	0.105	0.254	0.077
8	0.106	0.253	0.077
9	0.104	0.252	0.069
10	0.096	0.229	0.069
11	0.112	0.284	0.085

Arbitrary environment, signal standard deviation σ of 0.046 m without encoder input

Run	Mean error [m]	95 Percentile [m]	Standard deviation [m]
1	0.379	1.00	0.312
2	0.380	0.976	0.305
3	0.387	0.987	0.310
4	0.387	0.994	0.313
5	0.381	0.995	0.310
6	0.393	1.02	0.321
7	0.391	1.01	0.315
8	0.377	0.977	0.306
9	0.373	0.965	0.305
10	0.386	1.01	0.315
11	0.387	1.02	0.318

E. Results appendix

Arbitrary environment, signal standard deviation σ of 0.027 m with encoder input

Run	Mean error [m]	95 Percentile [m]	Standard deviation [m]
1	0.081	0.203	0.064
2	0.079	0.198	0.060
3	0.082	0.187	0.061
4	0.078	0.194	0.060
5	0.080	0.193	0.059
6	0.085	0.211	0.063
7	0.082	0.196	0.061
8	0.081	0.204	0.066
9	0.081	0.196	0.060
10	0.080	0.205	0.063
11	0.082	0.199	0.060

Arbitrary environment, signal standard deviation σ of 0.027 m without encoder input

Run	Mean error [m]	95 Percentile [m]	Standard deviation [m]
1	0.267	0.692	0.218
2	0.273	0.704	0.221
3	0.272	0.702	0.221
4	0.271	0.710	0.225
5	0.277	0.724	0.230
6	0.273	0.716	0.226
7	0.277	0.712	0.223
8	0.270	0.716	0.224
9	0.274	0.718	0.229
10	0.270	0.711	0.223
11	0.263	0.678	0.218

Square 56.5x56.5m, signal standard deviation σ of 0.046 m with encoder input

Run	Mean error [m]	95 Percentile [m]	Standard deviation [m]
1	0.187	0.477	0.145
2	0.177	0.418	0.130
3	0.190	0.469	0.159
4	0.203	0.466	0.136
5	0.189	0.490	0.158
6	0.183	0.432	0.128
7	0.183	0.419	0.125
8	0.176	0.449	0.130
9	0.199	0.469	0.144
10	0.202	0.544	0.170
11	0.201	0.522	0.157

Square 56.5x56.5m, signal standard deviation σ of 0.046 m without encoder input

Run	Mean error [m]	95 Percentile [m]	Standard deviation [m]
1	0.525	1.34	0.413
2	0.538	1.36	0.415
3	0.558	1.41	0.433
4	0.546	1.36	0.426
5	0.512	1.30	0.398
6	0.553	1.43	0.438
7	0.565	1.44	0.447
8	0.551	1.38	0.430
9	0.570	1.44	0.440
10	0.556	1.42	0.433
11	0.538	1.38	0.428

Circle 47m diameter, signal standard deviation σ of 0.046 m with encoder input

Run	Mean error [m]	95 Percentile [m]	Standard deviation [m]
1	0.232	0.646	0.197
2	0.215	0.562	0.174
3	0.195	0.537	0.165
4	0.229	0.660	0.200
5	0.209	0.549	0.170
6	0.180	0.459	0.145
7	0.258	0.677	0.204
8	0.208	0.536	0.168
9	0.175	0.431	0.143
10	0.198	0.521	0.164
11	0.217	0.558	0.176

Circle 47m diameter, signal standard deviation σ of 0.046 m without encoder input

Run	Mean error [m]	95 Percentile [m]	Standard deviation [m]
1	0.552	1.43	0.451
2	0.548	1.43	0.445
3	0.524	1.36	0.435
4	0.516	1.37	0.431
5	0.525	1.41	0.447
6	0.517	1.41	0.446
7	0.537	1.40	0.450
8	0.551	1.43	0.454
9	0.567	1.54	0.480
10	0.537	1.41	0.436
11	0.557	1.46	0.457

E. Results appendix

Square 30x30m, signal standard deviation σ of 0.027 m with encoder input

Run	Mean error [m]	95 Percentile [m]	Standard deviation [m]
1	0.090	0.237	0.073
2	0.100	0.259	0.077
3	0.103	0.268	0.081
4	0.097	0.246	0.077
5	0.099	0.237	0.072
6	0.088	0.236	0.071
7	0.100	0.254	0.079
8	0.094	0.238	0.071
9	0.101	0.255	0.078
10	0.095	0.258	0.078
11	0.093	0.234	0.080

Square 30x30m, signal standard deviation σ of 0.027 m without encoder input

Run	Mean error [m]	95 Percentile [m]	Standard deviation [m]
1	0.273	0.696	0.216
2	0.264	0.667	0.207
3	0.270	0.695	0.217
4	0.275	0.726	0.235
5	0.274	0.712	0.222
6	0.275	0.699	0.219
7	0.270	0.683	0.215
8	0.272	0.690	0.215
9	0.279	0.708	0.221
10	0.279	0.703	0.217
11	0.277	0.697	0.213

F

Schematics and circuit boards

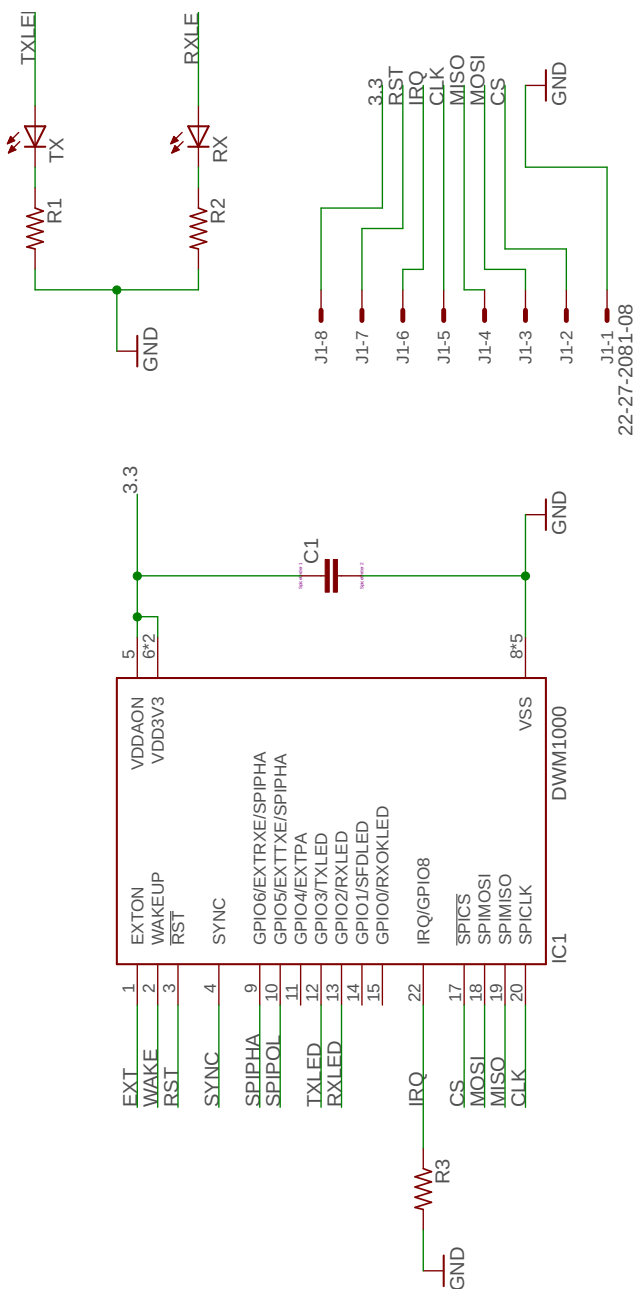


Figure F.1: DWM1000 breakout board schematic

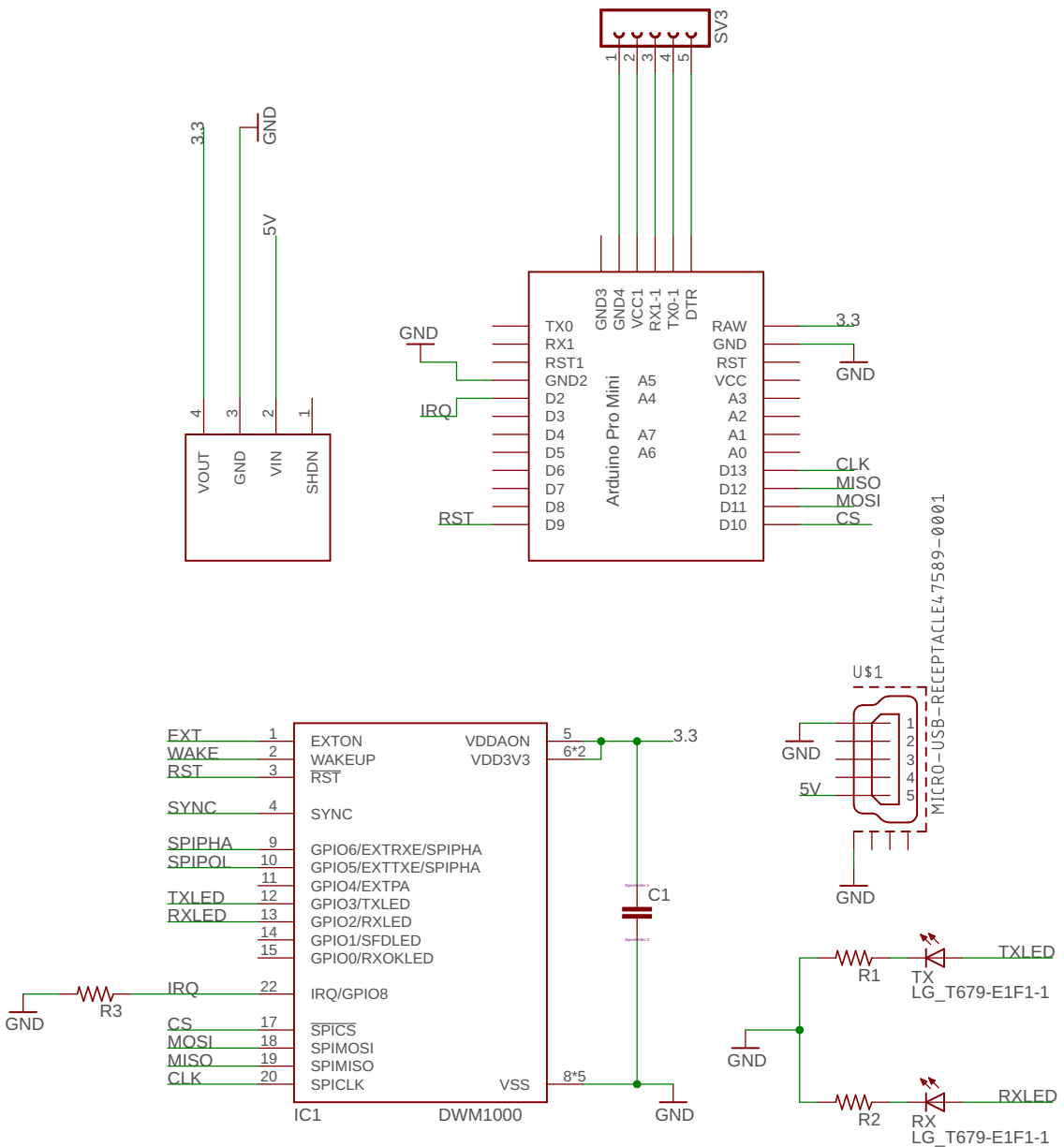


Figure F.2: Arduino tag schematic

F. Schematics and circuit boards

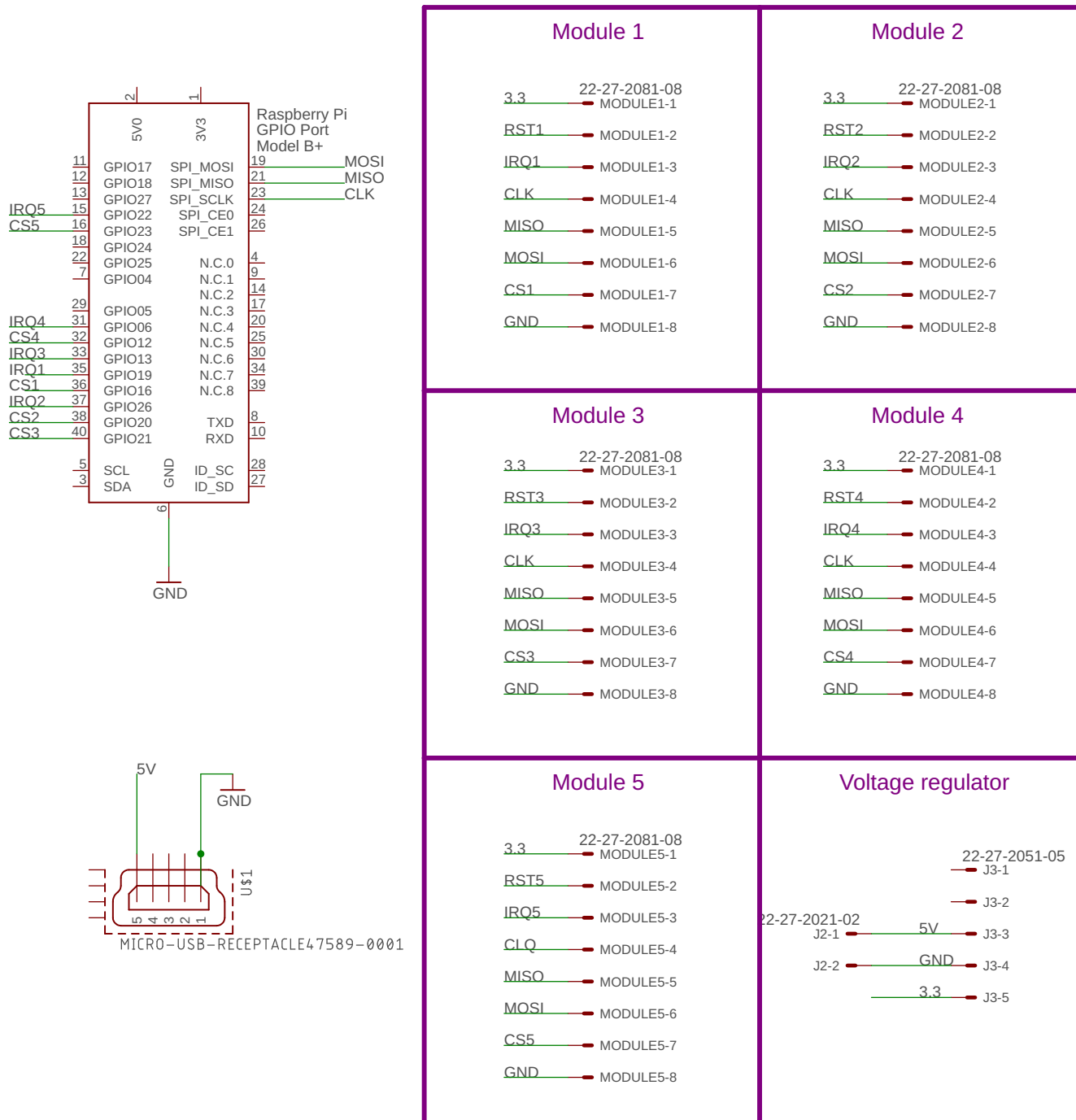


Figure F.3: Module connector board schematics

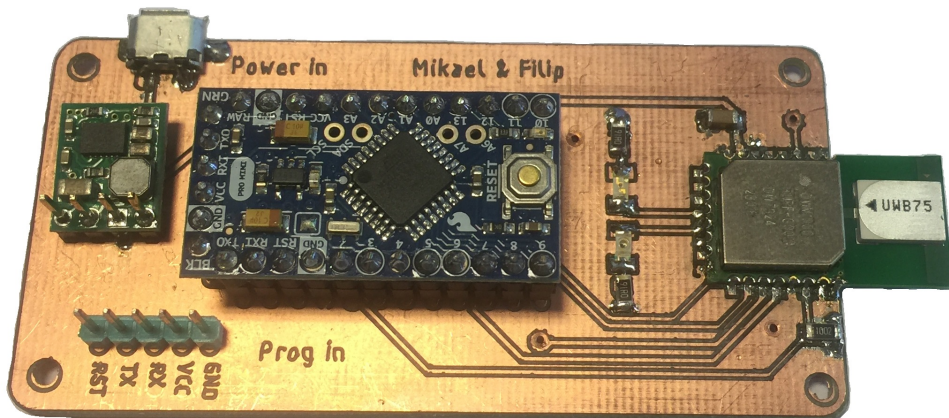


Figure F.4: Arduino tag PCB

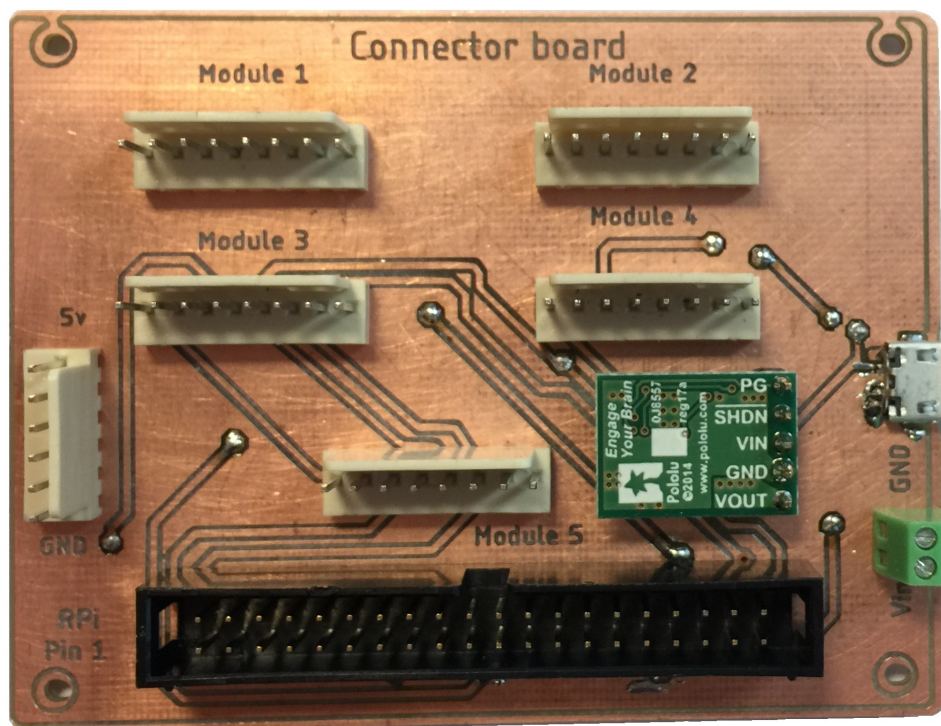


Figure F.5: Connectorboard PCB

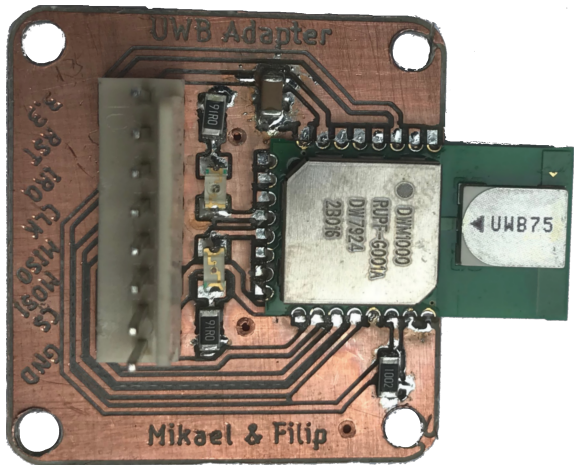


Figure F.6: DWM1000 breakoutboard PCB

G

Contributions

The work in this thesis was mainly done in collaboration between the authors but some separation of individual works can be identified. The research on the background study was made in collaboration. Considering the specific topics, Filip Lensund has been responsible for subtopics with regards to Ranging methods, Positioning techniques, Orientation angle and implementation/hardware while Mikael Sjöstedt has been responsible for Rover model, Radio, Filtering and simulations.

G. Contributions

H

Code

All the Matlab simulation programs as well as the software required to run the ranging and positioning protocols on the specified hardware are located at a GitLab repository. It can be accessed at <https://gitlab.com/Sjostedt/ExamensarbeteCybercom>

TRITA ITM-EX 2018:163